

# Journal Pre-proof

Selective contact self-assembled molecules for high-performance perovskite solar cells

Huan Bi, Jiaqi Liu, Liang Wang, Tuo Liu, Zheng Zhang, Qing Shen, Shuzi Hayase



PII: S2667-1417(24)00128-9

DOI: <https://doi.org/10.1016/j.esci.2024.100329>

Reference: ESCI 100329

To appear in: *eScience*

Received Date: 12 March 2024

Revised Date: 2 July 2024

Accepted Date: 15 October 2024

Please cite this article as: H. Bi, J. Liu, L. Wang, T. Liu, Z. Zhang, Q. Shen, S. Hayase, Selective contact self-assembled molecules for high-performance perovskite solar cells, *eScience*, <https://doi.org/10.1016/j.esci.2024.100329>.

This is a PDF file of an article that has undergone enhancements after acceptance, such as the addition of a cover page and metadata, and formatting for readability, but it is not yet the definitive version of record. This version will undergo additional copyediting, typesetting and review before it is published in its final form, but we are providing this version to give early visibility of the article. Please note that, during the production process, errors may be discovered which could affect the content, and all legal disclaimers that apply to the journal pertain.

© 2024 The Authors. Publishing services by Elsevier B.V. on behalf of Nankai University and KeAi.

## Selective contact self-assembled molecules for high-performance perovskite solar cells

Huan Bi<sup>1,2,\*</sup>, Jiaqi Liu<sup>1</sup>, Liang Wang<sup>1</sup>, Tuo Liu<sup>3</sup>, Zheng Zhang<sup>4</sup>, Qing Shen<sup>1,2,\*</sup>, and Shuzi Hayase<sup>1,2,\*</sup>

<sup>1</sup> *i-Powered Energy System Research Center (i-PERC), The University of Electro-Communications, Tokyo 182-8585, Japan*

<sup>2</sup> *Graduate School of Informatics and Engineering, The University of Electro-Communications, Tokyo 182-8585, Japan*

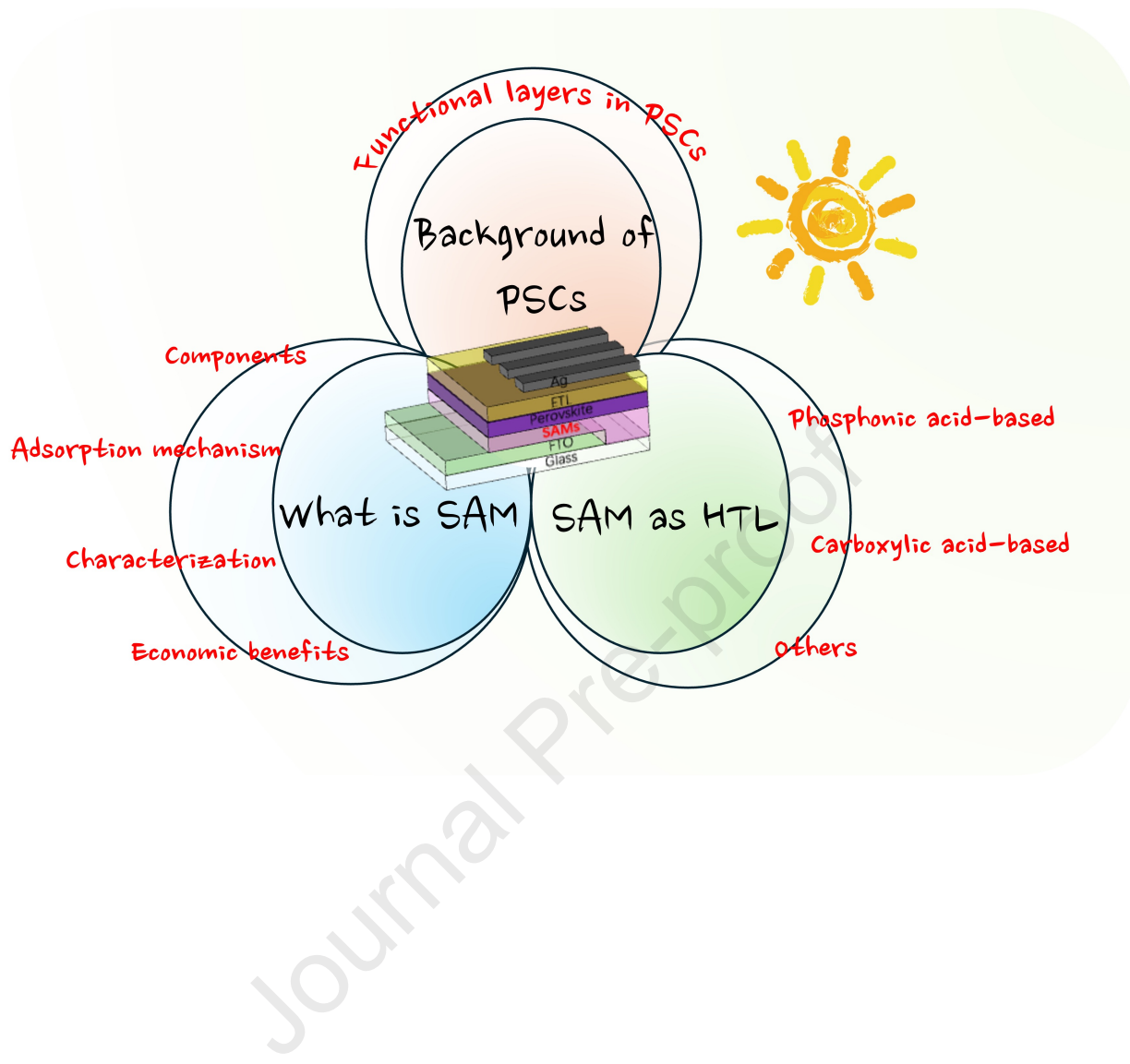
<sup>3</sup> *Department of Chemistry, University of Kentucky, Lexington, KY 40506, USA*

<sup>4</sup> *College of Physics Science and Technology, Hebei University, Hebei 050025, China*

\*Corresponding author.

E-mail: hbi.trans.sci@mail.uec.jp (Bi H.); shen@pc.uec.ac.jp (Shen Q.);

hayase@uec.ac.jp (Hayase S.)



# Selective contact self-assembled molecules for high-performance perovskite solar cells

Huan Bi<sup>1,2,\*</sup>, Jiaqi Liu<sup>1</sup>, Liang Wang<sup>1</sup>, Tuo Liu<sup>3</sup>, Zheng Zhang<sup>4</sup>, Qing Shen<sup>1,2,\*</sup>, and Shuzi Hayase<sup>1,2,\*</sup>

<sup>1</sup> *i-Powered Energy System Research Center (i-PERC), The University of Electro-Communications, Tokyo 182-8585, Japan*

<sup>2</sup> *Graduate School of Informatics and Engineering, The University of Electro-Communications, Tokyo 182-8585, Japan*

<sup>3</sup> *Department of Chemistry, University of Kentucky, Lexington, KY 40506, USA*

<sup>4</sup> *College of Physics Science and Technology, Hebei University, Hebei 050025, China*

\*Corresponding author.

E-mail: hbi.trans.sci@mail.uec.jp (Bi H.); shen@pc.uec.ac.jp (Shen Q.); hayase@uec.ac.jp (Hayase S.)

## Abstract

This review provides a comprehensive overview of the utilization of self-assembled monolayers (SAMs) in perovskite solar cells (PSCs), with a specific focus on their potential as hole transport layers (HTLs). Perovskite materials have garnered significant attention in photovoltaic technology owing to their unique optoelectronic properties. SAMs present a promising solution as efficient and stable HTLs by forming well-ordered thin films on transparent conductive oxide surfaces. This review commences with an introduction to the structure and properties of perovskite materials, followed by a discussion on the operational principles and compositions of functional layers in PSCs. It subsequently delves into the structure, preparation methodologies, and applications of SAMs in PSCs, highlighting their role in enhancing cell efficiency as HTLs. We also discuss their application as electron transport layers. The paper concludes by exploring the potential integration of SAMs into commercial PSC production processes and suggesting future research avenues.

## Keywords

Perovskite solar cell; Self-assembled monolayer; Hole-transport layer; Electron transport layer; Photovoltaic

## 1. Introduction

### 1.1. Background to perovskite solar cells

In recent years, the increasing depletion of natural energy sources has compelled us to seek new renewable energy alternatives. Solar energy, as a vital component of renewable energy, is essential in reducing reliance on fossil fuels, lowering greenhouse gas emissions, and mitigating climate change. Currently, common types of solar cells include silicon-based cells (c-Si), copper indium gallium selenide (CIGS) cells, organic photovoltaics (OPV), and solar cells in multi-junction devices (tandem cells). Perovskite solar cells (PSCs) have become an attractive alternative energy option due to their high photovoltaic conversion efficiency (PCE) and low production costs [1, 2, 3, 4]. Remarkably, single-junction PSCs have thus far achieved a PCE exceeding 26.1% and can compete with the most advanced c-Si-based solar cells in the traditional photovoltaic market [5].

Many researchers are dedicated to improving PSCs' power conversion efficiency and comprehending the perovskite structure is essential in this pursuit. The typical crystal structure of perovskite is depicted in Fig. 1. Here, A-site cations occupy the cubic vacancies of corner-sharing frameworks, while B-site cations and X-site anions form the octahedral structure ( $\text{BX}_6$ ). Common A-site cations include methylammonium ( $\text{MA}^+$ ), formamidinium ( $\text{FA}^+$ ), and cesium ( $\text{Cs}^+$ ). B-site cations typically comprise lead ( $\text{Pb}^{2+}$ ), tin ( $\text{Sn}^{2+}$ ), and germanium ( $\text{Ge}^{2+}$ ). Halogen ions such as iodide ( $\text{I}^-$ ), bromide ( $\text{Br}^-$ ), and chloride ( $\text{Cl}^-$ ) are commonly employed as X-site anions [6, 2, 7].

To assess the structural stability of perovskite materials, researchers always use the tolerance factor ( $t$ ), which is computed using the following equation [9, 10, 11, 12]:

$$t = \frac{r_A + r_X}{\sqrt{2}(r_B + r_X)} \quad (1)$$

where,  $r_A$ ,  $r_B$ , and  $r_X$  denote the A-site, B-site, and X-site ions' ionic radii. The ionic radii of elements constituting  $\text{ABX}_3$  perovskites are summarized in Table 1 [13, 14].

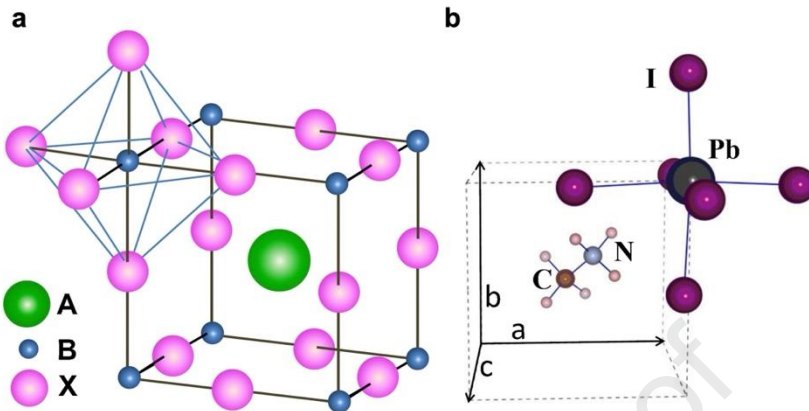


**Fig. 1.** (a)  $\text{ABX}_3$  perovskite structure, showing  $\text{BX}_6$  octahedral and larger A cation occupying the cubooctahedra site. (b) Unit cell of cubic  $\text{CH}_3\text{NH}_3\text{PbI}_3$  perovskite [8].  
Copyright 2015, Elsevier.

**Table 1.** Estimation of A-cation, B-cation, and X-cation radii in  $\text{ABX}_3$ .

Site	ionic radii ( $\text{\AA}$ )	Site	ionic radii ( $\text{\AA}$ )
A		B	
$\text{MA}^+$	2.17	$\text{Ge}^{2+}$	0.73
$\text{FA}^+$	2.53	$\text{Sn}^{2+}$	0.93
$\text{Li}^+$	1.13	$\text{Pb}^{2+}$	1.19
$\text{Na}^+$	1.39	X	
$\text{K}^+$	1.64	$\text{Cl}^-$	1.81
$\text{Rb}^+$	1.72	$\text{Br}^-$	1.96
$\text{Cs}^+$	1.88	$\text{I}^-$	2.2

Generally, materials with a  $t$  ranging from 0.9 to 1.0 exhibit an ideal cubic structure. Between 0.71 and 0.9 leads to a distorted perovskite structure with tilted octahedra. Structures deviating from the perovskite arrangement occur when the  $t$  exceeds 1 or falls below 0.71 [13]. Another approach to estimating the structural stability of the perovskite is to examine the octahedral factor ( $\mu$ ), which can be expressed as:[15, 16,

$$\mu = \frac{r_B}{r_X} \quad (2)$$

If  $\mu$  increases from 0.414 to 0.592, 7-coordinated octahedra would be more suitable, while  $\mu$  values below 0.592 would be better for stabilizing the  $\text{BX}_6$  octahedra [13, 11].

Table 2 summarizes different perovskite materials'  $t$  and  $\mu$  values [18].

**Table 2.** The  $t$  and  $\mu$  factors of  $\text{MABX}_3$ ,  $\text{FABX}_3$ , and  $\text{CsBX}_3$ .

Compound	$t$	$\mu$	Compound	$t$	$\mu$
$\text{MAPbI}_3$	0.912	0.541	$\text{FAPbI}_3$	0.987	0.541
$\text{CsPbI}_3$	0.851	0.541	$\text{MAPbI}_3$	0.927	0.607
$\text{FAPbBr}_3$	1.008	0.607	$\text{CsPbBr}_3$	0.862	0.607
$\text{MAPbCl}_3$	0.938	0.657	$\text{FAPbCl}_3$	1.023	0.657
$\text{CsPbCl}_3$	0.870	0.657	$\text{MASnI}_3$	0.987	0.423
$\text{FASnI}_3$	1.069	0.423	$\text{CsSnI}_3$	0.922	0.423
$\text{MASnBr}_3$	1.011	0.474	$\text{FASnBr}_3$	1.099	0.474
$\text{CsSnBr}_3$	0.940	0.474	$\text{MASnCl}_3$	1.027	0.514
$\text{FASnCl}_3$	1.120	0.514	$\text{CsSnCl}_3$	0.952	0.514
$\text{MAGeI}_3$	1.055	0.332	$\text{FAGeI}_3$	1.142	0.332
$\text{CsGeI}_3$	0.985	0.332	$\text{MAGeBr}_3$	1.086	0.372
$\text{FAGeBr}_3$	1.180	0.372	$\text{CsGeBr}_3$	1.009	0.372
$\text{MAGeCl}_3$	1.108	0.403	$\text{FAGeCl}_3$	1.208	0.403
$\text{CsGeCl}_3$	1.027	0.403	-	-	-

## 1.2. Functional layers in PSCs

Understanding the device structure is crucial for developing new functional layers, such as the hole transport layer (HTL) and electron transport layer (ETL), and for comprehending the conditions for modifying the device interface. Consequently, the device structure is introduced next.

In general, two typical structures of PSCs can be constructed: inverted-type (inverted planar) and regular-type (direct planar), illustrated in Fig. 2a [19]. Direct planar PSCs have functional layers arranged from bottom to top: a transparent conductive oxide (TCO, such as indium tin oxide (ITO) or fluorine-doped tin oxide (FTO)), ETL, perovskite layer, HTL, and metal electrode (such as gold (Au), silver (Ag), etc.). In inverted planar PSCs, the positions of the ETL and HTL are reversed compared to their locations in direct planar devices. Typically, sunlight illuminating the perovskite layer

triggers photon-induced transitions from the valence band to the conduction band, forming holes and electrons. Subsequently, holes and electrons diffuse to the interface and are extracted by the hole transport materials (HTM) and electron transport materials (ETM), respectively. Finally, they are collected by the cathode and anode electrodes and transmitted to the external circuit (Fig. 2b).

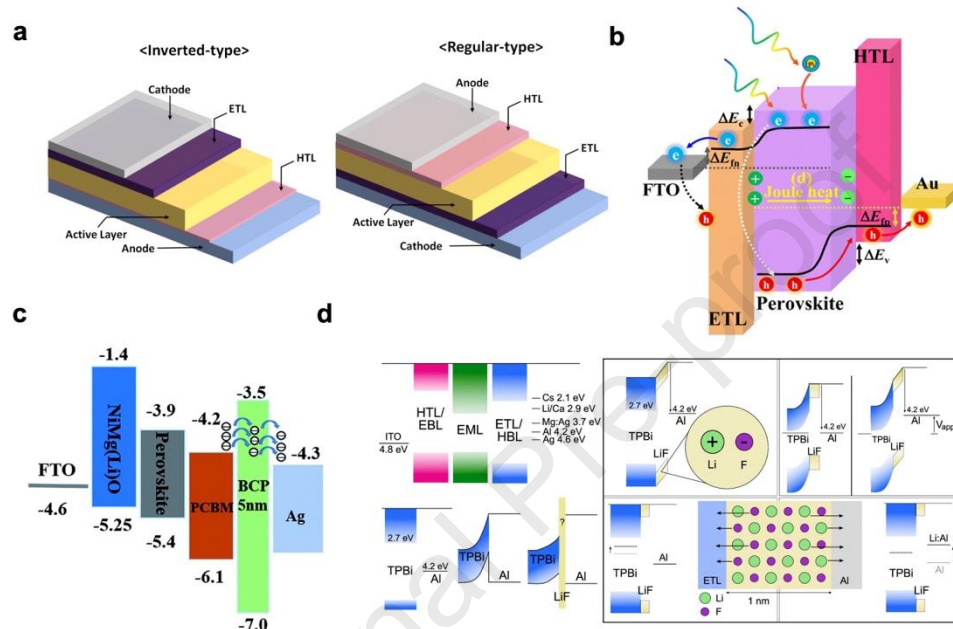


**Fig. 2.** (a) The device architectures of both inverted and regular perovskite solar cells [20]. (b) The operational mechanism of PSCs involves the following steps: Generation of photo-generated charge carriers. Extraction of charge carriers to the HTL and ETL. Transport of charge carriers to the electrodes [21]. Copyright 2020, American Chemical Society. (c) The energy diagram and charge transport mechanism of photovoltaic devices with bathocuproine [22]. (d) Proposed mechanisms for improved electroluminescence with thin-film LiF [23]. Copyright 2020, American Chemical Society.

The ETL is crucial in extracting and transmitting photo-generated electrons. A suitable ETL can facilitate electron transport and is a hole-blocking layer to suppress electron–hole recombination. The characteristics of the ETL, particularly its charge

mobility, energy-level alignment, trap state, morphology, and related interface properties, are vital in determining the final performance of PSCs [24]. Various materials have been chosen as ETLs, including TiO<sub>2</sub>, SnO<sub>2</sub>, and C60. Inverted-structure PSCs have additional requirements for selecting the ETL layer compared to normal-structure PSCs [25, 26, 27, 28]:

- (1) The deposition process must not damage the perovskite film; hence, the choice of solvent is critical.
- (2) The selected ETL material should not react with PSC components like Sn<sup>2+</sup>, Pb<sup>2+</sup>, MA<sup>+</sup>, or FA<sup>+</sup>, as such reactions could degrade performance and stability.
- (3) Optimal energy-level alignment and charge mobility as well as minimized trap states are essential to enhance PSCs' overall efficiency and longevity.

For inverted PSCs, C60 and some C60 derivatives (such as PC60BM, PC71BM, and ICBA) have long been selected as ETLs due to their contribution to charge separation and excellent PSC performance [29]. McNeill et al. utilized PCBM/P3HT double ETL layers to complement trap states in PSCs. Bathocuproine (BCP) and LiF have also been used to form multilayer ETLs with fullerenes to block holes (Figs. 2c and 2d) [30].

HTL also plays a crucial role in achieving high PCE and stability in PSCs, facilitating the transport of photo-generated holes from the perovskite layer to the TCO. To date, several materials have been adopted as HTLs, such as 2,2',7,7'-Tetrakis(N, N-di-*p*-methoxyphenylamine)-9,9'-spirobifluorene (Spiro-OMeTAD), Poly[bis(4-phenyl)(2,4,6-trimethylphenyl)amine] (PTAA), poly(3,4-ethylene-dioxythiophene):poly(styrene sulfonate) (PEDOT:PSS), and others. Ideally, the HTM should meet the following requirements [37, 38]:

- (1) Alignment of the highest occupied molecular orbital (HOMO) energy level with the valence band (VB) of the perovskite.

(2) Sufficient hole mobility to ensure effective hole transport and collection.

(3) Demonstrable chemical and thermal stability.

(4) Cost-effectiveness and scalability for commercial applications.

In inverted PSCs, PEDOT:PSS is commonly used as the HTL due to its favorable morphology, high conductivity, and low-temperature solution processing [39, 40, 41, 42, 43]. However, it has several persistent disadvantages. On the one hand, the natural acidity of PEDOT:PSS solutions can lead to the severe corrosion of ITO electrodes and perovskite. On the other hand, the energy level of PEDOT:PSS does not perfectly match that of perovskite, resulting in significant interfacial recombination [44, 45, 46, 47].

Table 3 lists the potential limits of the common functional layers.

**Table 3.** Summary of potential limits of the functional layers used in PSCs.

Materials	Function	Limits
TiO <sub>2</sub>	ETL	<ul style="list-style-type: none"> <li>1. Band structure mismatch [31].</li> <li>2. Pronounced hysteresis of the current–voltage curve [32].</li> <li>3. Complex preparation processes lead to higher manufacturing costs [33].</li> <li>4. Poor UV stability [34].</li> <li>5. <u>Relatively slow electron transfer rate [35].</u></li> </ul>
C <sub>60</sub>	ETL	<ul style="list-style-type: none"> <li>1. Poor solubility in common organic solvents.</li> <li>2. The preparation and purification costs are relatively high.</li> <li>3. <u>The interface stability between C<sub>60</sub> and the perovskite layer may not be ideal.</u></li> </ul>
SnO <sub>2</sub>	ETL	<ul style="list-style-type: none"> <li>1. Difficulties in adjusting the band structure.</li> <li>2. Interface defect sensitivity [36].</li> <li>3. <u>Tin can be toxic to living organisms.</u></li> </ul>
Spiro-OMeTAD	HTL	<ul style="list-style-type: none"> <li>1. Volatility of organic materials.</li> <li>2. Sensitive to doping.</li> <li>3. The production cost is relatively high.</li> <li>4. <u>The properties are unstable under light exposure or high-temperature conditions.</u></li> </ul>
PEDOT:PSS	HTL	<ul style="list-style-type: none"> <li>1. Acidity and alkalinity.</li> <li>2. Difficulty in controlling thickness.</li> <li>3. High manufacturing cost.</li> <li>4. <u>PEDOT:PSS is sensitive to moisture and prone to moisture absorption.</u></li> </ul>
PTAA	HTL	<ul style="list-style-type: none"> <li>1. Instability of doping.</li> <li>2. Volatility of organic materials.</li> <li>3. Complex preparation and high cost.</li> <li>4. Superhydrophobicity makes it unsuitable for inverting PSC.</li> </ul>

Inverted PSCs have emerged as a significant advancement in photovoltaic technology, offering notable benefits over traditional configurations. These cells are distinguished by their operational stability and minimal hysteresis, making them suitable for low-

temperature manufacturing processes. Inverted PSCs support the production of flexible solar cells due to their robust structure and performance under varying environmental conditions. With efficiencies surpassing 25%, achieved through optimized nanocrystalline films, effective interfaces, and electrode material management, inverted PSCs present a cost-effective solution for scalable solar energy applications. The simplicity of their fabrication process and enhanced stability position inverted PSCs as promising candidates for commercialization, especially in large-area solar modules [48, 49].

While the HTL and ETL are pivotal for the efficient functioning of PSCs, their roles and requirements are distinct. HTLs primarily support hole transport and must align closely with the HOMO level of the perovskite. In contrast, ETLs focus on electron mobility and barrier properties to optimize electron flow and minimize recombination. Recognizing and addressing these distinct roles is critical for designing more efficient and stable PSCs.

This review focuses on integrating self-assembled monolayers (SAMs) on inverted PSCs, particularly in novel selective-contact HTLs, to guide researchers wishing to enhance the efficiency and stability of PSCs. The review begins with an overview of SAMs, covering their structure, preparation techniques, and potential benefits. Subsequently, it explores SAMs as innovative selective-contact HTLs and their implementation in PSCs, with a brief mention of SAMs in ETLs. We then comprehensively address the potential integration of SAMs into the commercialization process of PSCs, along with challenges related to SAM technology and future research directions. The conclusion discusses the potential applications of SAMs in perovskite solar cells and outlines future research directions to address critical challenges in PSC technology.

## 2. A preliminary understanding of SAMs

SAMs of organic molecules are molecular assemblies formed spontaneously on surfaces by adsorption and are organized according to the size of their ordered domains [50]. In some cases, the molecules that form the monolayer do not interact strongly with the substrate. This phenomenon is observed in two-dimensional supramolecular networks, such as porphyrins on gold or perylene-3,4,9,10-tetracarboxylic dianhydride on highly oriented pyrolytic graphite. Conversely, in other scenarios, molecules feature a head group with a strong affinity for the substrate, anchoring them firmly onto the surface.

### 2.1. Composition and molecular design of SAMs

#### 2.1.1. Composition of SAMs

Generally, SAMs consist of three components: the headgroup or anchoring group, the spacer or linker, and the terminal or functional group, as shown in Fig. 3a. The headgroup/anchoring group and terminal/functional group play the most critical roles among these components. Anchoring groups are pivotal in SAM design, as they dictate the bonding strength between the substrate and the SAM. Various anchoring groups can form covalent bonds through chemical reactions and/or noncovalent bonds via physical adsorption. However, SAMs formed through physical adsorption often necessitate unique structural designs and processing methods, posing structural stability and reproducibility challenges. Consequently, anchoring groups based on chemical bonding are generally favored for solution-processed thin-film electronic devices. In addition, the anchoring group's chemical properties largely dictate the SAM's coverage ability [54]. Based on the substrate type for SAM deposition, anchoring groups capable of establishing chemical bonding can be categorized into two kinds: suitable for metals

and suitable for oxides. Commonly used headgroups include the thiol anchoring group, carboxylic acid anchoring group, phosphonic acid anchoring group, 2-cyanoacrylic acid (CA), or silane anchoring group.

The linker group in SAMs, which serves as a crucial backbone connecting anchoring and terminal groups, is primarily composed of non-conjugated alkyl chains or conjugated aromatic rings. These linkers control supramolecular structures through van der Waals interactions, influence molecular packing, and adjust the tilt angle during assembly. The choice between inactive aliphatic and photoactive conjugated linkers affects charge transfer properties, dipole moments, and tunneling lengths, which are vital for SAMs' electronic conductivity and optical properties, enhancing the performance and stability of devices like PSCs [55, 56].

The tail or functional group typically constitutes the functional end of the molecule, with its functionality determined by the head group itself. By varying the type of tail group, the surface energy of the device can be modified to either inhibit or promote the accumulation of moisture on the sample surface, thus altering its hydrophilicity and hydrophobicity. In PSCs, the most commonly used end groups include ammonium cation, hydroxyl, thiophene, thiol, and pyridine.

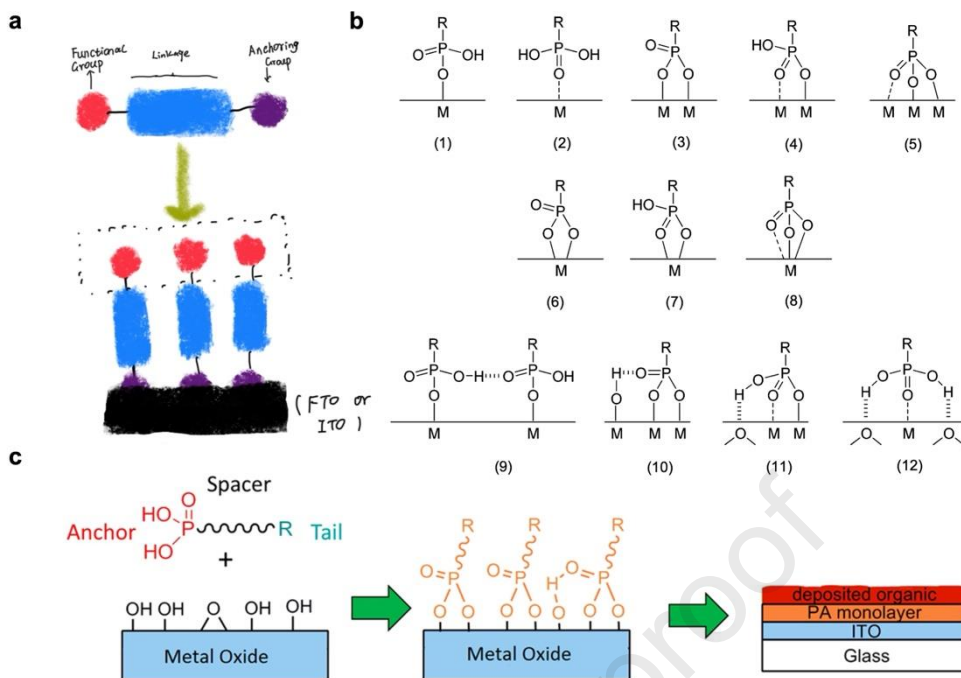


**Fig. 3.** (a) Schematic representation of SAMs. (b) Some possible binding modes of phosphonic acids to a metal oxide surface, where M = metal; monodentate (1 and 2), bridging bidentate (3 and 4), bridging tridentate (5), chelating bidentate (6 and 7), chelating tridentate (8), and some possible additional hydrogen bonding interactions (9–12) [51, 52]. Copyright 2008 American Chemical Society. (c) Surface modification with a phosphonic acid to increase the adhesion of a deposited organic on the surface [53, 51]. Copyright 2011 American Chemical Society.

### 2.1.2. SAM design strategy on PSCs

As discussed earlier, the molecular structure of SAMs consists of anchoring groups, linker groups, and terminal groups. Each component plays a crucial role in designing effective SAMs for PSCs. Table 4 lists the reported high-efficiency PSCs based on a SAM-HTL.

**Table 4.** The latest high-performance inverted PSCs achieving PCEs of over 23% based on a SAM as the HTL.

SAM-HTL	$J_{\text{SC}}$ ( $\text{mA cm}^{-2}$ )	$V_{\text{OC}}$ (V)	FF (%)	PCE (%)	Ref.
MeO-2PACz	25.58	1.18	84.9	25.6	[57]
2PACz+3-MPA	25.5	1.15	84.5	24.8	[58]
MPA-CPA	24.8	1.21	84.7	25.4	[59]
DMAcPA	25.69	1.19	84.7	25.9	[60]

Me-4PACz	24.78	1.19	83.1	24.5	[61]
DC-PA	24.45	1.19	84.2	24.5	[62]
DC-PA+IAHA	24.66	1.16	82.5	23.6	[63]
CBzNaph	24.69	1.17	83.4	24.1	[64]
Me-4PACz+Br-EPA	25.10	1.201	83.54	25.16	[65]

By analyzing the current HTL selections for high-efficiency PSCs, we can see that these molecules have the following characteristics:

- (1) Structural core units: Predominantly, these molecules comprise cyclic aromatic frameworks, including benzene and various heterocycles (e.g., carbazole, ethylene, hydrazone). These ring structures are pivotal for enhancing molecular stability and potentially modulating electronic characteristics.
- (2) Phosphate group: Each molecule incorporates a phosphate moiety (phosphonic acid)—a ubiquitous functional group employed to augment the molecule's polarity, enhance aqueous solubility, or facilitate binding with other entities, including biomolecules.
- (3) Functional substituents: Various substituents, such as methoxy groups and bromine atoms, are present. These groups influence the electronic properties and the lipophilicity/hydrophilicity balance, thereby impacting molecular behavior and suitability across different applications.
- (4) Alkyl chain linkages: Certain molecules feature alkyl chain segments, typically to boost intermolecular flexibility or alter the molecules' aggregation state.

Based on the above structural analysis, we need to consider the following aspects when designing new SAMs:

- (1) Enhance hole mobility:
  - Extend the conjugated system: Hole mobility can be enhanced by increasing the

molecule's conjugated length. For example, the molecule's conjugated system can be enhanced by introducing more conjugated connections in basic structures, such as carbazole or benzene rings, or by designing polycyclic structures.

- Optimization of molecular planarity: Maintaining high planarity when designing molecules can help with stacking and charge transport between molecules—for example, by introducing rigid ring structures or designing side groups that promote planar alignment.

(2) Maintain a balance between electron donors and acceptors:

- Adjustment of the electron donor structure: Introducing strong electron donor groups such as methoxy and amino groups into the molecular structure can increase the molecule's hole density.
- Controlling the characteristics of the electron acceptor: Properly adjusting the strength and position of the electron acceptor group (such as by introducing cyano and nitro groups) can help balance the charge distribution inside the molecule and optimize the hole transport performance.

(3) Optimize intermolecular interactions:

- Enhance intermolecular interactions through side chains or functional groups: Designing side chains to increase  $\pi$ - $\pi$  interactions or hydrogen bonding between molecules helps improve the molecules' order and transport properties in the film.
- Design of spatial arrangement: Consider the molecule's three-dimensional structure to optimize the stacking and arrangement of molecules, such as by introducing structural features that make the molecules stack in a specific direction.

(4) Utilize phosphate groups:

- Improvement of interfacial properties: Phosphate groups can provide a good polar interface, which helps the adsorption and arrangement of molecules on the electrode surface, thereby improving the injection and collection efficiency of charges.

(5) Make synthesis feasible and stable:

- Ensure synthesis feasibility: Consider the synthetic route of the molecule, and choose a structure that is easy both to synthesize and cost-effective.
- Thermal and photostability: Select a molecular structure with good thermal and photostability to meet battery materials' long-term use and environmental stability requirements.

## 2.2. Adsorption mechanism of SAMs

A SAM's adsorption mechanism relies on the anchoring group's chemical nature. For example, the phosphonic acid anchoring group consists of two hydroxyl groups and one phosphoryl group. Depending on the type of metal oxide surface and reaction conditions, it allows for single, bidentate, and tridentate binding modes, as exhibited in Fig. 3b. The -OH group binds to the metal oxide surface through protonation and then condenses to form a strong P-O-M bond, resulting in single and double bonds (Fig. 3c). For tridentate bonding, hydrogen atoms are transferred to the surface hydroxyl groups; this is followed by hetero-condensation, which generates oxygen vacancies in the SAM, forming an additional third bond. Therefore, various binding configurations based on surface type and conditions will facilitate the simultaneous connection of oxygen atoms to the same or different metal atoms [53, 51].

## 2.3. Characterization of SAM binding mode (phosphonic acid group as the example)

So far, although various techniques have been used to observe the vibration modes

and states of molecules, understanding the adsorption modes of SAMs remains challenging due to SAMs' unique properties, and only a few methods have been adopted. Armstrong et al. investigated the adsorption behavior and molecular orientation of SAMs on ITO surfaces using various phosphonic acids, including n-hexyl phosphonic acid (HPA), n-octadecyl phosphonic acid (ODPA), and others (see Fig. 4a). They employed photonic modulation infrared reflection-absorption spectroscopy (PM-IRRAS) for in-depth analysis, contrasting it with conventional Fourier-transform infrared spectroscopy (FT-IR) to demonstrate the former's superior signal-to-noise ratio and resolution. Initially, PM-IRRAS was used to analyze an unmodified ITO surface for a baseline spectrum. Subsequent analyses on ODPA-modified ITO surfaces revealed distinct vibrational modes, such as the  $\nu(\text{P}=\text{O})$  vibration at  $1230\text{ cm}^{-1}$  and P–O–(H) stretching vibrations at  $955\text{ cm}^{-1}$  and  $930\text{ cm}^{-1}$ , indicating significant differences between surface-bound and bulk materials. These findings suggest a predominantly bidentate binding of ODPA, with some monodentate attachment evident by the weak signals from free P–O–H moieties (Fig. 4b). Additionally, different binding modes of SAMs are illustrated in Fig. 4c. For TFBdiPA-modified surfaces, PM-IRRAS showed vibrational differences indicative of unique molecular orientations compared to their powder form, suggesting two potential adsorption orientations (Fig. 4d) [66]. Marder et al. employed IRRAS to examine the formation of an ODPA monolayer on zinc oxide (ZnO) surfaces, focusing on chain conformation and surface interactions. Using dodecyl phosphate-d25 modified ZnO/Au substrates as a background, they observed distinct methylene C–H stretching vibrations consistent with an anti-conformation of alkyl chains, indicative of a dense and stable monolayer. Analysis of the binding mode of ODPA to the ZnO surface revealed tridentate bonding of phosphonic acid, with a broad peak at  $1016\text{ cm}^{-1}$  and a shoulder representing  $\nu_{\text{a}}(\text{PO}_3^{2-})$ , without any P=O or

P–O–H bands, confirming the tridentate attachment (Fig. 4c) [67]. These studies demonstrate that IRRAS and PM-IRRAS are vital for elucidating SAMs' molecular orientation and binding modes on surfaces, establishing the techniques' effectiveness in revealing detailed molecular interactions.

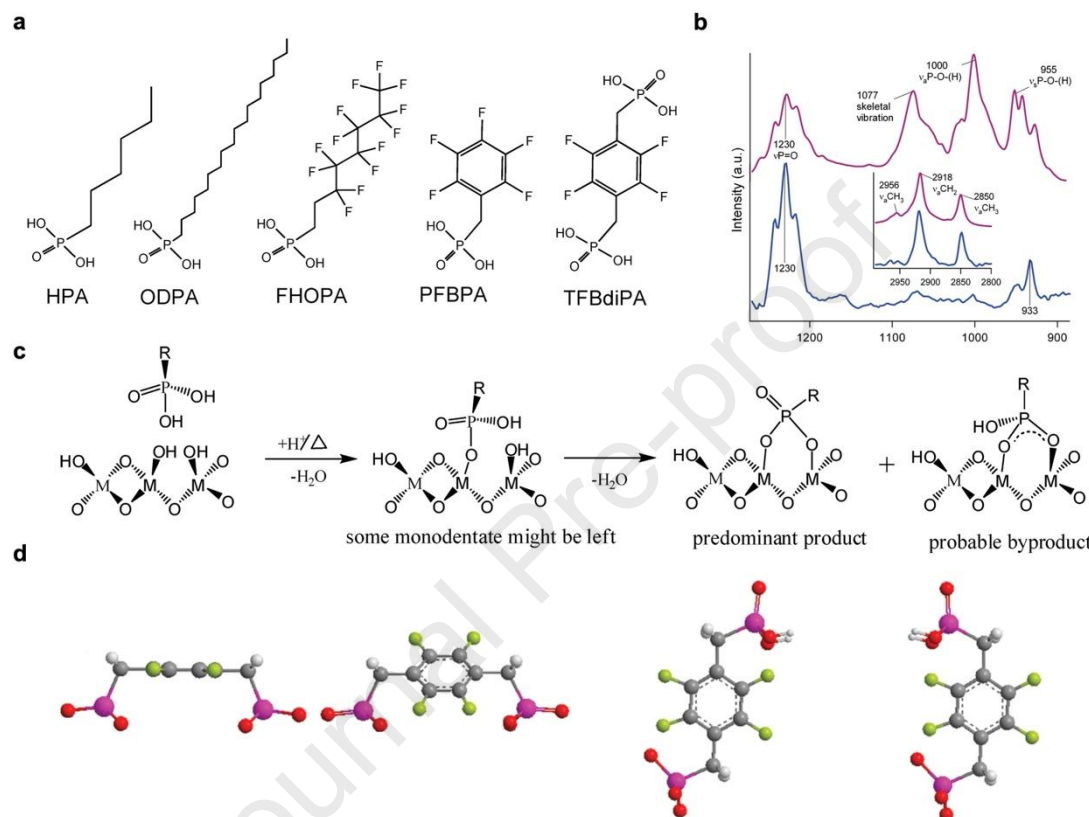


**Fig. 4.** (a) Structures of several phosphonic acid modifiers. (b) Comparison of the ODPA transmission FT-IR spectrum (top spectrum) and the PM-IRRAS spectrum for an ODPA-modified DSC/OP-treated ITO surface (bottom spectrum) in the  $\nu(\text{P-O})$  region. Inset: Same spectral comparisons for the  $\nu(\text{C-H})$  region. (c) Proposed reaction steps for OP-treated ITO with ODPA, based on the PM-IRRAS characterization data. (d) Most probable conformations for TFBdiPA bonded to ITO [66]. Copyright 2008 American Chemical Society.

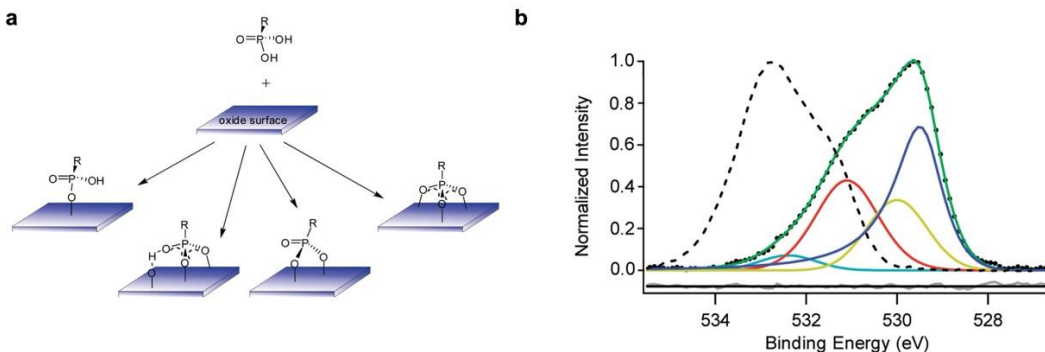


**Fig. 5.** (a) Common adsorption modes of SAMs on ITO surfaces. (b) Experimental oxygen (O1s) core-level XPS spectrum for ODPA adsorbed on the ITO surface is represented by dots, with components fitted using DFT calculations illustrated by colored lines [68]. Copyright 2008 American Chemical Society.

X-ray photoelectron spectroscopy (XPS) coupled with density functional theory (DFT) calculations has been established as a robust method to study the adsorption patterns of SAMs on metal oxide substrates [68, 69, 70]. Bredas et al. highlighted that this combination can provide deep insights into the binding modes of phosphonic acids [68]. Initially, comparing the O 1s XPS spectra of ODPA powder and ODPA-modified ITO films revealed shifts in O 1s binding energies, indicating a chemical interaction between ODPA and ITO. DFT calculations were instrumental in further elucidating these binding modes and comparing core-level binding energy shifts. The XPS and DFT results, which were in excellent agreement, identified bidentate and tridentate binding as the predominant attachment geometries of phosphonic acids on the ITO surface, as shown in Figs. 5a and 5b. Recent studies also corroborate the alignment between DFT-calculated shifts in O 1s core-level binding energies and XPS observations for ODPA surface modifiers on ZnO and gallium-doped ZnO substrates. Tempel et al. noted that the peak at +3.2 eV in the XPS spectrum, indicative of oxygen atoms in a non-surface-bound bidentate configuration, corresponded closely to the +3.75 eV predicted by DFT calculations, highlighting the method's accuracy [71].

Wakamiya et al. developed a series of SAMs with selective contact sites, labeled as 1PATAT-C3, 2PATAT-C3, 3PATAT-C3, and 3PATAT-C4, showcasing a straightforward synthesis process with significant yields: 1PATAT-C3 at 45%, 2PATAT-C3 at 37%, 3PATAT-C3 at 77%, and 3PATAT-C4 at 74%, as depicted in Fig. 6a [72]. They analyzed the vibration bands of 3PATAT-C3 in both film and powder forms on Si/ITO substrates using IRRAS and attenuated total reflection (ATR) spectroscopy. Compared with DFT calculations, the IRRAS results identified each vibration peak, showing a notable decrease in the P-O-H stretching vibration intensity that was indicative of the deprotonation of phosphonic acid groups-critical evidence of SAM adsorption on the substrate, as illustrated in Fig. 6b. Furthermore, an increase in the intensity of the P=O stretching band relative to P-O-H bands suggested all three phosphonic acid groups are bidentate bound to the ITO surface without chemical interaction from P=O groups. To verify the molecular orientation of 3PATAT-C3 on the ITO surface, ultraviolet photoelectron spectroscopy (UPS) and metastable atom electron spectroscopy (MAES) were employed. UPS assessed the valence states' density of states (DOS), while MAES targeted the outermost atomic orbitals, providing insights into the molecular surface orientation. The disparities between the UPS and MAES spectra and the calculated DOS helped deduce the molecular orientation, as shown in Fig. 6c. The MAES results highlighted a pronounced contribution from  $\pi$  states compared to  $\sigma$  states, indicating that 3PATAT-C3 molecules are vertically aligned on the ITO surface. This preferred vertical orientation was further supported by DFT calculations, confirming that the most stable configuration for all three phosphonic acid groups is their vertical anchorage to the ITO surface, as shown in Figs. 6d and 6e.

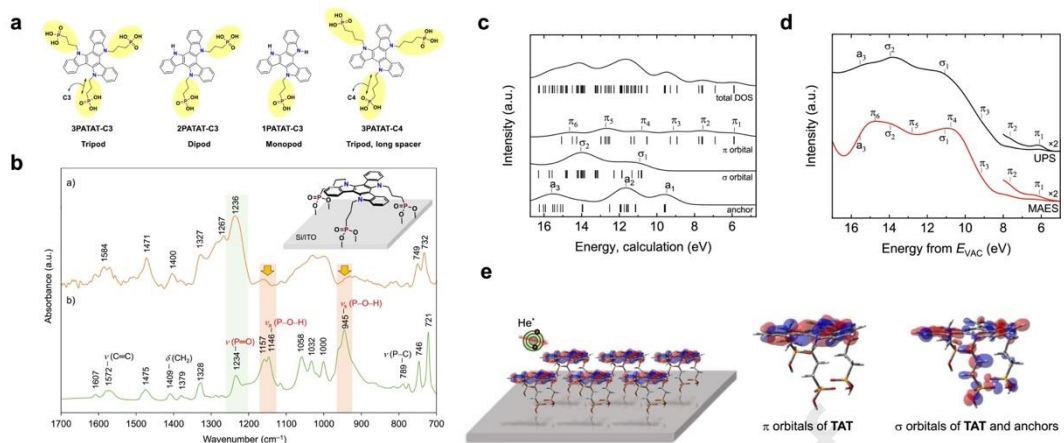


**Fig. 6.** (a) The molecular structures of triazatruxene-based materials for hole collection; (b) the IRRAS spectrum of 3PATAT-C3 on a Si/ITO substrate, obtained with p-polarized light at an  $80^\circ$  angle alongside the ATR spectrum of 3PATAT-C3 in powder form; (c) the DOS and MO energies, as determined through DFT calculations; (d) a comparative analysis of the helium I ultraviolet photoelectron spectroscopy (He I UPS) and metastable atom electron spectroscopy (He\* MAES) spectra of 3PATAT-C3 on the ITO substrate; and (e) a schematic of the face-on orientation of 3PATAT-C3 molecules on ITO, illustrating typical distributions of molecular orbitals [72].

Copyright 2023 American Chemical Society.

In summary, although many techniques have been used to characterize the orientation of SAMs, the mechanism of action of SAMs remains controversial, so developing and exploring more precise characterization methods to detect SAM orientations and action mechanisms is a matter of urgency.

#### 2.4. Why choose SAMs?

Compared to traditional first- and second-generation solar cells, PSCs' significant

advantages are their low cost and ease of fabrication. Although the perovskite layer is low-cost, the functional layer is expensive, challenging to synthesize, and complex with respect to influencing factors, reducing PSCs' advantages. For example, it has been noted that the molecular weight of polymers like P3HT and PTAA, HTMs widely used as inverted PSCs, significantly impacts device performance [73, 74, 75]. Another commonly used HTM, Spiro-OMeTAD, undergoes a complex synthesis process, involves expensive raw materials, and requires multiple additives, contributing to the slow commercialization of PSCs [76]. In contrast, SAMs offer significant advantages:

- (1) The reported effective SAM structures are relatively simple, with synthesis steps that do not require expensive noble metal catalysts or complex reaction conditions.
- (2) The molecules of a SAM-based HTL can be purified through recrystallization instead of traditional column chromatography.
- (3) Only a small concentration of SAMs is required to fabricate efficient devices, mainly due to the thinness of the SAM layer. These cost advantages become even more pronounced when scaled up for commercial production.

In addition to the abovementioned advantages, the tremendous thinness of SAMs utilized as HTLs effectively reduces optical losses and enhances device performance. Commonly used hole transport materials like PEDOT:PSS, NiO<sub>x</sub>, etc. typically have greater thicknesses (>10nm), leading to reduced light absorption in the perovskite layer (Fig. 7a). According to reports illustrated in Fig. 7b, using SAMs as HTLs does not compromise the optical transparency of the substrate (ITO or FTO), which is crucial for enhancing the device's current [80, 77].

SAMs' high carrier transfer performance and conductivity contribute to reduced device resistance, minimizing unnecessary losses. Researchers generally aim to reduce material resistance and enhance conductivity through doping. However, the uniformity

and controllability of doping are challenging, and ion migration induced by doping can impact the quality of the perovskite thin film. SAMs effectively address these issues. Levine's group investigated charge transfer rates and electron capture in buried interfaces in SAM-based PSCs using photoelectron spectroscopy (PES) (Fig. 7c) [78]. They found that SAMs maintain excellent selectivity, achieving faster transfer rates and lower trap density. This study reasonably explains the record-breaking 29.2% efficiency in perovskite/c-Si tandem cells.

Finally, as exhibited in Figs. 7d and 7e, since SAMs can easily form uniform thin films, they are conducive to preparing large-area perovskite solar cells, thereby promoting the commercialization process of perovskite photovoltaics [78, 79].

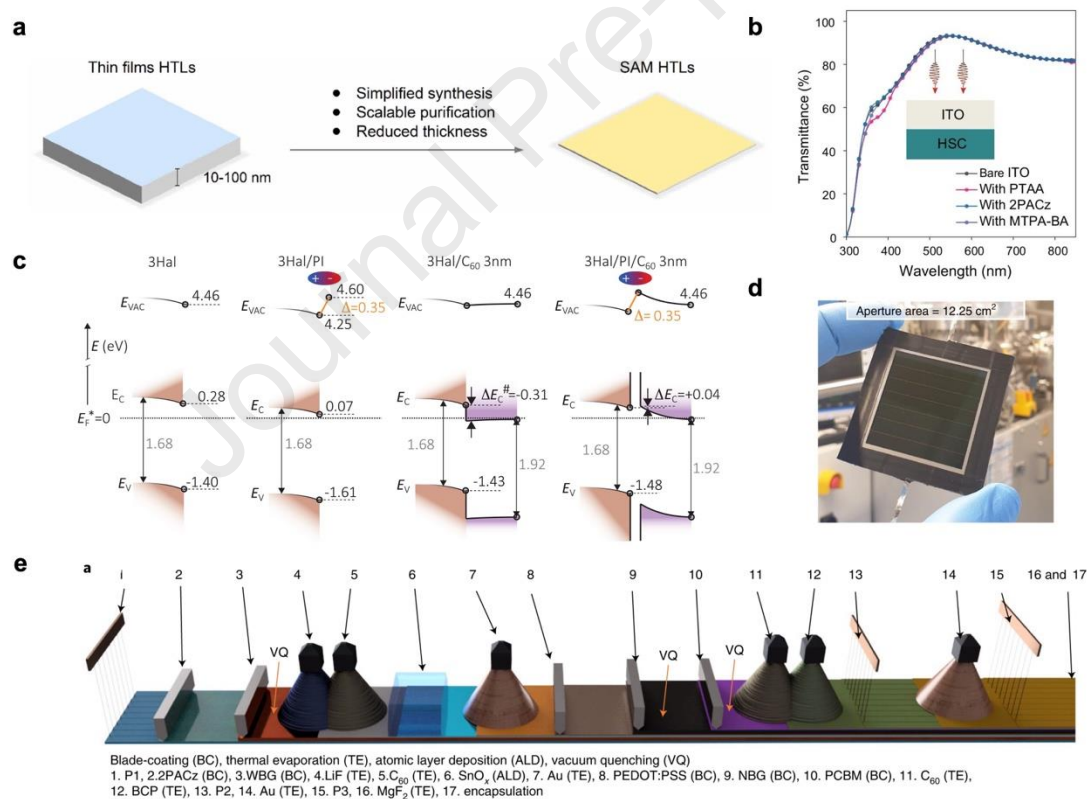


**Fig. 7.** (a) A schematic representation of the varying thicknesses in different HTLs; (b) transmittance spectra for perovskite film developed on ITO glass/different HTMs [77]; (c) the energy-level alignment at the interface between 3Hal-PI and 3Hal- PI-C60, as

determined through UPS and a complementary fitting system (CFSYS) [78]; (d) depiction of a tandem module's front side, featuring seven cell strips and an aperture area measuring 12.25 cm<sup>2</sup>; and (e) a schematic outlining the tandem modules' scalable fabrication sequence, which utilizes a blend of blade-coating and vacuum-deposition techniques [79].

## 2.5. Challenges of SAM

Characterizing the microstructure of SAM-based HTLs, which are composed of thin, organically adsorbed molecules on metal oxides, is complex due to their fine structure. Techniques like XPS, atomic force microscopy, and water contact-angle measurements are typically used to confirm SAM formation, while sum-frequency generation vibrational spectroscopy helps understand the adsorption and molecular ordering at interfaces [81, 82]. However, these methods fail to reveal the monolayers' detailed state on such complex surfaces, particularly issues like defects and continuity. Furthermore, due to monolayer thinness, understanding the charge transport within these HTLs remains challenging, engendering ongoing debates about their function in modifying work functions or assisting with charge extraction and transport [83, 84, 85, 86]. Consequently, more advanced surface- and interface-sensitive techniques are necessary to explore the properties and mechanisms of SAM-based HTLs thoroughly.

The structural simplicity and low molecular weight of SAM-based HTLs contribute to their unique properties but also raise concerns regarding their thermal and light stability, especially for the SAM-based HTL in single-junction inverted PSCs, wherein the SAM layer is located at the light incident side. Efforts to enhance stability have led to the exploration of various anchoring groups. Wu et al. revealed that the –PO<sub>3</sub>H<sub>2</sub> group bonds more robustly to ITO in a tridentate fashion than the –SO<sub>3</sub>H and –COOH groups, with notably higher adsorption energy [87]. DFT analysis reveals that the

adsorption energy for  $-PO_3H_2$  on the most stable ITO (111) surface is measured at  $-2.71$  eV. Comparatively, the corresponding values for  $-SO_3H$  and  $-COOH$  are  $-2.49$  and  $-2.15$  eV, respectively. Further testing demonstrated that ITO/TPT-P6's excellent adhesion enhances film quality and charge collection efficiency while reducing complexation at the interface. The study also discovered that MeO-2PACz, commonly used for photostability, undergoes significant degradation under light and electrochemical conditions. The molecule was modified to enhance stability by substituting alkyl linkers with a conjugated phenylene group. This adjustment promotes charge delocalization and spatial separation between the HOMO and LUMO orbitals, enhancing the light and electrochemical stability of the SAM. This has led to the development of conjugated SAM-based hole-selective contacts, which contribute to more efficient and durable inverted PSCs. In a similar vein, the Palomares group improved the thermal stability of carbazole carboxylic acid (EADR04) by incorporating an additional phenyl linker, increasing its decomposition temperature significantly from  $180$  to  $354$  °C. Conversely, acid-based solid anchors were detrimental to ITO's longevity, leading to a milder boric acid anchoring approach that demonstrated covalent solid bonding and resistance to environmental degradation, substantially enhancing interfacial stability and extending device operational life.

### **3. SAMs as HTLs to enhance the performance of PSCs**

#### **3.1. SAM-HTL of phosphonic acid anchoring groups**

Molecules with phosphonic acid anchoring groups are recognized for their ability to form bidentate solid/tridentate bonds with oxide surfaces. This results in dense, uniform monolayers forming on various oxides, ITO or FTO, even at room temperature. These monolayers have applications in multiple fields, such as dye-sensitized solar cells (DSSC) and electrochromic devices [53, 88, 68]. Table 5 presents recent efficiency

statistics for PSCs utilizing phosphonate-based SAMs as HTLs; Fig. 8 provides the chemical structures of common phosphonic acid-based SAMs.

In 2018, Gauthet et al. pioneered the utilization of phosphonic acid-based SAMs as HTLs in PSCs [89]. They successfully synthesized a novel hole-transporting material, V1036 (2-{3,6-bis[di-(4-methoxyphenyl) amino]-9H-carbazol-9-yl} ethyl) phosphonic acid (Fig. 9a), featuring a phosphonic acid anchoring group and a carbazole core, a known efficient hole transporter. The carbazole core's dimethoxy substituent group enhances molecular solubility and facilitates SAM formation in solution. UV-vis spectroscopy indicated that compared to PTAA ( $\lambda_{\text{max}} = 387 \text{ nm}$ ), V1036 ( $\lambda_{\text{max}} = 304 \text{ nm}$ ) exhibits maximal absorption in a shorter wavelength range and weaker absorption in the visible range, along with higher optical transparency. Additionally, as shown in Figure 9b, V1036 demonstrates excellent thermal stability with a high decomposition temperature ( $T_d = 343^\circ\text{C}$ ). Furthermore, by blending SAMs (V1036 and n-butylphosphonic acid (C4)), they further reduced the SAM interface contact angle (Fig. 9c). Vibrational sum-frequency generation spectroscopy confirmed a single-layer molecule structure on ITO surfaces, with the mixed SAM containing approximately 62% of the surface coverage of a pure V1036 SAM. Adding a small molecule, resulting in mixed SAMs, positively impacted the overall performance of SAM-based HTL devices. Finally, a PCE of 17.8% for a 10% V1036 and 90% C4 mixture SAMs-based HTL device was achieved.

Subsequently, Albrecht and his collaborators synthetically developed two phosphonic acid-based SAMs, [2-(3,6-dimethoxy-9H-carbazol-9-yl) ethyl] phosphonic acid (MeO-2PACz) and [2-(9H-carbazol-9-yl)ethyl] phosphonic acid (2PACz) [90]. They achieved high coverage using a simple spin-coating process. As a molecular-specific surface-sensitive technique, IRRAS was further used to uncover the structure

and bonding mode of adsorbed molecules on metal substrates. IRRAS results indicated that the phosphonic acid-based SAM-HTLs prepared by spin-coating were single-layer rather than multilayer structures, with the peak at  $1010\text{cm}^{-1}$  assigned to the P–O species bound to ITO (Fig. 9d). The appearance of the P–O peak, along with the disappearance of the prominent P–OH peak around  $950\text{ cm}^{-1}$  in the raw material, provided more evidence for the deprotonation of the phosphonic acid anchoring group and the formation of a single layer. Due to improved perovskite film quality and reduced nonradiative recombination in devices, the three-cation PSCs based on 2PACz exhibited a high open-circuit voltage ( $V_{oc}$ ) of 1.19 V and a PCE of 20.9% (certified as 20.28%). Moreover, the PCE of the reverse PSCs based on MeO-2PACz increased by 21.1%. Applying MeO-2PACz to single-junction CIGS/perovskite tandem solar cells achieved a certified stable PCE of 23.26% over an effective area of  $1.02\text{ cm}^2$ .

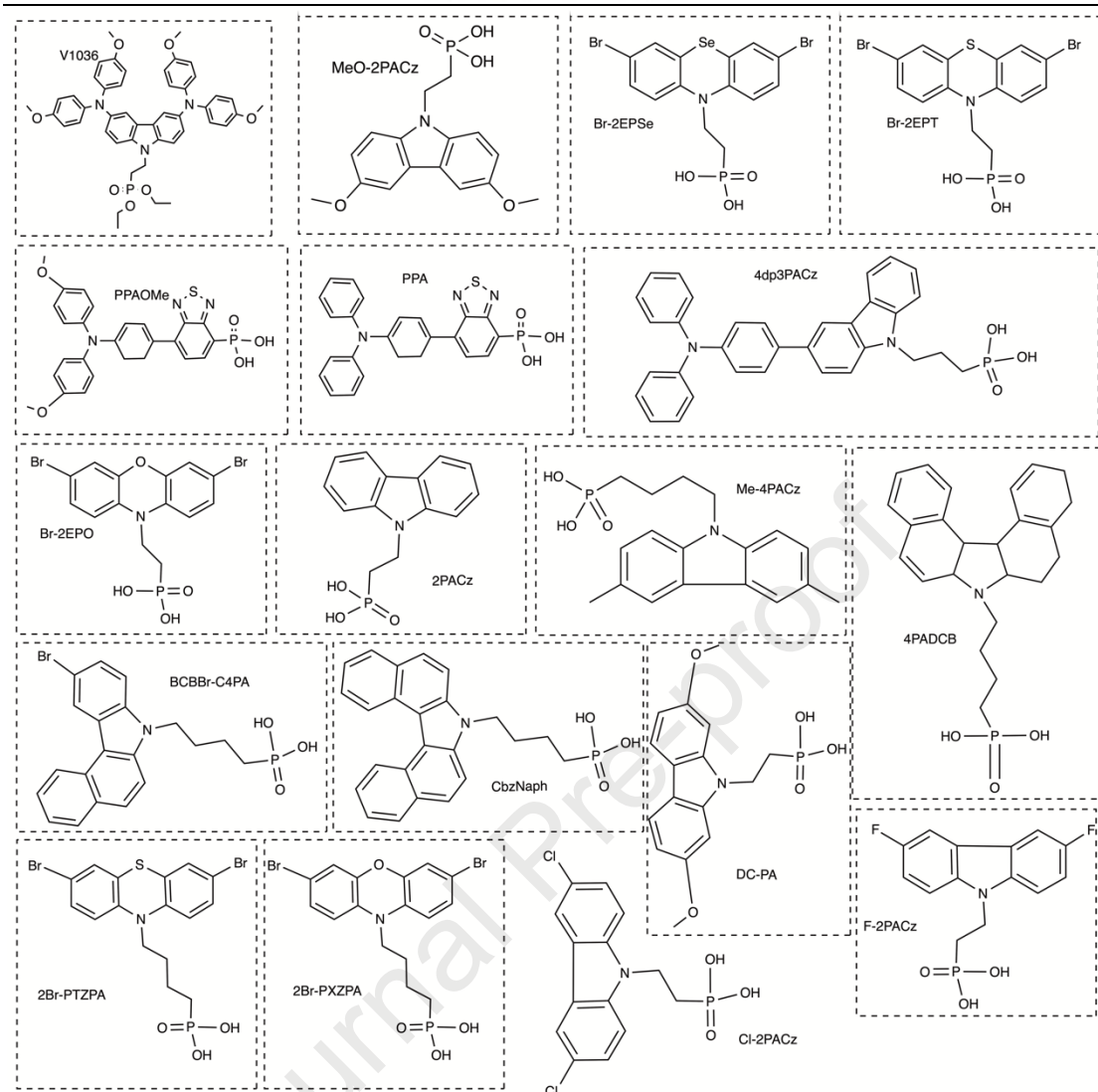


**Fig. 8.** Summary of SAM molecules with phosphonic acid as an anchoring group.

Subsequently, they further investigated the impact of alkyl chain length and different substitutions of carbazole units on the performance of PSCs and found that Me-4PACz ([4-(3,6-dimethyl-9H-carbazol-9-yl) butyl] phosphonic acid) exhibited optimal performance among a series of carbazole-based molecules [91]. The introduction of Me-4PACz improved the thin film quality and enhanced charge extraction at the interface, thereby minimizing nonradiative recombination (Fig. 9e). Consequently, the fill factor (FF) of the single-junction PSCs integrated with Me-4PACz approached 84%. Simultaneously, a single-junction perovskite/silicon tandem solar cell achieved a record

FF of up to 80% and a remarkable PCE of 29.15%.

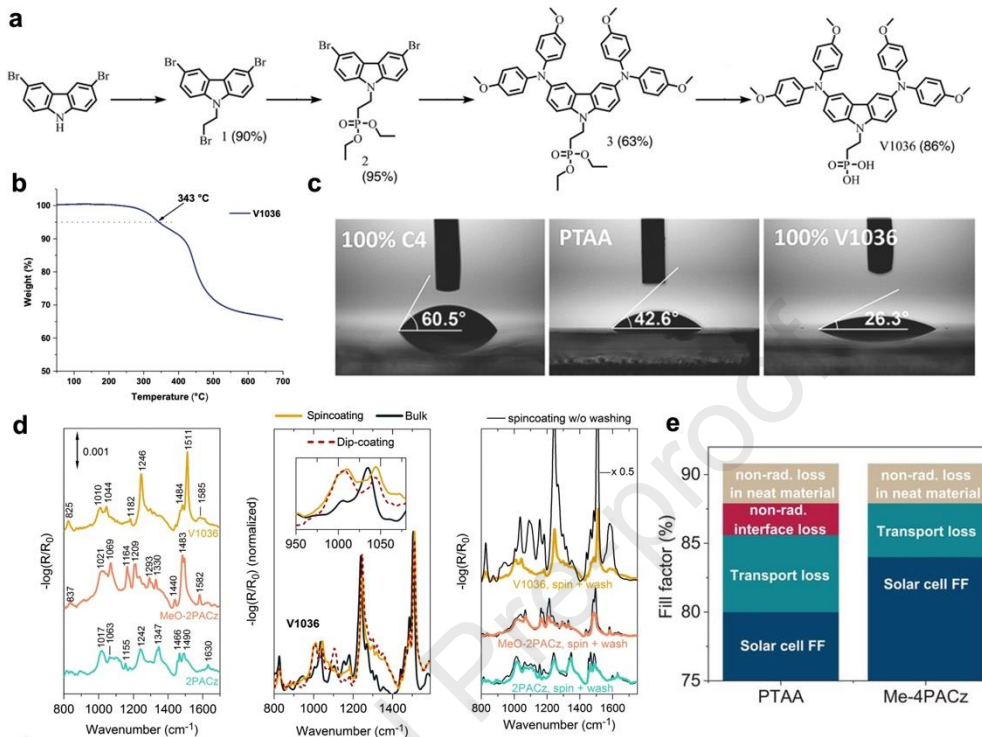


**Fig. 9.** (a) The synthesis of a phosphonic acid functionalized carbazole derivative, V1036; (b) the thermogravimetric analysis heating curve of V1036; (c) the water contact-angle measurements for a perovskite solution on various surfaces, including a 100% C4 SAM, PTAA, and a 100% V1036 SAM [89]; Copyright 2018 Wiley. (d) The spectra analysis for V1036, MeO-2PACz, and 2PACz following spin-coating on Si/ITO substrates and subsequent washing with ethanol and chlorobenzene. This includes comparing bulk V1036 material versus SAM formation through spin-coating and dip-coating techniques and the impact of the washing step on the RAIRS spectra of spin-coated SAMs. Notably, MeO-2PACz and 2PACz exhibit monolayer characteristics without the need for a washing step [90]; (e) an evaluation of loss mechanisms that reduce the FF of the cell below the detailed balance limit,

comparing PTAA and Me-4PACz cells. This includes the identification of nonradiative loss in the neat material, nonradiative interface loss, and transport loss, which collectively influence the discrepancy between the predicted fill factor (pFF) of the neat film and the full cell, and the measured FF of the solar cell [91].

The same year, they successfully applied MeO-2PACz to PSCs prepared via co-evaporation [92]. The results demonstrated that MeO-2PACz offers a wider processing window than PTAA. Particularly, MeO-2PACz surpassed PTAA performance-wise, exhibiting higher FF and Voc. Ultimately, combining vapor-deposited perovskite with SAMs achieved a stable PCE of 20.6% for a co-evaporated p-i-n solar cell structure.

A set of SAMs derived from the phenothiazine moiety and featuring different anchoring groups, namely TPT-S6, TPT-C6, and TPT-P6, were examined by Zhu and colleagues, as shown in Fig. 10a [87]. Among these molecules, TPT-P6 exhibited the quickest adsorption rate and the highest loading amount on the ITO substrate, attributed to the phosphonic acid group's strong adsorption energy on the ITO surface. Employing a triple-cation perovskite  $\text{Cs}_{0.05}\text{MA}_{0.12}\text{FA}_{0.83}\text{Pb}(\text{I}_{0.85}\text{Br}_{0.15})_3$ , they achieved a PCE of 21.43% (active area = 0.09 cm<sup>2</sup>, Voc = 1.125 V, FF = 0.811). In light of the poor wettability of TPT-P6, caused by its large hydrophobic triphenylamine group and long aliphatic chain, Hong et al. designed a novel SAM named 2-(3,7-dibromo-10H-benzo[d][1,2] thiazin-10-yl)ethyl phosphonic acid (Br-2EPT) by introducing halogen groups [93]. UPS revealed that Br-2EPT has a bandgap more aligned with CsFAMA than two commonly used HTLs, PTAA and MeO-2PACz (Fig. 10b). Additionally, the perovskite film quality based on Br-2EPT was significantly enhanced, while bulk and interface nonradiative recombination of the devices were notably suppressed. Finally, they demonstrated Br-2EPT to be an excellent HTL, effectively improving the performance

of PSCs composed of  $\text{Cs}_{0.05}\text{FA}_{0.874}\text{MA}_{0.076}\text{PbI}_{2.76}\text{Br}_{0.24}$  (referred to as CsFAMA). This design concept resulted in PSCs with an average PCE exceeding 22%, surpassing the current standard polymer PTAA and commercial MeO-2PACz. Importantly, the Br-2EPT-based unencapsulated PSCs demonstrated excellent long-term stability, with no initial PCE loss after continuous maximum power point (MPP) tracking for 100 hours (Fig. 10c).

Following that, they also synthesized two variants of Br-2EPT, namely 2-(3,7-dibromo-10H-phenoxazine-10-yl)ethyl phosphonic acid (Br-2EPO) and 2-(3,7-dibromo-10H-phenoselenazine-10-yl)ethyl phosphonic acid (Br-2EPSe), by incorporating O or Se into the tricyclic aromatic head group, and reported their applications as hole-selective interlayers in inverted PSCs [94]. They investigated the impact of different head atoms on the electronic structure of the molecules and device performance. The results revealed that varying the core heteroatom from O to Se could finely control the folding angle of the peripheral benzene rings along the fused aromatic ring X...N vector and influence the photovoltaic performance of inverted PSCs due to differences in atomic size and orbital overlap. The different core heteroatom effects resulted in subtle differences in the optical bandgap and energy alignment with the perovskite layer (Figs. 10d–f). They found that the interface interaction energy between the Br-2EPX series SAM and the perovskite layer was strongly influenced by the polarization of the core heteroatoms, increasing in the order of Se > S > O. Adopting the Br-2EPX series SAM decreased the interface of the device trap density, prolonging the perovskite film lifetime of charge carriers. These favorable factors simultaneously improved the PSCs' efficiency and long-term stability. As a result, the PSC based on Br-2EPSe exhibited excellent performance, with a maximum PCE of 22.73% and almost no initial PCE loss even after 500 hours of continuous MPP tracking tests under

environmental conditions.

Jen et al. successfully developed high-efficiency, large-area blade-coated PSCs using MeO-2PACz as HTLs (Fig. 10g) [95]. In contrast to the hydrophobic PTAA, the more hydrophilic surface of MeO-2PACz promotes the nucleation and growth of a perovskite thin film, resulting in a dense and uniform buried interface. Additionally, better energy alignment between the HOMO level of MeO-2PACz and the VBM of the perovskite also benefits device performance. Due to the high-quality embedding of perovskite on the MeO-2PACz substrate, champion devices prepared via the blade-coating method in high-humidity air (50% RH) achieved PCEs of 18.47% and 14.64% for devices with effective areas of 0.105 and 1.008 cm<sup>2</sup>, respectively (Fig. 10h). Furthermore, MeO-2PACz-based devices exhibited good stability, maintaining 90% of the initial efficiency after continuous operation for over 500 hours at 40 °C in an inert atmosphere. Additionally, the PCE of perovskite mini-modules based on MeO-2PACz reached 14.13%, with an aperture area of 18.0 cm<sup>2</sup>.

**Table 5.** Performance statistics of SAMs based on phosphonic acid groups as single-junction PSCs for HTLs

SAM-HTL	ETL	$J_{sc}$ (mA cm <sup>-2</sup> )	$V_{oc}$ (V)	FF (%)	PCE (%)	Ref.
10% V1036+90% C4	C <sub>60</sub> +BCP	21.4	1.09	76.5	17.8	[89]
MeO-2PACz	C <sub>60</sub> +BCP	22.2	1.144	80.5	20.2	[90]
2PACz	C <sub>60</sub> +BCP	21.9	1.188	80.2	20.8	[90]
Me-4PACz	C <sub>60</sub> , BCP, LiF	20.3	1.150	84.0	20.0	[91]
MeO-2PACz	C <sub>60</sub> +BCP	22.43	1.150	79.6	20.5	[92]
MeO-2PACz	C <sub>60</sub> +BCP	24.96	1.06	80.0	20.99	[93]
Br-2EPT	C <sub>60</sub> +BCP	25.11	1.09	82.0	22.44	[93]
Br-2EPO	C <sub>60</sub> +BCP	24.25	1.074	80.74	21.02	[94]
Br-2EPT	C <sub>60</sub> +BCP	24.41	1.09	81.3	21.63	[94]
Br-2EPSe	C <sub>60</sub> +BCP	24.49	1.12	82.86	22.73	[94]
MeO-2PACz (0.1 cm <sup>2</sup> )	C <sub>60</sub> +BCP	21.57	1.081	78.9	18.39	[95]
MeO-2PACz (1.0 cm <sup>2</sup> )	C <sub>60</sub> +BCP	19.83	1.073	68.8	14.64	[95]

4dp3PACz	C <sub>60</sub> +BCP	17.8	1.214	79.44	17.17	[96]
4PACz	C <sub>60</sub> +BCP	17.8	1.26	75.49	16.93	[97]
4PADCB	C <sub>60</sub> +BCP	17.84	1.30	78.70	18.28	[97]
MeO-2PACz (annealed +PVK annealed)	C <sub>60</sub> +BCP	22.4	1.08	80.3	18.0	[98]
MeO-2PACz (annealed +PVK unannealed)	C <sub>60</sub> +BCP	21.2	1.11	78.0	17.5	[98]
MeO-2PACz (unannealed +PVK unannealed)	C <sub>60</sub> +BCP	20.4	1.09	76.6	16.6	[98]
2BrCzPA	PCBM+BCP	11.43	1.10	33.7	4.24	[99]
2BrPTZPA	PCBM+BCP	23.26	1.18	80.02	22.06	[99]
2BrPXZPA	PCBM+BCP	23.59	1.19	81.69	22.93	[99]
2PACz	C <sub>60</sub> BCP	32.83	0.86	76.0	21.39	[100]
MPA	C <sub>60</sub> +BCP	32.75	0.84	77.0	21.08	[100]
2PACz+MPA	C <sub>60</sub> +BCP	33.13	0.88	80.0	23.23	[100]
BCBBr-C4PA	C <sub>60</sub> +ALD-SnO <sub>2</sub>	17.54	82.61	80.0	18.63	[101]
PPA	PCBM+BCP	24.83	1.14	82.0	23.24	[102]
PPAOMe	PCBM+BCP	24.70	1.10	79.2	21.52	[102]
MeO-2PACz	C <sub>60</sub> +BCP	22.47	1.14	76.5	19.6	[103]
MeO-2PACz (CIGSe tandem)	C <sub>60</sub> +BCP	16.48	1.65	66.9	18.2	[103]
IPA-2PACz	C <sub>60</sub> +BCP	23.90	1.135	79.61	21.59	[104]
Cos-2PACz	C <sub>60</sub> +BCP	23.80	1.167	82.58	22.93	[104]
IPA-MeO-2PACz	C <sub>60</sub> +BCP	23.84	1.108	81.68	21.57	[104]
Cos-MeO-2PACz	C <sub>60</sub> +BCP	23.78	1.134	84.86	22.89	[104]
IPA-CbzNaph	C <sub>60</sub> +BCP	23.69	1.152	83.32	22.73	[104]
Cos-CbzNaph	C <sub>60</sub> +BCP	23.80	1.170	86.26	24.02	[104]
Hybrid IL	C <sub>60</sub> +BCP	24.80	1.18	82.9	24.5	[105]
2PACz	C <sub>60</sub> +BCP	32.3	0.86	75	20.9	[106]
9CPA	C <sub>60</sub> +BCP	32.5	0.89	76	22.1	[106]
9CAA	C <sub>60</sub> +BCP	22.8	0.89	79	23.1	[106]
CbzPh	C <sub>60</sub> +BCP	23.80	1.08	78.42	20.22	[107]
CbzBF	C <sub>60</sub> +BCP	24.0	1.09	83.04	21.72	[107]
CbzBT	C <sub>60</sub> +BCP	23.93	1.10	84.20	22.08	[107]
2PACz (DMSO)	C <sub>60</sub> +BCP	18.05	1.194	81.75	17.62	[108]
Me-4PACz (DMSO)	C <sub>60</sub> +BCP	17.93	1.163	82.97	17.30	[108]
MeO-2PACz (DMSO)	C <sub>60</sub> +BCP	17.94	1.147	78.25	16.10	[108]
BCB-C4PA	C <sub>60</sub> +BCP	24.4	1.13	80	22.2	[109]
CZ-C4PA	C <sub>60</sub> +BCP	22.6	1.02	79	18.2	[109]
CZ-C4Br	C <sub>60</sub> +BCP	14.0	0.79	59	6.6	[109]

(sc)BCB-C4PA	C <sub>60</sub> +BCP	22.6	1.09	73	17.9	[109]
2PACz	345FAn+C <sub>60</sub> +BCP	25.9	1.14	82.3	24.3	[58]
2PACz+3-MPA	F-PEAI+C <sub>60</sub> +BCP	25.9	1.16	84.2	25.3	[58]
MPA-CPA	345FAn+C <sub>60</sub> +BCP	24.27	1.192	80.91	23.41	[59]
4dp3PACz	C <sub>60</sub> +BCP	24.95	1.150	82.00	23.53	[110]

In our group, we also synthesized novel SAMs based on phosphonic acid groups, namely [3-[4-(diphenylamino) phenyl]-9H-carbazol-9-yl] propylphosphonic acid (4dp3PACz), as effective SAMs in wide-bandgap PSCs [96]. In this work, inspired by the structure of PTAA, we selected PTAA monomers as functional groups to improve the molecular structure of 2PACz. Considering the hydrophilic and hydrophobic properties of the material, we discarded the hydrophobic functional groups (methyl groups). 4dp3PACz improved the quality of the perovskite film by reducing its defect density, thereby minimizing nonradiative recombination and enhancing carrier transport. Finally, a high efficiency of 17.71% was achieved for wide-bandgap PSCs (1.77 eV). The efficiency of all the perovskite tandem solar cells, with WBG PSCs as the top cell and narrow-bandgap PSC as the bottom cell, reached 26.47%. Our working site molecular design suggested that combining reported effective HTMs as modified functional groups should further improve the performance of SAMs. Zhao et al. developed a SAM named 4-(7H-dibenzo[c,g]carbazole-7-yl) butylphosphonic acid (4PADCB), aimed at enhancing the coverage and surface wetting of the perovskite film by incorporating a new 7H-dibenzo[c,g]carbazole (DCB) terminal group [97]. This modification facilitated rapid hole extraction and suppressed interface nonradiative recombination, ultimately leading to impressive PCE improvement in the devices. The all-perovskite tandem cells utilizing 4PADCB achieved a remarkable PCE of 26.90%.

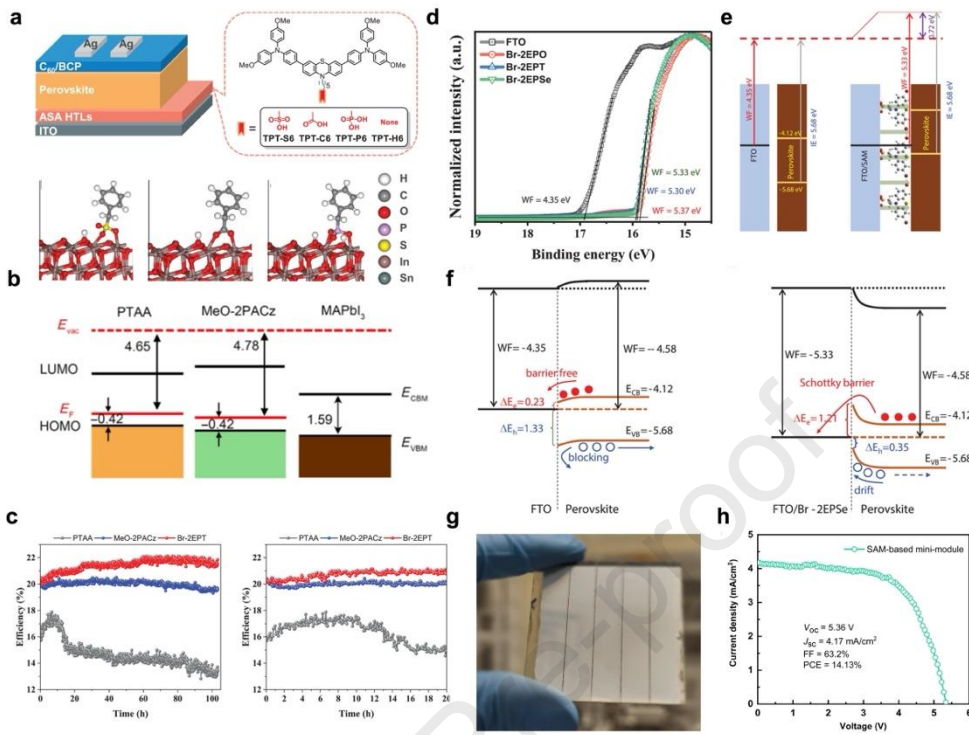


**Fig. 10.** (a-left) shows a schematic of p-i-n structured perovskite solar cells with ASA HTLs. (a-right) the chemical structures of phenothiazine-based molecular HTMs. (a-bottom) the theoretical SA, CA, and PA adsorption model on the ITO (111) surface. [87] Copyright 2021 Wiley. (b) The energetic alignment of various HTL contacts and CsMAFA perovskite around the vacuum level is depicted, with the dashed red lines indicating the Fermi energy levels measured via UPS. (c) The long-term continuous MPPT of PSCs utilizing the explored HTLs under ambient conditions with controlled humidity (RH 15–25%) and without encapsulation [93]. Copyright 2021 Wiley. (d) UPS spectra showing the secondary electron cutoff region of bare FTO and FTO/SAMs. (e) A schematic representation of the energy-level diagram at the FTO/perovskite interface before and after Br-2EPSe modification, detailing the interface energy levels of (f-left) FTO/perovskite and (f-right) FTO/Br-

2EPSe/perovskite [94]. Copyright 2023 American Chemical Society. (g) A photograph of a SAM-based perovskite mini-module ( $5\text{ cm} \times 5\text{ cm}$ ) fabricated using the blade-coating method. (h) The  $J$ - $V$  characteristics of the blade-coated, SAM-based perovskite mini-module with an aperture area of  $18\text{ cm}^2$  [95].

Lidzey et al. creatively eliminated the annealing step typically used during the deposition of SAM molecules as HTLs [98]. Upon omitting the annealing process for MeO-2PACz, only a slight loss in device performance was observed. By combining unannealed MeO-2PACz film with unannealed 1:9 THF:2-ME perovskite layers, devices with a high PCE stability of up to 17.1% were created. This represents the highest device performance demonstrated by a fully unannealed PSC. Lidzey et al. also introduced a novel binary solvent system for fabricating fully annealing-free PSCs except for the non-annealed SAM layer [98]. A mixture of 2-methoxyethanol and tetrahydrofuran was used to deposit high-quality perovskite films at room temperature, eliminating the need for post-deposition annealing. This approach yields p-i-n devices with stabilized PCEs up to 18.0%. By integrating MeO-2PACz as the HTL without annealing, they further advanced the fabrication of fully annealing-free devices, achieving PCEs up to 17.1% and thereby marking a significant achievement in annealing-free PSC production compatible with roll-to-roll manufacturing processes.

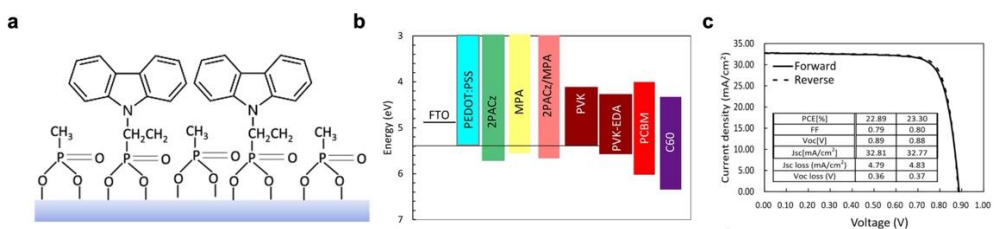


**Fig. 11.** (a) A schematic illustrating the potential for 2PACz/MPA bilayer formation on the substrate. (b) An energy diagram providing insights into the HOMO and

LUMO levels of different components within the constructed PSCs. (c) The J-V characteristics of the best-performing PSC fabricated using the 2PACz/MPA bilayer [100]. Copyright 2022 American Chemical Society.

He et al. developed three novel SAMs: 2BrCzPA, 4-(3,7-dibromo-10H-phenothiazin-10-yl) butyl phosphonic acid (2BrPTZPA), and 4-(3,7-dibromo-10H-phenoxazin-10-yl) butyl phosphonic acid (2BrPXZPA) [99]. The thermogravimetric analysis result demonstrated the superior thermal stability of these SAMs, with decomposition temperatures substantially surpassing the annealing and operating temperatures of PSCs, which is very important for the PSC commercialization process. The decomposition temperatures ( $T_d$ ) for 2BrCzPA, 2BrPTZPA, and 2BrPXZPA were 264, 234, and 225 °C, respectively. UV-vis absorption spectroscopy showed that these SAMs exhibit similar  $\pi$ - $\pi^*$  absorption characteristics in dilute tetrahydrofuran (THF) solutions ( $10^{-5}$  M), with absorption peaks at 304, 349, and 363 nm for 2BrCzPA, 319 nm for 2BrPTZPA, and 334 nm for 2BrPXZPA, indicating minimal light absorption in the visible spectrum. Notably, 2BrPTZPA and 2BrPXZPA demonstrated enhanced energy-level alignment with the perovskite layer, facilitating reduced energy losses in PSCs. Furthermore, ITO substrates coated with 2BrPTZPA and 2BrPXZPA were found to promote the growth of high-quality perovskite films (Fig. 11d). Inverted PSCs incorporating these SAMs achieved PCEs of 22.06% for 2BrPTZPA and 22.93% for 2BrPXZPA, with the latter certified at 22.38%. Encapsulated devices based on 2BrPXZPA maintained 97% of their initial efficiency after 600 hours under continuous illumination, demonstrating exceptional durability.

In addition to employing single-layer SAMs as HTLs, integrating mixed SAMs has been identified as a strategy to enhance the efficiency of devices. Our study incorporated a mixed solution of 2PACz+MPA as the HTL, leading to an increase in the PCE of SnPb-PSCs to 23.23% (Figs. 11a–c) [100]. Conventionally, PEDOT:PSS serves as the ubiquitous HTL in SnPb PSCs. However, our findings indicate that not only a considerable energy band gap between PEDOT:PSS and the perovskite material but also the added thickness of the PEDOT:PSS layer further obstruct light absorption, consequently diminishing the devices' short-circuit current density ( $J_{sc}$ ) and  $V_{oc}$  (Fig. 11g). Substitution of the HTL with 2PACz+MPA markedly enhanced device efficiency, alongside significant improvements in various photovoltaic parameters. This enhancement is primarily attributed to the optimized band alignment, which facilitated smoother carrier transport and reduced nonradiative recombination due to improved film quality.

Sargent et al. introduce a novel conformal SAM as a hole-selective contact on textured substrates, which significantly enhanced the efficiency and stability of inverted PSCs [58]. By employing molecular dynamics simulations, the research identified the phosphonic acid cluster formation issue that leads to incomplete SAM coverage. To address this, a co-adsorbent strategy was developed, effectively disassembling high-order clusters and achieving a more uniform distribution of the SAM, minimizing interfacial recombination, and optimizing the electronic structure. This method achieved a remarkable laboratory-measured PCE of 25.3% and a certified quasi-steady-state PCE of 24.8%. The encapsulated device demonstrated exceptional stability, retaining 95% of its performance

after over 1,000 hours under stress conditions, making this one of the most stable PSCs to date, with a PCE exceeding 24%. This work paves the way for using engineered adsorption strategies on textured substrates to enhance the efficiency and durability of PSCs and potentially other optoelectronic devices.

Seok-In Na et al. presented a groundbreaking approach for enhancing the efficiency and stability of PSCs [111]. By employing a novel mixed SAM that combines MeO-2PACz and Me-4PACz, the research demonstrates significant advancements in the interface engineering of PSCs. This mixed SAM optimizes the hole-transport properties by maintaining favorable wettability and adjusting the energy levels for efficient charge transfer, features crucial for high-quality film formation and effective charge extraction. Notably, the stability of the PSCs is remarkably improved, showing less efficiency loss over extended operational hours and under thermal stress; this is attributed to the synergistic effects of the mixed SAM components, which mitigate the individual weaknesses of each component. The approach leads to a robust design that enhances the longevity and performance of PSCs, a critical step towards their commercial viability.

### 3.2. SAM-HTL of carboxylic acid anchoring groups

In addition to employing phosphonic acid groups, numerous SAMs also incorporate carboxylic acid as anchoring groups. The preference for carboxylic acid groups stems from their ability to engage in dehydration esterification reactions with hydroxyl groups on metal oxides' surfaces, thus securely affixing the SAMs to the metal oxide substrates.

Table 6 presents the efficiency statistics from recent studies of PSCs that utilize carboxylic acid-based SAMs as HTLs; Fig. 12 lists the chemical formula structures of

common carboxylic acid-based SAMs.

**Table 6.** Performance statistics of SAMs based on carboxylic acid groups as single-junction PSCs for HTLs

SAM-HTL	ETL	$J_{sc}$ (mA cm <sup>-2</sup> )	$V_{oc}$ (V)	FF (%)	PCE (%)	Ref.
TPA-PT-C6	PCBM+BCP	21.8	1.04	77.4	17.19	[80]
MC-54	C <sub>60</sub> +BCP	22.32	1.10	79.15	19.52	[112]
MC-45	C <sub>60</sub> +BCP	20.56	1.09	74.35	16.69	[112]
MC-55	C <sub>60</sub> +BCP	21.90	1.09	79.32	18.99	[112]
Spiro-Acid	chC <sub>60</sub> +BCP	22.20	0.990	82.6	18.15	[113]
RC-24	C <sub>60</sub> +BCP	22.3	1.123	79	19.8	[114]
RC-25	C <sub>60</sub> +BCP	22.1	1.116	79	19.6	[114]
RC-34	C <sub>60</sub> +BCP	22.5	1.109	79	19.7	[114]
P3HT-COOH	PCBM+BCP	22.07	1.09	81	19.21	[115]
AC-3	PCBM+BCP	24.27	1.108	82.56	22.2	[116]
AC-5	PCBM+BCP	24.42	1.130	84.05	23.19	[116]
AB	C <sub>60</sub> +BCP	19.92	0.534	71.9	7.6	[117]
AM	C <sub>60</sub> +BCP	17.83	0.530	56.1	5.3	[117]
AE	C <sub>60</sub> +BCP	15.46	0.522	64.1	5.2	[117]
NB	C <sub>60</sub> +BCP	13.96	0.532	61.0	4.5	[117]
EADR03	C <sub>60</sub> +BCP+LiF	22.9	1.156	80	21.2	[85]
EADR04	C <sub>60</sub> +BCP+LiF	22.6	1.164	80	21.0	[85]

TPA	PCBM	19.4	1.06	76.9	15.9	[118]
MC-43	PCBM	20.1	1.08	80.0	17.3	[118]
EA-41	PCBM+Ca	16.69	1.019	69.86	11.89	[119]
EA-46	PCBM+Ca	16.37	1.006	62.18	10.24	[119]
EA-49	PCBM+Ca	17.25	1.024	68.15	12.03	[119]
EA-51	PCBM+Ca	15.59	1.035	56.30	9.09	[119]
EA-53	PCBM+Ca	15.05	1.023	56.56	8.71	[119]
EA-54	PCBM	17.95	0.982	63.64	11.22	[120]
EA-63	PCBM	18.13	1.021	60.71	11.24	[120]
EA-58	PCBM	18.56	0.967	76.37	13.71	[120]
SAM1	PCBM+BCP	21.70	1.109	78.3	18.86	[121]
SAM2	PCBM+BCP	20.32	1.093	79.3	17.61	[121]
SAM3	PCBM+BCP	21.03	1.130	73.8	17.55	[121]
EADR03	PCBM+BCP	21.89	1.149	80.24	20.18	[121]
TT1	C <sub>60</sub> +BCP	17.92	1.049	69.7	13.11	[122]
2F	C <sub>60</sub> +BCP	17.93	1.31	82.31	19.33	[123]
2F	C <sub>60</sub> +BCP	32.55	0.872	81.89	23.24	[123]

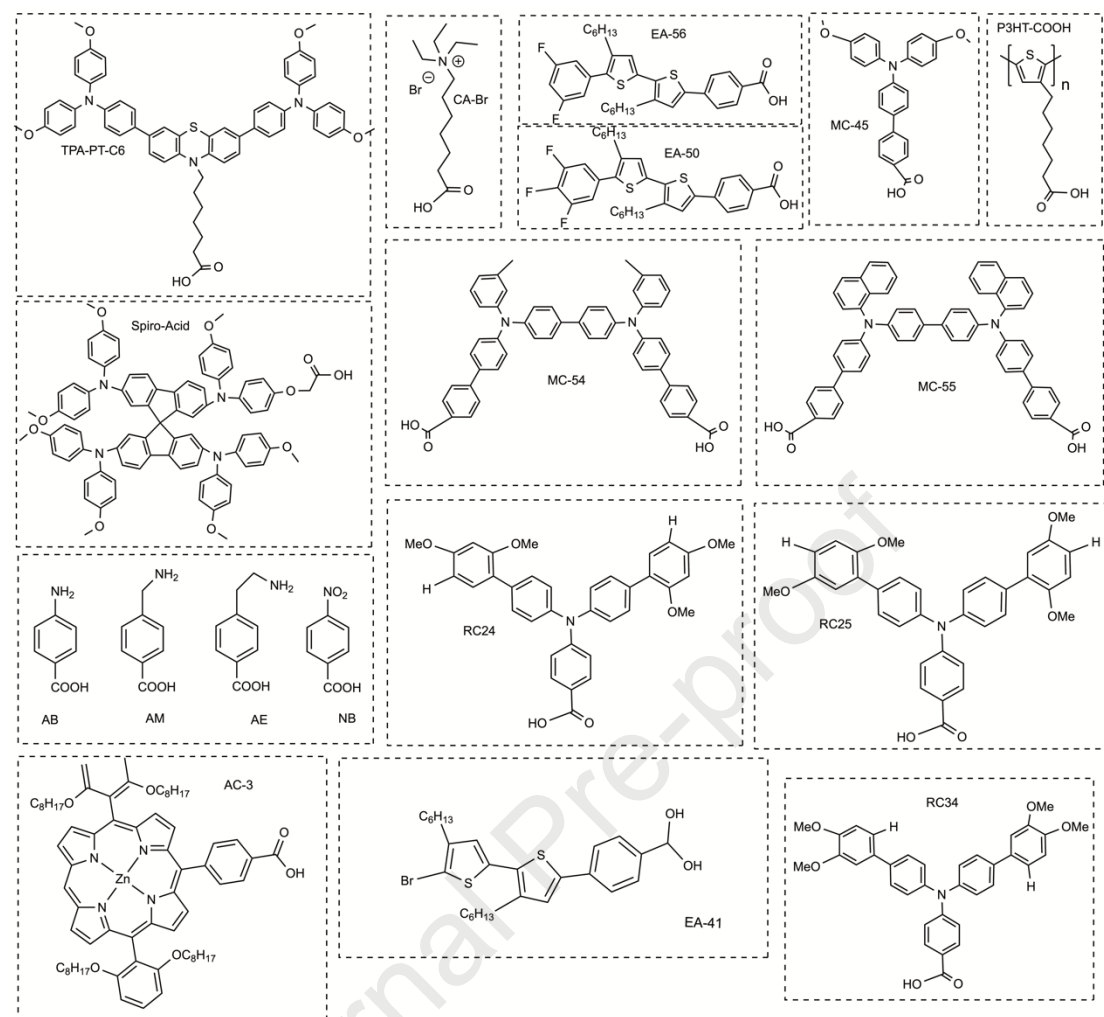
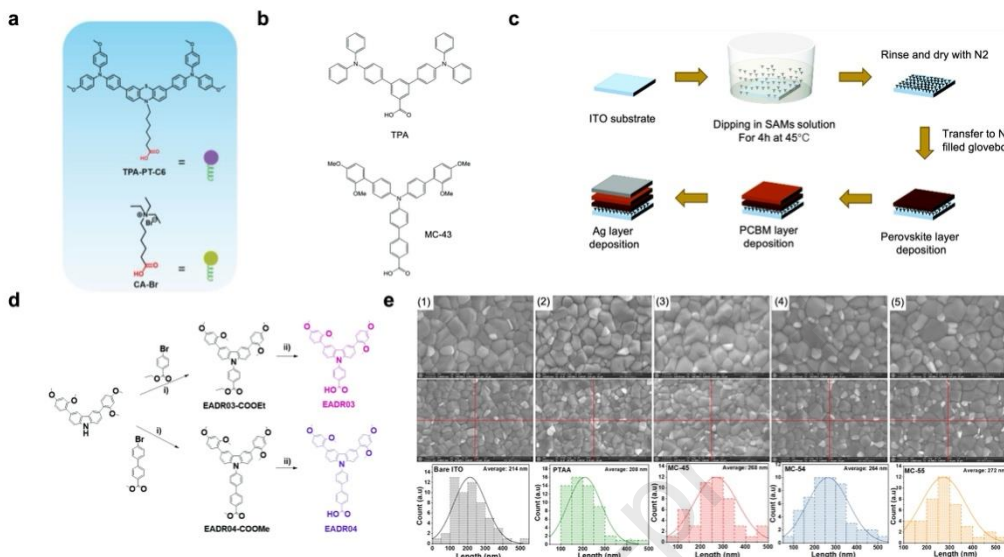


**Fig. 12.** Summary of SAM molecules with carboxylic acid as an anchoring group.

Zhu's team created a new SAM-based HTM, TPA-PT-C6, featuring carboxylic acid as its anchoring group, depicted in Fig. 13a [80]. This HTM was combined with CA-Br to produce ultra-thin, evenly wettable films that effectively covered extensive perovskite surfaces. The HOMO and LUMO energy levels of TPA-PT-C6 were  $-5.20$  and  $-2.34$  eV, respectively, compatible with the perovskite film energies. CA-Br integration improved mechanical and electronic interactions at the HTL/perovskite interface, increasing stability by mitigating ionic vacancies. PSCs incorporating this HTL recorded a PCE of 17.49% and maintained 89% of their efficiency after 120 days, without encapsulation, in

30% RH conditions. Their practical application was confirmed by producing smaller modules with a 36 cm<sup>2</sup> aperture, which achieved a PCE of 12.67%.



E. Palomares et al. synthesized two SAMs, 4,-[bis(2',4,-dimethoxybiphenyl-4-yl) amino] biphenyl-4-carboxylic acid (MC-43) and 4,4',-bis(diphenyl amino)-1, 1,:3', 1"-terphenyl-5,-carboxylic acid (TPA), as shown in Figs. 13b and 13d [118, 124]. These SAMs were applied to ITO substrates using immersion, resulting in uniform adsorption. Electrochemical analysis indicated that MC-43 had a lower HOMO energy level than

PEDOT:PSS, enhancing hole transport to the HTL. The introduction of SAMs increased the contact angle at the interface, which did not negatively impact device performance and confirmed the uniform coverage of SAMs on ITO. The MC-43-coated ITO also facilitated perovskite deposition by means of more defined grain boundaries and larger grains, reducing nonradiative recombination. Devices with MC-43 reported an average PCE of 16.8% and a peak PCE of 17.3%. These devices displayed stable J-V characteristics with minimal hysteresis. Encapsulated devices maintained 90% of their initial efficiency after 20 days in dark, low-humidity conditions.

Two new SAMs, EADR04 (4'-(3,6-bis (2,4-methoxyphenyl)-9H-carbazol-9-yl)-[1,1'-biphenyl]-4-carboxylic acid) and EADR03 (4-(3,6-bis(2,4-methoxyphenyl)-9H-carbazol-9-yl)benzoic acid), feature carboxylic acid groups and carbazole as the electron-donating unit, as shown in Fig. 13d [85]. These SAMs were modified by adding electron-rich groups to the carbazole structure to better match energy levels with perovskite materials and enhance solubility in organic solvents. Water contact-angle tests showed lower angles than PTAA, promoting denser and more uniform perovskite film formation. XPS analysis identified ester bond formations between the SAMs, carboxylic acid groups, and ITO or solvent residues, confirming a SAM presence on the ITO. TRPL measurements indicated that the photoluminescence lifetimes of EADR03 and EADR04 were longer than those of the perovskite alone, suggesting better film quality and lower defect density. Devices incorporating these SAMs achieved PCEs of 20.5% for EADR03 and 20.6% for EADR04, surpassing PTAA's peak efficiency of 18.9%. Enhanced Voc and FF were observed, affirming the superior electron-blocking properties of the SAMs.

compared to PTAA.

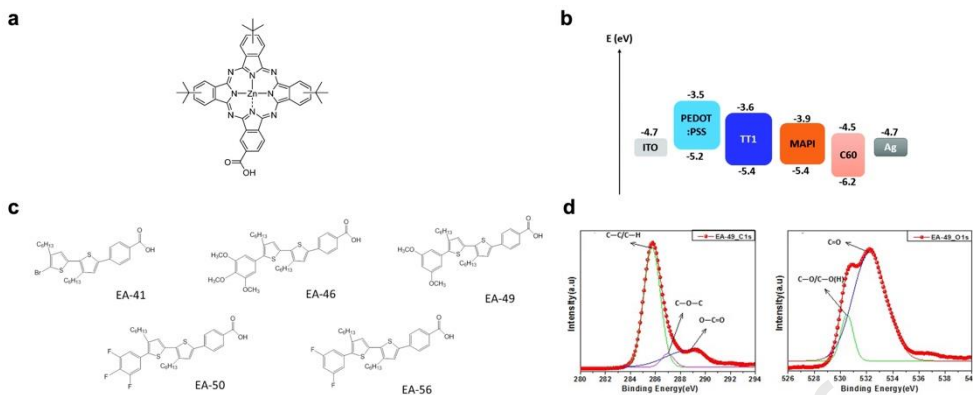


**Fig. 14.** (a) The molecular structure of phthalocyanine TT1. (b) An energy-level diagram of the materials employed in constructing MAPI-based solar cells [122]. (c) The molecular structure of SAM molecules. (d) The XPS high-resolution survey spectra of C 1s and O 1s for ITO/EA-49 [119]. Copyright 2020 Elsevier.

In 2023, the same group reported three new molecules capable of forming SAMs as alternatives to the commonly used p-type contact material, PTAA [112]. Two of these molecules feature bidentate anchoring groups ( $4',4''$ -([1,1'-biphenyl]-4,4'-diylbis(m-tolylazanediyl)) bis([1,1,-biphenyl]-4-carboxylic acid) (MC-54), and  $4',4''$ - ([1,1'-biphenyl]-4,4'-diylbis(naphthalene-1-alkanediyl)) bis([1, 1'-biphenyl]-4-carboxylic acid) (MC-55)), while the last one is monodentate ( $4'$ -(bis(4-methoxyphenyl)amino)-[1, 1'-biphenyl]-4-carboxylic acid (MC-45)). The qualities of perovskite films on different substrates (bare ITO, PTAA, and SAMs) were found to be significantly different, including their grain size and bulk defects, as shown in Fig. 13d. Devices fabricated using MC-54 and MC-55 exhibited significantly higher FF (approximately 80%) and JSC, resulting in higher solar cell efficiencies than MC-45 and PTAA. SAM-based PSCs also

demonstrated higher stability and reproducibility than PTAA-based ones.

Zhao et al. engineered a donor–acceptor molecule, MPA2FPh-BT-BA (2F), combining a hole-transporting 4-methoxy-N-(4-methoxyphenyl)N-phenylaniline (MPA) donor and a structurally planar benzo[c][1,2,5]thiadiazole (BT) acceptor [123]. The molecular structure optimizes photoelectric performance through improved intermolecular stacking, facilitated by the flatness of BT and the electron-donating properties of MPA. The presence of sulfur and fluorine in 2F enhances interaction with under-coordinated ions, aiding in surface defect passivation and perovskite growth control. Carboxylic acid groups anchor ITO, promoting face-up orientation for better hole transport and multilayer formation potential for further perovskite interactions. Fluorine inclusion lowers the HOMO level, reducing unwanted absorption and improving defect passivation. The simple four-step synthesis of 2F makes it economically viable. For tin–lead perovskite cells, 2F mitigates  $\text{Sn}^{2+}$  oxidation and slows crystal growth, enhancing film quality and interface performance. In practical applications, 2F-based single-junction and tandem perovskite solar cells achieved PCEs of 19.33% and 23.24% for wide and narrow bandgap cells, respectively, with all-perovskite tandems reaching up to 27.22% (certified at 26.3%). Tandem devices maintained 80% of their initial efficiency after 301 hours, indicating notable stability improvements over conventional PTAA-based cells.

Emilio Palomares and colleagues reported a synthesis method for the common zinc phthalocyanine (ZnPc) molecule TT1 (Fig. 14a), widely used in dye-sensitized solar cells.[122] TT1, with a carboxylic acid as a linker group, can firmly adsorb onto the ITO surface. The introduction of TT1 slightly reduces the optical transparency of ITO and

increases the surface water contact angle. However, the significantly improved film quality and better bandgap matching resulted in a higher PCE, and the tested devices even exhibited voltages exceeding 1 V, while the control PEDOT:PSS devices showed lower  $V_{OC}$  due to the higher HOMO energy level (Fig. 14b). Ultimately, devices based on TT1 achieved a maximum efficiency of 13.11% with a voltage of 1.049 V.

Serafettin and colleagues explored the impact of five different SAMs on ITO electrode properties, focusing on how these modifications influence perovskite film formation and solar cell performance (Fig. 14c) [119]. Using Kelvin probe force microscopy, they observed a significant increase in the work function (WF) of ITO after SAM modification, with values ranging from 5.03 to 5.30 eV for the different SAMs, compared to 4.62 eV for unmodified ITO. The results indicated that SAMs with electron-donating groups enhanced hole collection more effectively than those with electron-withdrawing groups, which suffered from poor energy alignment and problematic hydrogen bonding, potentially impairing charge extraction and photovoltaic performance. XPS surface chemistry analysis revealed changes due to SAMs, particularly for ITO modified with EA-41, where bonding interactions involving carboxylic and hydroxyl groups were evident. XRD analysis further confirmed that SAM-modified ITO showed improved film characteristics, such as larger grain sizes and more compact coverage, compared to traditional PEDOT:PSS. Among the tested SAMs, EA-49 significantly improved solar cell performance, achieving a peak PCE of 12.03%, with advantageous photovoltaic parameters such as a  $V_{OC}$  of 1.024 V and a  $J_{SC}$  of  $17.25 \text{ mA cm}^{-2}$ . This improvement was attributed to better energy barrier management and the ability of the methoxy groups on

EA-49 to passivate trap states through coordination bonding.

Spiro-OMeTAD has long been widely used as the benchmark HTM for traditional PSCs. However, due to its intrinsic low conductivity and hole mobility, Spiro-OMeTAD requires chemical dopants to enhance hole mobility, and these often compromise the long-term stability of solar cells. Palomares et al. synthesized SAM HTMs of Spiro-Acid, comprising spiro-OMeTAD derivatives with carboxylic acid units serving as anchor groups [113]. By introducing carboxylic acid anchoring groups into the Spiro-OMeTAD molecule, Spiro-Acid can form a stable self-assembled monolayer on the surface of ITO. This self-assembly process does not require additional chemical dopants, simplifying the manufacturing process and reducing costs. Moreover, Spiro-Acid is expected to improve the selective transport of holes by optimizing the molecular structure to reduce the energy loss of holes between the perovskite layer and the HTL, thereby enhancing the efficiency of solar cells. PSCs based on spin-coated Spiro-Acid achieved a PCE of 18.15% and an FF of 82.6% without encapsulation or interface passivation. These devices exhibited improved stability under illumination due to the removal of PbI<sub>2</sub> from the perovskite.

### 3.3. SAM-HTLs with other additional anchoring groups

In addition to phosphonic acid and carboxylic acid groups as anchoring groups, other anchoring groups have also been used to design SAM-HTLs (Table 7).

**Table 7.** Performance statistics of SAMs based on other acid groups as single-junction PSCs for HTL

SAM-HTL	ETL	$J_{sc}$ (mA cm <sup>-2</sup> )	$V_{oc}$ (V)	FF (%)	PCE (%)	Ref.
MPA-BT-CA	C <sub>60</sub> +BCP	22.37	1.13	82.2	20.7	[125]

MPA-BT-CA	C <sub>60</sub> +BCP	23.18	1.15	82.0	21.81	[126]
MPA-BT-BA	C <sub>60</sub> +BCP	22.76	1.12	81.0	20.58	[126]
MPA-BT-RA	C <sub>60</sub> +BCP	22.03	1.10	81.1	19.65	[126]
MPA-BT-CA	C <sub>60</sub> +BCP	22.73	1.106	82.3	20.70	[127]
FMPA-BT-CA	C <sub>60</sub> +BCP	23.33	1.151	83.3	22.37	[127]
2FMPA-BT-CA	C <sub>60</sub> +BCP	22.81	1.143	83.1	21.68	[127]
NBA	PCDTBT:PC <sub>70</sub> BM	14.65	0.98	76.5	10.93	[128]
ADAI	PCBM+LiF	19.9	1.04	77	15.9	[129]
ADA (p-i-n)	PCBM	16.28	0.94	51	8.49	[130]
ADAI (p-i-n)	PCBM	19.88	1.04	77	15.5	[130]
ADA (n-i-p)	SnO <sub>2</sub> +PCBM	18.77	0.89	44	6.61	[130]
ADAI (n-i-p)	SnO <sub>2</sub> +PCBM	20.46	1.07	70	15.3	[130]
MTPA-BA-R	PCBM+C <sub>60</sub> +BCP	23.24	1.14	85.2	22.62	[77]
MTPA-BA-R	PCBM+C <sub>60</sub> +BCP	23.00	1.10	83.2	21.04	[77]
MTPA-BA-R	PCBM+C <sub>60</sub> +BCP	20.09	1.16	82.9	19.28	[77]
EA-59	PCBM+Ca	17.98	1.043	71.56	13.19	[131]
PDI	C <sub>60</sub> +BCP	28.8	0.78	71	16	[132]
PDAI	C <sub>60</sub> +BCP	29.0	0.77	72	16	[132]

Guo and colleagues synthesized a novel SAM, named MPA-BT-CA, using 4-methoxy-N-(4-methoxyphenyl) benzylamine (MPA) as the donor unit, benzo[c] [1,2,5] thiadiazole (BT) as the acceptor unit, and acrylic acid (CA) as the anchoring group (Fig. 15a) [125]. In MPA-BT-CA, MPA as the donor unit exhibits good oxidation capability and high hole transport ability, while BT as the acceptor unit enhances intermolecular stacking due to its planar structure, with the sulfur (S) atom in BT interacting with under-coordinated Pb<sup>2+</sup> ions via coordination bonds. As the anchoring group, CA is attached to one end of the molecule, introducing multifunctionalities on the perovskite active layer, such as solubility adjustment, level modulation, interface modification, and passivation effects. UV-vis analysis shows that MPA-BT-CA does not affect photon transmittance, although it exhibits weak absorption in the visible range. Thermal analysis confirms the excellent thermal stability of SAM, which is crucial given the impact of operating temperature on the commercialization of perovskite solar cells.

UPS reveals that after modification with MPA-BT-CA molecules, the WF of ITO glass increases to 4.79 eV, compared to 4.40 eV for bare ITO glass, indicating better alignment of the ITO electrode with the valence band of the perovskite, which should facilitate efficient hole collection. The effective adjustment of ITO WF can be attributed to the high dipole moment of MPA-BT-CA, which may induce interfacial dipoles, thereby enhancing the ITO's work function. MPA-BT-CA interacts strongly with ITO and the perovskite layer, greatly suppressing interface charge recombination, passivating interface defects, and promoting interfacial charge transfer. Finally, inverted PSCs based on MPA-BT-CA achieve an impressive PCE of 21.24%, with good long-term and thermal stability. More importantly, PSCs based on MPA-BT-CA processed with ethanol as a non-toxic solvent achieve an extremely high PCE of 20.52%, indicating significant progress in developing a new category of HTM combining low-cost synthesis, environmentally friendly processability, and high performance.

They then synthesized a series of D-A type SAMs, namely MPA-BT-CA, MPA-BT-BA, and MPA-BT-RA, incorporating different functional groups to enhance the interface properties on ITO substrates [126]. Using XPS, they confirmed successful SAM deposition, highlighted by specific peaks such as C 1s at 284.7 eV and S 2p at 165.6 eV. MPA-BT-RA SAMs exhibited a propensity for aggregation, resulting in thicker and rougher multilayer films as deduced from Beer–Lambert law calculations. DFT analyses suggested that the sp<sup>3</sup> hybridized carbon in the RA group of MPA-BT-RA allows high molecular rotation, which disrupts monolayer uniformity. In contrast, the BA group in MPA-BT-BA creates a 32.7° dihedral angle with the BT unit, reducing the planarity and π-π stacking essential for ordered self-assembly and hence leading to uneven and less stable films. The CA group in MPA-BT-CA demonstrated the strongest

performance, enabling strong chemical adsorption with the ITO surface due to covalent bonds formed between its carboxylic acid group and ITO's hydroxyl groups. This interaction and the large dipole moment introduced by the CA group facilitated a tight, ordered monolayer, which is crucial for uniform film formation. UPS revealed that the work function of MPA-BT-CA-modified ITO was significantly higher (4.79 eV) than that of bare ITO (4.40 eV), aligning well with the perovskite's valence band to yield improved hole transfer and Voc. As a result, devices incorporating MPA-BT-CA achieved an impressive PCE of 21.81%, maintaining high efficiency even as the device area expanded to 0.80 cm<sup>2</sup>. This indicates the potential of MPA-BT-CA SAMs for optimizing photovoltaic device performance through enhanced molecular ordering and interface engineering.

Huang et al. synthesized two novel fluorinated molecules, FMPA-BT-CA and 2FMPA-BT-CA [127]. Methoxy-substituted triphenylamine (MPA) and benzo[c][1,2,5]thiadiazole (BT) were utilized as donor and acceptor building blocks, respectively. At the same time, polar cyanoacetic acid (CA) served as an interface modifier and solubility-enhancing functional group in environmentally friendly solvents. DFT calculations were conducted to investigate the structure and electronic properties of the fluorinated molecules. The results revealed that the introduction of fluorine atoms led to slightly larger dihedral angles between the phenyl moiety and the BT unit in FMPA-BT-CA (31.2°) and 2FMPA-BT-CA (31.0°) compared to MPA-BT-CA (27.7°), primarily due to increased steric hindrance of the fluorine atoms compared to hydrogen atoms (Fig. 15d). Additionally, computational results indicated that fluorine atoms played a crucial role in lowering the HOMO levels of FMPA-BT-CA (-4.99 eV) and 2FMPA-BT-CA (-4.97 eV) to below that of MPA-BT-CA (-4.89 eV). Deeper HOMO levels typically lead to higher open-circuit voltages in PSCs. Fluorine atoms also

increased the maximum negative potential of the CA group in FMPA-BT-CA, affecting hole contact and interactions with the perovskite surface. Due to its better energy level alignment with perovskite, FMPA-BT-CA achieved a higher PCE. An inverted PSC device based on FMPA-BT-CA processed with environmentally friendly solvents demonstrated efficient and stable performance, with a PCE of 22.37%.

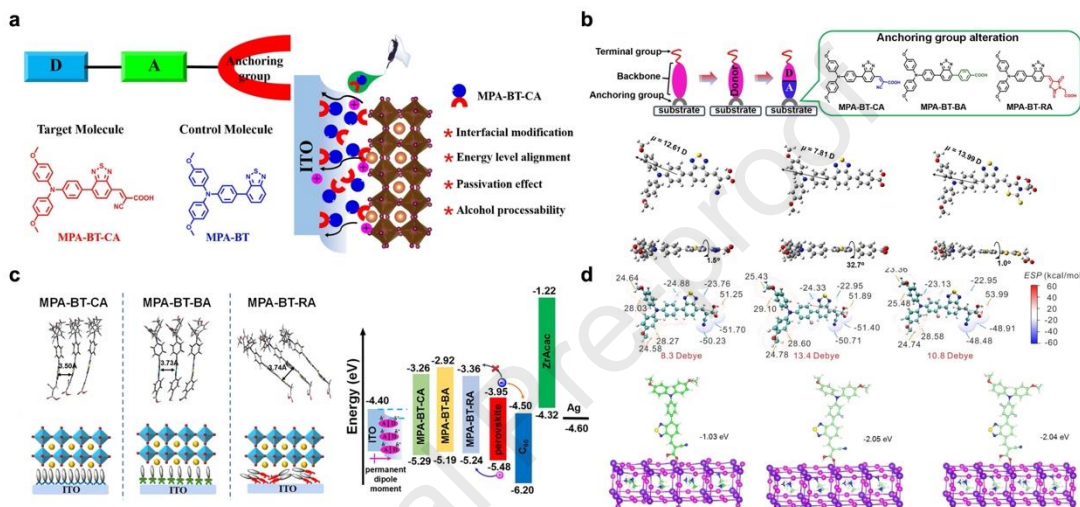


**Fig. 15.** (a) Chemical structures and a schematic diagram, highlighting the multifunctionality of MPA-BT-CA [125]. Copyright 2020 American Chemical Society. (b) A schematic diagram of SAMs as hole contacts in PSCs, alongside the chemical structures of newly designed SAMs. This includes optimized ground-state molecular configurations and dipole moments for MPA-BT-CA, MPA-BT-BA, and MPA-BT-RA. (c) Optimized stacking models derived from DFT calculations, plus a schematic diagram outlining potential molecular organization behaviors in the self-assembled films for the three SAMs, and a schematic illustration of the device's energy-level diagram [126]. Copyright 2022 Elsevier. (d) Geometry-optimized structures of hole contact molecules adsorbed onto perovskite surfaces [127].

Copyright 2022 American Chemical Society.

#### 4. Other applications

As the foregoing sections have shown, SAMs are effective as HTMs in PSCs. Their potential application as ETMs has also been explored. However, in n-i-p structures, SAMs used as ETMs tend to yield lower performance than traditional metal oxide substrates like TiO<sub>2</sub> and SnO<sub>2</sub>. Fig. 16 exhibits the molecular structures of some SAMs used as ETMs.

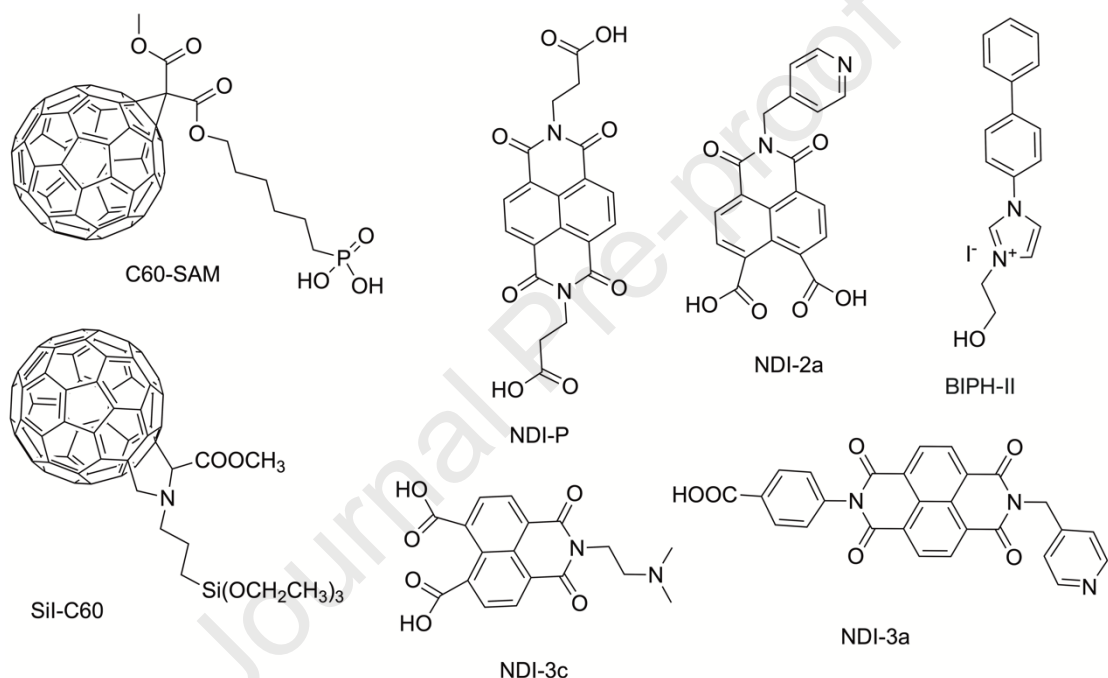


**Fig. 16. The molecular structures of SAMs as ETMs.**

Hou et al. significantly enhanced the mitigation of hysteresis in PSCs by applying SAMs [133]. Specifically, using a phosphonic acid-based mixed C60/organic SAM on transparent conductive oxide substrates notably reduced the hysteresis effect. Their key findings indicate that SAM-treated devices exhibit substantially less hysteresis than TiO<sub>2</sub>-based devices, with transition thresholds for hysteresis observed at approximately 1 kHz. This reduction is attributed to the strong phosphonate bond formed with the ITO substrate, which effectively suppresses ion migration, the primary cause of hysteresis, stabilizing the interface and reducing the density of ionic defects. Impedance studies

also highlighted that SAM-based devices show considerably lower capacitance at low and intermediate frequencies, suggesting a minimized ionic defect migration, which correlates directly with the observed stability improvements. They also emphasize the effectiveness of SAMs in enhancing operational stability and improving efficiency, with a demonstrated maximum PCE of 17.1%. These results underscore the potential of SAMs to significantly improve the long-term performance and reliability of perovskite solar cells by addressing fundamental issues related to ionic migration and electronic interface stability. A similar effect has been proven by Topolovsek et al., who employed the siloxane-functionalized C60 SAM SiI-C60 [134].

Cheng et al. presented an innovative approach to enhance the stability and performance of PSCs by using a self-assembled ionic liquid on the conductive substrate [135]. This method addresses the critical challenges associated with ETL-free PSCs by improving interfacial electron extraction and reducing charge recombination rates. They found that when a SAM was used as the ETL, the PCE of the PSC increased from 9.01% to 17.31%. This significant improvement is attributed mainly to the enhanced electron extraction capabilities and minimized interfacial charge recombination facilitated by the strong chemical interaction between the ionic liquid and the conductive substrate. Moreover, PSCs in ambient conditions with a relative humidity of 10–15% showed notable stability and durability, maintaining high efficiency over extended periods. This self-assembled ionic liquid approach simplifies the device architecture by eliminating the need for an ETL, thereby lowering production costs and complexity and offering a promising avenue for scalable, cost-effective PSC production.

Li et al. explored a naphthalene-imide compound to adjust the energy level, improving the PCE of devices employing NDI-P (3,3'-(1,3,6,8-tetraoxo-1,3,6,8-tetrahydrobenzo[lmn][3,8] phenanthroline-2,7-diyl) dipropionic acid) to 16% [136].

Additionally, Fürer et al. introduced naphthalene-imide-based SAMs (NDI-2a, 2c, 3a) as a surface modification to enhance device thermal stability [137].

## 5. Device stability with SAMs

Several challenges need to be addressed to achieve effective PSC utilization. Degradation caused by oxygen, light, and water is a major factor contributing to their reduced stability. For instance, UV exposure produces PbI<sub>2</sub> at the perovskite layer interface, which diminishes device stability; additionally, water and oxygen infiltration degrades the perovskite layers. This results in inefficient charge transport at the interfaces and a substantial decrease in the PCE [134]. Introducing SAMs as the HTL at the PSC layer interfaces can help mitigate these degradation factors, thus enhancing PSC performance during exposure to environmental conditions such as air and light over time.

Magomedov et al. provided significant insights into improving the stability of PSCs through the use of a novel HTM [89]. Their SAM, comprising a phosphonic acid-based molecule V1036, is directly applied to ITO substrates, bypassing the need for high-temperature processes and reducing parasitic absorption. The study shows that devices incorporating V1036 exhibit less degradation over time than traditional approaches. This was evidenced by the extended operational stability witnessed in their study, with devices retaining over 95% of their initial efficiency after 1000 hours of stress testing under illumination and thermal conditions. Introducing mixed SAMs, particularly with butyl phosphonic acid, further enhanced this effect by optimizing the interfacial layer's coverage and uniformity, reducing recombination losses, and providing a more robust barrier against environmental factors. Azmi et al. introduced significant advancements in PSC stability by using boronic acid-based fluorine-terminated SAMs on ITO [138]. Applying these SAMs was shown to significantly enhance ITO's work function and

overall device stability. Key stability improvements were quantitatively evident, as the device efficiency of the 2F-SAM modified cells exhibited only a 20% decrease after 30 days of testing, compared to a 75% efficiency loss in non-modified devices under similar conditions. The marked improvement in stability is attributed to the SAMs' ability to create a permanent dipole on the ITO surface, effectively increasing its work function and improving the interface with the hole transport layer (PEDOT:PSS). This modification enhances charge collection efficiency and acts as a protective barrier that mitigates the degradation typically induced by the acidic nature of PEDOT:PSS and environmental factors. Additionally, the optimized interfacial energy alignment facilitated by the SAMs reduces recombination losses and stabilizes the device's electrical characteristics over time. Including fluorinated SAMs significantly alters the surface wettability and energy barrier at the ITO/PEDOT:PSS interface, improving hole extraction and reducing device performance hysteresis. Overall, their study showcases a novel approach to improving the longevity and efficiency of planar heterojunction PSCs, suggesting that SAMs can be a viable solution for enhancing the operational stability of these devices in practical applications.

Chih-Yu Chang et al. addressed the stability of PSCs through innovative surface engineering.[139] Using thiol-functionalized SAMs on nickel oxide nanoparticles enhanced the interface between the perovskite layer and the electrode, a crucial change for improving device stability. Specifically, they reported on the employment of two SAM molecules, 3-mercaptopropyltrimethoxysilane (MPTMS) and (11-mercaptoundecyl) trimethylammonium bromide (MUTAB), which contributed significantly to device stability. These SAMs enhanced the adhesion and uniformity of an ultrathin Ag film used as the transparent electrode, leading to a PCE of up to 16.2% and maintaining high PCEs (approximately 16%) for large-area devices ( $1.2\text{ cm}^2$ ).

Meanwhile, the devices also exhibited good ambient stability without rigorous encapsulation. The improved device stability was mainly due to two factors: (1) the thiol-functionalized SAMs, specifically MPTMS and MUTAB, played a crucial role in enhancing the interfacial properties. They improved the adhesion and uniformity of the ultrathin Ag film, which served as the transparent electrode. This optimized interface contributed to reduced degradation pathways for the perovskite material; and (2) the SAMs helped tailor the work function of the electrodes and optimize the energy level alignment at the interface, which reduced recombination losses and enhanced charge carrier extraction. This optimization was critical for maintaining efficiency under ambient conditions. These findings represent a significant step towards practically applying stable, large-area, ITO-free PSCs.

## 6. Concluding remarks and perspectives

The SAM has recently emerged as a promising type of molecule for wide use as the HTL of high-performance PSCs. However, understanding the impact of such molecules on perovskite material and device performance remains elusive and requires further investigation. In the pursuit of more efficient perovskite solar cells for eventual use at the interface of tandem solar cells with silicon films or organic semiconductor films, countless new SAMs have been synthesized.

To aid in this pursuit, we have provided a comprehensive overview of the rational design and synthesis of all molecules used, to date, as SAMs in PSCs, from original pioneering work employing commercial molecules to the most complex structures prepared in this field. Undeniably, numerous organic chemists and materials scientists have made many efforts to develop new SAMs, but they still face several key challenges. Here, we provide some suggestions on how to design high-performance SAMs:

- (1) Anchoring groups: Choosing an anchoring group that forms a strong covalent bond

with the surface of the TCO is vital. Phosphonic acid and carboxylic acid are common anchoring groups because they form stable monolayers with metal oxide surfaces.

Consider introducing functional groups with strong affinity, such as thiol or silane groups, to enhance the binding force with TCO.

(2) Functional groups: When designing functional groups, consider their impact on electronic structure and energy levels. For example, introducing heterocyclic structures containing nitrogen or sulfur (such as thiophene, pyridine, etc.) can increase the molecule's electron affinity and facilitate hole transport. At the same time, the selection of functional groups should also consider their impact on film morphology and stability.

(3) Molecular configuration: Molecular planarity and intermolecular interactions (such as  $\pi$ - $\pi$  stacking) are crucial for forming ordered SAMs. Molecular configuration should be considered during design to promote the close packing and orderly arrangement of molecules.

(4) Intermolecular interactions: Groups with strong intermolecular interactions (such as hydrogen bond donor or acceptor groups) can enhance the stability and uniformity of SAMs.

(5) Environmental stability: Since PSCs may be used outdoors, SAMs molecules should have good thermal and photostability to ensure long-term performance.

At the same time, we believe that SAMs are very promising when applied as HTLs for PSCs, because SAMs can achieve the following:

(1) Better efficiency: By optimizing the electronic structure and energy level of SAMs, interface recombination can be reduced, and hole transmission efficiency can be improved, thereby boosting the overall photoelectric conversion efficiency of PSCs.

(2) Better stability: SAMs can serve as an interface layer to protect the perovskite layer from moisture and oxygen, thereby improving PSCs' environmental stability and

service life.

(3) Simplified manufacturing process: Compared with traditional HTL materials, SAMs can be prepared through a straightforward solution-processing method, which helps simplify the PSC manufacturing process and reduce production costs.

(4) Scalability: SAMs' self-assembly properties allow their application on large areas and flexible substrates, providing new opportunities for PSC commercialization and scalability.

(5) Environmental friendliness: The development of SAMs based on green solvents and low-toxic materials can reduce the environmental impact of PSC production and meet the requirements for sustainable development.

### Author contributions

Huan Bi: Visualization, Conceptualization, Writing - original draft (lead). Jiaqi Liu: Review and editing. Liang Wang: Review and editing. Tuo Liu: Review and editing. Zheng Zhang: Review and editing. Qing Shen: Supervision, Writing - review and editing. Shuzi Hayase: Supervision, Writing - review and editing.

### Competing financial interests

The authors declare no competing financial interests.

### Acknowledgments

This research did not receive any specific grant from funding agencies in the public, commercial, or not-for-profit sectors.

### References

- [1] H.Zhang, N.-G. Park, Towards sustainability with self-healing and recyclable perovskite solar cells, eScience 2 (2022) 567-572.
- [2] Z. Zhang, L. Qiao, K. Meng, R. Long, G. Chen, P. Gao, Rationalization of passivation strategies toward high-performance perovskite solar cells, Chem. Soc. Rev. 52 (2023) 163–195.
- [3] C. Wang, Y. Jiang, H. Xu, N. Zheng, G. Bai, Y. Zha, H. Qi, Z. Bian, X. Zhan, Z. Liu, Enhancing performance of tin-based perovskite solar cells via fused-ring electron acceptor, eScience 3 (2023) 100113.

- [4] Y. Yu, Y. Tang, B. Wang, K. Zhang, J.-X. Tang, Y.-Q. Li, Red perovskite light-emitting diodes: Recent advances and perspectives, *Laser Photonics Rev.* 17 (2023) 2200608.
- [5] Best research-cell efficiency chart | photovoltaic research | NREL, accessed on Feb. 8th, 2024 (2024). URL <https://www.nrel.gov/pv/cell-efficiency.html>
- [6] H. Bi, G. Han, M. Guo, C. Ding, S. Hayase, H. Zou, Q. Shen, Y. Guo, W. Hou, Top-contacts-interface engineering for high-performance perovskite solar cell with reducing lead leakage, *Solar RRL* 6 (2022) 2200352.
- [7] B. Liu, X. Ren, R. Li, Y. Chen, D. He, Y. Li, Q. Zhou, D. Ma, X. Han, X. Shai, K. Yang, S. Lu, Z. Zhang, J. Feng, C. Chen, J. Yi, J. Chen, Stabilizing top interface by molecular locking strategy with polydentate chelating biomaterials toward efficient and stable perovskite solar cells in ambient air, *Adv. Mater.* 36 (2024) 2312679.
- [8] N.-G. Park, Perovskite solar cells: an emerging photovoltaic technology, *Mater. Today* 18 (2015) 65-72.
- [9] H. W. Qiao, S. Yang, Y. Wang, X. Chen, T. Y. Wen, L. J. Tang, Q. Cheng, Y. Hou, H. Zhao, H. G. Yang, A gradient heterostructure based on tolerance factor in high-performance perovskite solar cells with 0.84 fill factor, *Adv. Mater.* 31 (2019) 1804217.
- [10] W. Travis, E. N. K. Glover, H. Bronstein, D. O. Scanlon, R. G. Palgrave, On the application of the tolerance factor to inorganic and hybrid halide perovskites: a revised system, *Chem. Sci.* 7 (2016) 4548-4556.
- [11] Z. Xiao, Y. Yan, Progress in theoretical study of metal halide perovskite solar cell materials, *Adv. Energy Mater.* 7 (2017) 1701136.
- [12] A. E. Fedorovskiy, N. A. Drigo, M. K. Nazeeruddin, The role of goldschmidt's tolerance factor in the formation of  $a2bx6$  double halide perovskites and its optimal range, *Small Methods* 4 (2020) 1900426.
- [13] C. Li, X. Lu, W. Ding, L. Feng, Y. Gao, Z. Guo, Formability of  $ABX_3$  ( $X = F, Cl, Br, I$ ) halide perovskites, *Acta Crystallogr. Sect. B* 64 (2008) 702-707.
- [14] R. D. Shannon, Revised effective ionic radii and systematic studies of interatomic distances in halides and chalcogenides, *Acta Crystallogr. Sect. A* 32 (1976) 751-767.
- [15] S. F. Hoefler, G. Trimmel, T. Rath, Progress on lead-free metal halide perovskites for photovoltaic applications: a review, *Monatsh. Chem.* 148 (2017) 795-826.
- [16] Z. Li, M. Yang, J.-S. Park, S.-H. Wei, J. J. Berry, K. Zhu, Stabilizing perovskite structures by tuning tolerance factor: Formation of formamidinium and cesium lead iodide solid-state alloys, *Chem. Mat.* 28 (2016) 284-292.
- [17] M. D. Sampson, J. S. Park, R. D. Schaller, M. K. Y. Chan, A. B. F. Martinson, Transition metal-substituted lead halide perovskite absorbers, *J. Mater. Chem. A* 5 (2017) 3578-3588.
- [18] T. Oku, Crystal structures of perovskite halide compounds used for solar cells, *Rev. Adv. Mater. Sci.* 59 (2020) 264-305.
- [19] L. Gollino, T. Pauperté, Lead-less halide perovskite solar cells, *Solar RRL* 5 (2021) 2000616.
- [20] Q. B. Ke, J.-R. Wu, C.-C. Lin, S. H. Chang, Understanding the pedot:pss, PTAA and P3HT-x hole-transport-layer-based inverted perovskite solar cells, *Polymers* 14

- (2022) 823.
- [21] Y. An, C. Wang, G. Cao, X. Li, Heterojunction perovskite solar cells: Opto-electro-thermal physics, modeling, and experiment, *ACS Nano* 14 (2020) 5017-5026.
  - [22] C. Chen, S. Zhang, S. Wu, W. Zhang, H. Zhu, Z. Xiong, Y. Zhang, W. Chen, Effect of BCP buffer layer on eliminating charge accumulation for high performance of inverted perovskite solar cells, *RSC Adv.* 7 (2017) 35819-35826.
  - [23] R. Quintero-Bermudez, J. Kirman, D. Ma, E. H. Sargent, R. Quintero-Torres, Mechanisms of lif interlayer enhancements of perovskite light-emitting diodes, *J Phys. Chem. L* 11 (2020) 4213-4220.
  - [24] M. Okuya, N. A. Prokudina, K. Mushika, S. Kaneko, TiO<sub>2</sub> thin films synthesized by the spray pyrolysis deposition (spd) technique, *J. Eur. Ceram. Soc.* 19 (1999) 903-906.
  - [25] Y. Kuang, V. Zardetto, R. van Gils, S. Karwal, D. Koushik, M. A. Verheijen, L. E. Black, C. Weijtens, S. Veenstra, R. Andriessen, W. M. Kessels, M. Creatore, Low-temperature plasma-assisted atomic-layer-deposited SnO<sub>2</sub> as an electron transport layer in planar perovskite solar cells, *ACS Appl. Mater. Interfaces* 10 (2018) 30367-30378.
  - [26] T. Yokoyama, Y. Nishitani, Y. Miyamoto, S. Kusumoto, R. Uchida, T. Matsui, K. Kawano, T. Sekiguchi, Y. Kaneko, Improving the open-circuit voltage of Sn-based perovskite solar cells by band alignment at the electron transport layer/perovskite layer interface, *ACS Appl. Mater. Interfaces* 12 (2020) 27131-27139.
  - [27] H. Bi, B. Liu, D. He, L. Bai, W. Wang, Z. Zang, J. Chen, Interfacial defect passivation and stress release by multifunctional KPF6 modification for planar perovskite solar cells with enhanced efficiency and stability, *Chem. Eng. J.* 418 (2021) 129375.
  - [28] H. Bi, X. Zuo, B. Liu, D. He, L. Bai, W. Wang, X. Li, Z. Xiao, K. Sun, Q. Song, Z. Zang, J. Chen, Multifunctional organic ammonium salt-modified SnO<sub>2</sub> nanoparticles toward efficient and stable planar perovskite solar cells, *J. Mater. Chem. A* 9 (2021) 3940-3951.
  - [29] A. A. Said, J. Xie, Q. Zhang, Recent progress in organic electron transport materials in inverted perovskite solar cells, *Small* 15 (2019) 1900854.
  - [30] W. Huang, E. Gann, L. Thomsen, A. Tadich, Y.-B. Cheng, C. R. McNeill, Metal evaporation-induced degradation of fullerene acceptors in polymer/fullerene solar cells, *ACS Appl. Mater. Interfaces* 8 (2016) 2247-2254.
  - [31] J. P. Correa Baena, L. Steier, W. Tress, M. Saliba, S. Neutzner, T. Matsui, F. Giordano, T. J. Jacobsson, A. R. Srimath Kandada, S. M. Zakeeruddin, A. Petrozza, A. Abate, M. K. Nazeeruddin, M. Grätzel, A. Hagfeldt, Highly efficient planar perovskite solar cells through band alignment engineering, *Energy Environ. Sci.* 8 (2015) 2928–2934.
  - [32] K. Wojciechowski, S. D. Stranks, A. Abate, G. Sadoughi, A. Sadhanala, N. Kopidakis, G. Rumbles, C.-Z. Li, R. H. Friend, A. K.-Y. Jen, H. J. Snaith, Heterojunction modification for highly efficient organic-inorganic perovskite solar cells, *ACS Nano* 8 (2014) 12701–12709.
  - [33] W. Ke, G. Fang, J. Wang, P. Qin, H. Tao, H. Lei, Q. Liu, X. Dai, X. Zhao, Perovskite

- solar cell with an efficient  $\text{TiO}_2$  compact film, *ACS Appl. Mater. Interfaces* 6 (2014) 15959–15965.
- [34] T. Leijtens, G. E. Eperon, S. Pathak, A. Abate, M. M. Lee, H. J. Snaith, Overcoming ultraviolet light instability of sensitized  $\text{TiO}_2$  with meso-superstructured organometal tri-halide perovskite solar cells, *Nat. Commun.* 4 (2013) 2885.
- [35] P. Tiwana, P. Docampo, M. B. Johnston, H. J. Snaith, L. M. Herz, Electron mobility and injection dynamics in mesoporous  $\text{ZnO}$ ,  $\text{SnO}_2$ , and  $\text{TiO}_2$  films used in dye-sensitized solar cells, *ACS Nano* 5 (2011) 5158–5166.
- [36] P. Zhu, S. Gu, X. Luo, Y. Gao, S. Li, J. Zhu, H. Tan, Simultaneous contact and grain-boundary passivation in planar perovskite solar cells using  $\text{SnO}_2\text{-KCl}$  composite electron transport layer, *Adv. Energy Mater.* 10 (2020) 1903083.
- [37] D. Bi, L. Yang, G. Boschloo, A. Hagfeldt, E. M. J. Johansson, Effect of different hole transport materials on recombination in  $\text{CH}_3\text{NH}_3\text{PbI}_3$  perovskite-sensitized mesoscopic solar cells, *J Phys. Chem. L* 4 (2013) 1532–1536.
- [38] X. Ding, M. Yan, C. Chen, M. Zhai, H. Wang, Y. Tian, L. Wang, L. Sun, M. Cheng, Efficient and stable tin-lead mixed perovskite solar cells using post-treatment additive with synergistic effects, *Angew. Chem. Int. Ed.* 63 (2024) e202317676.
- [39] Z. Zhang, J. Liang, Y. Zheng, X. Wu, J. Wang, Y. Huang, Y. Yang, Z. Zhou, L. Wang, L. Kong, K. M. Reddy, C. Qin, C.-C. Chen, Balancing crystallization rate in a mixed Sn-Pb perovskite film for efficient and stable perovskite solar cells of more than 20% efficiency, *J. Mater. Chem. A* 9 (2021) 17830–17840.
- [40] J.-S. Nam, K. Kim, J. Han, D. Kim, I. Chung, D. H. Wang, I. Jeon, A facile and effective ozone exposure method for wettability and energy-level tuning of hole-transporting layers in lead-free tin perovskite solar cells, *ACS Appl. Mater. Interfaces* 13 (2021) 42935–42943.
- [41] H. Guo, H. Zhang, S. Liu, D. Zhang, Y. Wu, W.-H. Zhu, Efficient and stable methylammonium-free tin-lead perovskite solar cells with hexaazatrinaphthylene-based hole-transporting materials, *ACS Appl. Mater. Interfaces* 14 (2022) 6852–6858.
- [42] J. Chen, X. Zhao, Y. Cheng, J. Qian, M. Wang, W. Shen, K. Cao, Y. Huang, W. Hui, Y. Gu, Y. Chen, X. Gao, S. Chen, Hydroxyl-rich d-sorbitol to address transport layer/perovskite interfacial issues toward highly efficient and stable 2D/3D tin-based perovskite solar cells, *Adv. Opt. Mater.* 9 (2021) 2100755.
- [43] W.-F. Yang, J.-J. Cao, J. Chen, K.-L. Wang, C. Dong, Z.-K. Wang, L.-S. Liao, Nicotinamide-modified PEDOT:PSS for high performance indoor and outdoor tin perovskite photovoltaics, *Solar RRL* 5 (2021) 2100713.
- [44] P. Lin, W. Zhang, L. Tian, L. Jia, F. Wen, G. Duan, X. Zhou, S. Zhou, F. Zhang, Y. Jiang, T. Chen, F. Liu, S. Yang, Y. Huang, Surface modification of PEDOT:PSS for enhanced performance of inverted perovskite solar cells, *ACS Appl. Energ. Mater.* 4 (2021) 4408–4415.
- [45] H. Ma, Y. Shao, C. Zhang, Y. Lv, Y. Feng, Q. Dong, Y. Shi, Enhancing the interface contact of stacking perovskite solar cells with hexamethylenediammonium diiodide-modified PEDOT:PSS as an electrode, *ACS Appl. Mater. Interfaces* 12

(2020) 42321-42327.

- [46] J. Kim, M. A. Mat Teridi, A. R. b. Mohd Yusoff, J. Jang, Stable and null current hysteresis perovskite solar cells based nitrogen doped graphene oxide nanoribbons hole transport layer, *Sci. Rep.* 6 (2016) 27773.
- [47] M. Chen, G. Kapil, L. Wang, S. Razey Sahamir, A. K. Baranwal, K. Nishimura, Y. Sanehira, Z. Zhang, M. Akmal Kamarudin, Q. Shen, S. Hayase, High-performance wide bandgap lead-free perovskite solar cells by monolayer engineering, *Chem. Eng. J.* 436 (2022) 135196.
- [48] S. Liu, V. P. Biju, Y. Qi, W. Chen, Z. Liu, Recent progress in the development of high-efficiency inverted perovskite solar cells, *NPG Asia Mater.* 15 (2023) 27.
- [49] W. Zhang, X. Guo, Z. Cui, H. Yuan, Y. Li, W. Li, X. Li, J. Fang, Strategies for improving efficiency and stability of inverted perovskite solar cells, *Adv. Mater.* (2024) 2311025.
- [50] J. C. Love, L. A. Estroff, J. K. Kriebel, R. G. Nuzzo, G. M. Whitesides, Self-assembled monolayers of thiolates on metals as a form of nanotechnology, *Chem. Rev.* 105 (2005) 1103-1170.
- [51] P. J. Hotchkiss, S. C. Jones, S. A. Paniagua, A. Sharma, B. Kippelen, N. R. Armstrong, S. R. Marder, The modification of indium tin oxide with phosphonic acids: Mechanism of binding, tuning of surface properties, and potential for use in organic electronic applications, *Accounts Chem. Res.* 45 (2012) 337-346.
- [52] F. Brodard-Severac, G. Guerrero, J. Maquet, P. Florian, C. Gervais, P. H. Mutin, High-field  $^{17}\text{O}$  mas nmr investigation of phosphonic acid monolayers on titania, *Chem. Mat.* 20 (2008) 5191-5196.
- [53] S. A. Paniagua, A. J. Giordano, O. L. Smith, S. Barlow, H. Li, N. R. Armstrong, J. E. Pemberton, J.-L. Brédas, D. Ginger, S. R. Marder, Phosphonic acids for interfacial engineering of transparent conductive oxides, *Chem. Rev.* 116 (2016) 7117-7158.
- [54] M. Li, M. Liu, F. Qi, F. R. Lin, A. K.-Y. Jen, Self-assembled monolayers for interfacial engineering in solution-processed thin-film electronic devices: Design, fabrication, and applications, *Chem. Rev.* 124 (2024) 2138-2204.
- [55] S. Y. Kim, S. J. Cho, S. E. Byeon, X. He, H. J. Yoon, Self-assembled monolayers as interface engineering nanomaterials in perovskite solar cells, *Adv. Energy Mater.* 10 (2020) 2002606.
- [56] S. Zhang, R. Wu, C. Mu, Y. Wang, L. Han, Y. Wu, W.-H. Zhu, Conjugated self-assembled monolayer as stable hole-selective contact for inverted perovskite solar cells, *ACS Mater. Lett.* 4 (2022) 1976-1983.
- [57] Q. Jiang, R. Tirawat, R. A. Kerner, E. A. Gaulding, Y. Xian, X. Wang, J. M. Newkirk, Y. Yan, J. J. Berry, K. Zhu, Towards linking lab and field lifetimes of perovskite solar cells, *Nature* 623 (2023) 313-318.
- [58] S. M. Park, M. Wei, N. Lempesis, W. Yu, T. Hossain, L. Agosta, V. Carnevali, H. R. Atapattu, P. Serles, F. T. Eickemeyer, H. Shin, M. Vafaie, D. Choi, K. Darabi, E. D. Jung, Y. Yang, D. B. Kim, S. M. Zakeeruddin, B. Chen, A. Amassian, T. Filleter, M. G. Kanatzidis, K. R. Graham, L. Xiao, U. Rothlisberger, M. Grätzel, E. H. Sargent, Low-loss contacts on textured substrates for inverted perovskite solar cells,

Nature 624 (2023) 289-294.

- [59] S. Zhang, F. Ye, X. Wang, R. Chen, H. Zhang, L. Zhan, X. Jiang, Y. Li, X. Ji, S. Liu, M. Yu, F. Yu, Y. Zhang, R. Wu, Z. Liu, Z. Ning, D. Neher, L. Han, Y. Lin, H. Tian, W. Chen, M. Stolterfoht, L. Zhang, W.-H. Zhu, Y. Wu, Minimizing buried interfacial defects for efficient inverted perovskite solar cells, Science 380 (2023) 404-409.
- [60] Q. Tan, Z. Li, G. Luo, X. Zhang, B. Che, G. Chen, H. Gao, D. He, G. Ma, J. Wang, J. Xiu, H. Yi, T. Chen, Z. He, Inverted perovskite solar cells using dimethylacridine-based dopants, Nature 620 (2023) 545-551.
- [61] X. Zheng, Z. Li, Y. Zhang, M. Chen, T. Liu, C. Xiao, D. Gao, J. B. Patel, D. Kuciauskas, A. Magomedov, R. A. Scheidt, X. Wang, S. P. Harvey, Z. Dai, C. Zhang, D. Morales, H. Pruett, B. M. Wieliczka, A. R. Kirmani, N. P. Padture, K. R. Graham, Y. Yan, M. K. Nazeeruddin, M. D. McGehee, Z. Zhu, J. M. Luther, Co-deposition of hole-selective contact and absorber for improving the processability of perovskite solar cells, Nat.Energy 8 (2023) 462-472.
- [62] F. Li, X. Deng, Z. Shi, S. Wu, Z. Zeng, D. Wang, Y. Li, F. Qi, Z. Zhang, Z. Yang, S.-H. Jang, F. R. Lin, S. Tsang, X.-K. Chen, A. K. Y. Jen, Hydrogen-bond-bridged intermediate for perovskite solar cells with enhanced efficiency and stability, Nat. Photonics 17 (2023) 478-484.
- [63] X. Deng, F. Qi, F. Li, S. Wu, F. R. Lin, Z. Zhang, Z. Guan, Z. Yang, C.-S. Lee, A. K.-Y. Jen, Co-assembled monolayers as hole-selective contact for high-performance inverted perovskite solar cells with optimized recombination loss and long-term stability, Angew. Chem. Int. Ed. 61 (2022) e202203088.
- [64] W. Jiang, F. Li, M. Li, F. Qi, F. R. Lin, A. K.-Y. Jen,  $\pi$ -expanded carbazoles as hole-selective self-assembled monolayers for high-performance perovskite solar cells, Angew. Chem. Int. Ed. 61 (2022) e202213560.
- [65] Y. Zhao, X. Luan, L. Han, Y. Wang, Post-assembled alkylphosphonic acids for efficient and stable inverted perovskite solar cells, Adv. Funct. Mater. (2024) 2405646.
- [66] S. A. Paniagua, P. J. Hotchkiss, S. C. Jones, S. R. Marder, A. Mudalige, F. S. Marrikar, J. E. Pemberton, N. R. Armstrong, Phosphonic acid modification of indiumtin oxide electrodes: Combined xps/ups/contact angle studies, J Phys. Chem. C 112 (2008) 7809-7817.
- [67] P. J. Hotchkiss, M. Malicki, A. J. Giordano, N. R. Armstrong, S. R. Marder, Characterization of phosphonic acid binding to zinc oxide, J. Mater. Chem. 21 (2011) 3107-3112.
- [68] P. B. Paramonov, S. A. Paniagua, P. J. Hotchkiss, S. C. Jones, N. R. Armstrong, S. R. Marder, J.-L. Brédas, Theoretical characterization of the indium tin oxide surface and of its binding sites for adsorption of phosphonic acid monolayers, Chem. Mat. 20 (2008) 5131-5133.
- [69] M. Wagstaffe, A. G. Thomas, M. J. Jackman, M. Torres-Molina, K. L. Syres, K. Handrup, An experimental investigation of the adsorption of a phosphonic acid on the anatase TiO<sub>2</sub>(101) surface, J Phys. Chem. C 120 (2016) 1693-1700.
- [70] C. Di Valentin, D. Costa, Anatase tio2 surface functionalization by alkyl

- phosphonic acid: A DFT+d study, *J Phys. Chem. C* 116 (2012) 2819-2828.
- [71] M. Timpel, M. V. Nardi, S. Krause, G. Ligorio, C. Christodoulou, L. Pasquali, A. Giglia, J. Frisch, B. Wegner, P. Moras, N. Koch, Surface modification of ZnO (0001)-Zn with phosphonate-based self-assembled monolayers: Binding modes, orientation, and work function, *Chem. Mat.* 26 (2014) 5042-5050.
- [72] M. A. Truong, T. Funasaki, L. Ueberricke, W. Nojo, R. Murdey, T. Yamada, S. Hu, A. Akatsuka, N. Sekiguchi, S. Hira, L. Xie, T. Nakamura, N. Shioya, D. Kan, Y. Tsuji, S. Iikubo, H. Yoshida, Y. Shimakawa, T. Hasegawa, Y. Kanemitsu, T. Suzuki, A. Wakamiya, Tripodal triazatruxene derivative as a face-on oriented hole-collecting monolayer for efficient and stable inverted perovskite solar cells, *J. Am. Chem. Soc.* 145 (2023) 7528-7539.
- [73] N. Yaghoobi Nia, M. Bonomo, M. Zendehdel, E. Lamanna, M. M. H. Desoky, B. Paci, F. Zurlo, A. Generosi, C. Barolo, G. Viscardi, P. Quagliotto, A. Di Carlo, Impact of P3HT regioregularity and molecular weight on the efficiency and stability of perovskite solar cells, *ACS Sustain. Chem. Eng.* 9 (2021) 5061-5073.
- [74] N. Yaghoobi Nia, M. Méndez, B. Paci, A. Generosi, A. Di Carlo, E. Palomares, Analysis of the efficiency losses in hybrid perovskite/PTAA solar cells with different molecular weights: Morphology versus kinetics, *ACS Appl. Energ. Mater.* 3 (2020) 6853-6859.
- [75] I. Lee, N. Rolston, P.-L. Brunner, R. H. Dauskardt, Hole-transport layer molecular weight and doping effects on perovskite solar cell efficiency and mechanical behavior, *ACS Appl. Mater. Interfaces* 11 (2019) 23757-23764.
- [76] R. Chen, S. Liu, X. Xu, F. Ren, J. Zhou, X. Tian, Z. Yang, X. Guanz, Z. Liu, S. Zhang, Y. Zhang, Y. Wu, L. Han, Y. Qi, W. Chen, Robust hole transport material with interface anchors enhances the efficiency and stability of inverted formamidinium-cesium perovskite solar cells with a certified efficiency of 22.3%, *Energy Environ. Sci.* 15 (2022) 2567-2580.
- [77] H. Guo, C. Liu, H. Hu, S. Zhang, X. Ji, X.-M. Cao, Z. Ning, W.-H. Zhu, H. Tian, Y. Wu, Neglected acidity pitfall: boric acid-anchoring hole-selective contact for perovskite solar cells, *Natl. Sci. Rev.* 10 (2023) nwad057.
- [78] S. Mariotti, E. Köhnen, F. Scheler, K. Sveinbjörnsson, L. Zimmermann, M. Piot, F. Yang, B. Li, J. Warby, A. Musiienko, D. Menzel, F. Lang, S. Keßler, I. Levine, D. Mantione, A. Al-Ashouri, M. S. Härtel, K. Xu, A. Cruz, J. Kurpiers, P. Wagner, H. Köbler, J. Li, A. Magomedov, D. Mecerreyes, E. Unger, A. Abate, M. Stolterfoht, B. Stannowski, R. Schlatmann, L. Korte, S. Albrecht, Interface engineering for high-performance, triple-halide perovskite-silicon tandem solar cells, *Science* 381 (2023) 63-69.
- [79] B. AbdollahiNejand, D. B. Ritzer, H. Hu, F. Schackmar, S. Moghadamzadeh, T. Feeney, R. Singh, F. Laufer, R. Schmager, R. Azmi, M. Kaiser, T. Abzieher, S. Gharibzadeh, E. Ahlsweide, U. Lemmer, B. S. Richards, U. W. Paetzold, Scalable two-terminal all-perovskite tandem solar modules with a 19.1% efficiency, *Nat. Energy* 7 (2022) 620–630.
- [80] E. Li, E. Bi, Y. Wu, W. Zhang, L. Li, H. Chen, L. Han, H. Tian, W.-H. Zhu, Synergistic coassembly of highly wettable and uniform hole- extraction

monolayers for scaling-up perovskite solar cells, *Adv. Funct. Mater.* 30 (2020) 1909509.

- [81] L. Li, Y. Wang, X. Wang, R. Lin, X. Luo, Z. Liu, K. Zhou, S. Xiong, Q. Bao, G. Chen, Y. Tian, Y. Deng, K. Xiao, J. Wu, M. I. Saidaminov, H. Lin, C.-Q. Ma, Z. Zhao, Y. Wu, L. Zhang, H. Tan, Flexible all-perovskite tandem solar cells approaching 25% efficiency with molecule- bridged hole-selective contact, *Nat. Energy* 7 (2022) 708-717.
- [82] S. Gharibzadeh, P. Fassl, I. M. Hossain, P. Rohrbeck, M. Frericks, M. Schmidt, T. Duong, M. R. Khan, T. Abzieher, B. A. Nejand, F. Schackmar, O. Almora, T. Feeney, R. Singh, D. Fuchs, U. Lemmer, J. P. Hofmann, S. A. L. Weber, U. W. Paetzold, Two birds with one stone: dual grain-boundary and interface passivation enables >22%. *Energy Environ. Sci.* 14 (2021) 5875-5893.
- [83] Z. Dai, S. K. Yadavalli, M. Chen, A. Abbaspourtamijani, Y. Qi, N. P. Padture, Interfacial toughening with self-assembled monolayers enhances perovskite solar cell reliability, *Science* 372 (2021) 618-622.
- [84] X. Lin, A. N. Jumabekov, N. N. Lal, A. R. Pascoe, D. E. Gómez, N. W. Duffy, A. S. R. Chesman, K. Sears, M. Fournier, Y. Zhang, Q. Bao, Y.-B. Cheng, L. Spiccia, U. Bach, Dipole-field-assisted charge extraction in metal-perovskite-metal back-contact solar cells, *Nat. Commun.* 8 (1) (2017) 613.
- [85] E. Aktas, N. Phung, H. Köbler, D. A. González, M. Méndez, I. Kafedjiska, S.-H. Turren-Cruz, R. Wenisch, I. Lauermann, A. Abate, E. Palomares, Understanding the perovskite/self-assembled selective contact interface for ultra-stable and highly efficient p-i-n perovskite solar cells, *Energy Environ. Sci.* 14 (2021) 3976-3985.
- [86] W. Jiang, F. Li, M. Li, F. Qi, F. R. Lin, A. K. Y. Jen, ĪA-expanded carbazoles as hole-selective self-assembled monolayers for high-performance perovskite solar cells, *Angew. Chem. Int. Ed.* 61 (2022) e202213560.
- [87] E. Li, C. Liu, H. Lin, X. Xu, S. Liu, S. Zhang, M. Yu, X.-M. Cao, Y. Wu, W.-H. Zhu, Bonding strength regulates anchoring-based self-assembly monolayers for efficient and stable perovskite solar cells, *Adv. Funct. Mater.* 31 (2021) 2103847.
- [88] L. Zhang, J. M. Cole, Anchoring groups for dye-sensitized solar cells, *ACS Appl. Mater. Interfaces* 7 (2015) 3427-3455.
- [89] A. Magomedov, A. Al-Ashouri, E. Kasparavičius, S. Strazdaite, G. Niaura, M. Jošt, T. Malinauskas, S. Albrecht, V. Getautis, Self-assembled hole transporting monolayer for highly efficient perovskite solar cells, *Adv. Energy Mater.* 8 (2018) 1801892.
- [90] A. Al-Ashouri, A. Magomedov, M. Roß, M. Jošt, M. Talaikis, G. Chistiakova, T. Bertram, J. A. Márquez, E. Könen, E. Kasparavičius, S. Levcenco, L. Gil-Escríg, C. J. Hages, R. Schlatmann, B. Rech, T. Malinauskas, T. Unold, C. A. Kaufmann, L. Korte, G. Niaura, V. Getautis, S. Albrecht, Conformal monolayer contacts with lossless interfaces for perovskite single junction and monolithic tandem solar cells, *Energy Environ. Sci.* 12 (2019) 3356-3369.
- [91] A. Al-Ashouri, E. Könen, B. Li, A. Magomedov, H. Hempel, P. Caprioglio, J. A. Márquez, A. B. M. Vilches, E. Kasparavicius, J. A. Smith, N. Phung, D. Menzel, M. Grischek, L. Kegelmann, D. Skroblin, C. Gollwitzer, T. Malinauskas, M. Jošt, G.

- Matič, B. Rech, R. Schlatmann, M. Topič, L. Korte, A. Abate, B. Stannowski, D. Neher, M. Stolterfoht, T. Unold, V. Getautis, S. Albrecht, Monolithic perovskite/silicon tandem solar cell with >29% efficiency by enhanced hole extraction, *Science* 370 (2020) 1300–1309.
- [92] M. Roß, L. Gil-Escríg, A. Al-Ashouri, P. Tockhorn, M. Jošt, B. Rech, S. Albrecht, Co-evaporated p-i-n perovskite solar cells beyond 20% efficiency: Impact of substrate temperature and hole-transport layer, *ACS Appl. Mater. Interfaces* 12 (2020) 39261–39272.
- [93] A. Ullah, K. H. Park, H. D. Nguyen, Y. Siddique, S. F. A. Shah, H. Tran, S. Park, S. I. Lee, K.-K. Lee, C.-H. Han, K. Kim, S. Ahn, I. Jeong, Y. S. Park, S. Hong, Novel phenothiazine-based self-assembled monolayer as a hole selective contact for highly efficient and stable p-i-n perovskite solar cells, *Adv. Energy Mater.* 12 (2022) 2103175.
- [94] A. Ullah, K. H. Park, Y. Lee, S. Park, A. B. Faheem, H. D. Nguyen, Y. Siddique, K.-K. Lee, Y. Jo, C.-H. Han, S. Ahn, I. Jeong, S. Cho, B. Kim, Y. S. Park, S. Hong, Versatile hole selective molecules containing a series of heteroatoms as self-assembled monolayers for efficient p-i-n perovskite and organic solar cells, *Adv. Funct. Mater.* 32 (2022) 2208793.
- [95] J. Zeng, L. Bi, Y. Cheng, B. Xu, A. K.-Y. Jen, Self-assembled monolayer enabling improved buried interfaces in blade-coated perovskite solar cells for high efficiency and stability, *Nano Res. Energy* 1 (2022) 9120004.
- [96] H. Bi, J. Liu, Z. Zhang, L. Wang, R. Beresneviciute, D. Tavgeniene, G. Kapil, C. Ding, A. K. Baranwal, S. R. Sahamir, Y. Sanehira, H. Segawa, S. Grigalevicius, Q. Shen, S. Hayase, All-perovskite tandem solar cells approach 26.5% efficiency by employing wide bandgap lead perovskite solar cells with new monomolecular hole transport layer, *ACS Energy Lett.* 8 (2023) 3852-3859.
- [97] R. He, W. Wang, Z. Yi, F. Lang, C. Chen, J. Luo, J. Zhu, J. Thiesbrummel, S. Shah, K. Wei, Y. Luo, C. Wang, H. Lai, H. Huang, J. Zhou, B. Zou, X. Yin, S. Ren, X. Hao, L. Wu, J. Zhang, J. Zhang, M. Stolterfoht, F. Fu, W. Tang, D. Zhao, Improving interface quality for 1-cm<sup>2</sup> all-perovskite tandem solar cells, *Nature* 618 (2023) 80-86.
- [98] E. J. Cassella, E. L. Spooner, J. A. Smith, T. Thornber, M. E. O’Kane, R. D. Oliver, T. E. Catley, S. Choudhary, C. J. Wood, D. B. Hammond, H. J. Snaith, D. G. Lidzey, Binary solvent system used to fabricate fully annealing-free perovskite solar cells, *Adv. Energy Mater.* 13 (2023) 2203468.
- [99] Z. Li, Q. Tan, G. Chen, H. Gao, J. Wang, X. Zhang, J. Xiu, W. Chen, Z. He, Simple and robust phenoxazine phosphonic acid molecules as self-assembled hole selective contacts for high-performance inverted perovskite solar cells, *Nanoscale* 15 (2023) 1676-1686.
- [100] G. Kapil, T. Bessho, Y. Sanehira, S. R. Sahamir, M. Chen, A. K. Baranwal, D. Liu, Y. Sono, D. Hirotani, D. Nomura, K. Nishimura, M. A. Kamarudin, Q. Shen, H. Segawa, S. Hayase, Tin-lead perovskite solar cells fabricated on hole selective monolayers, *ACS Energy Lett.* 7 (2022) 966-974.
- [101] W. Wang, X. Liu, J. Wang, C. Chen, J. Yu, D. Zhao, W. Tang, Versatile self-

assembled molecule enables high-efficiency wide-bandgap perovskite solar cells and organic solar cells, *Adv. Energy Mater.* 13 (2023) 2300694.

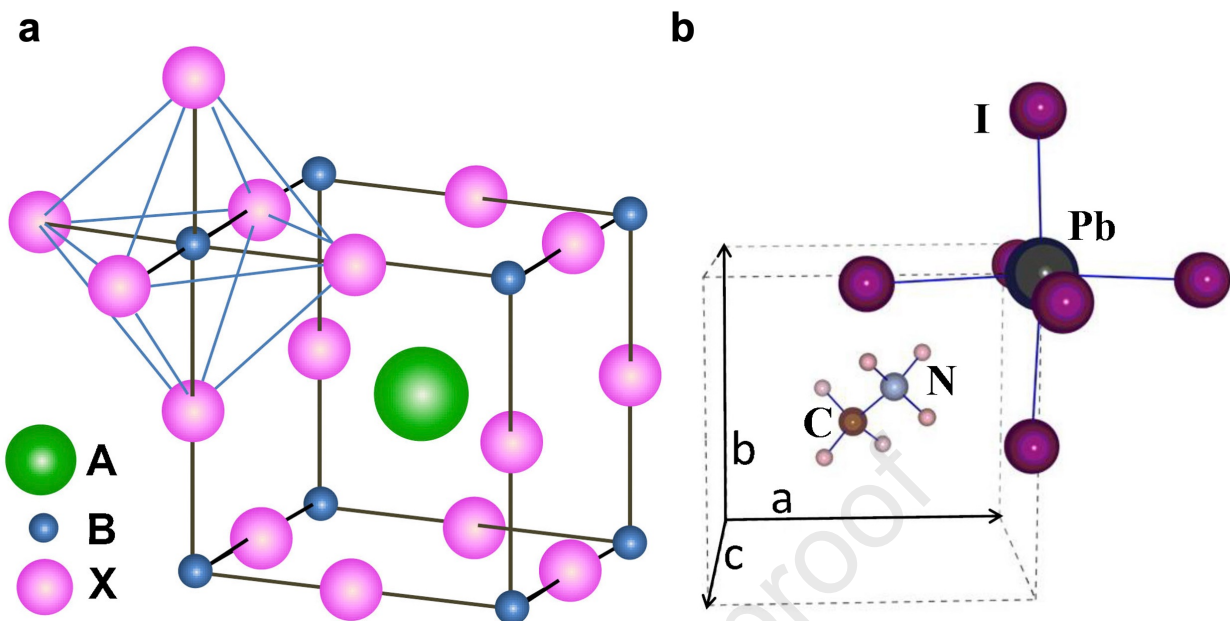
- [102] R. Guo, X. Zhang, X. Zheng, L. Li, M. Li, Y. Zhao, S. Zhang, L. Luo, S. You, W. Li, Z. Gong, R. Huang, Y. Cui, Y. Rong, H. Zeng, X. Li, Tailoring multifunctional self-assembled hole transporting molecules for highly efficient and stable inverted perovskite solar cells, *Adv. Funct. Mater.* 33 (2023) 2211955.
- [103] I. Kafedjiska, I. Levine, A. Musiienko, N. Maticiu, T. Bertram, A. Al-Ashouri, C. A. Kaufmann, S. Albrecht, R. Schlatmann, I. Lauermann, Advanced characterization and optimization of NiOx:Cu-SAM hole-transporting bi-layer for 23.4% efficient monolithic Cu(In,Ga)Se<sub>2</sub>-perovskite tandem solar cells, *Adv. Funct. Mater.* 33 (2023) 2302924.
- [104] M. Liu, L. Bi, W. Jiang, Z. Zeng, S.-W. Tsang, F. R. Lin, A. K.-Y. Jen, Compact hole-selective self-assembled monolayers enabled by disassembling micelles in solutionfor efficient perovskite solar cells, *Adv. Mater.* 35 (2023) 2304415.
- [105] B. Niu, H. Liu, Y. Huang, E. Gu, M. Yan, Z. Shen, K. Yan, B. Yan, J. Yao, Y. Fang, H. Chen, C.-Z. Li, Multifunctional hybrid interfacial layers for high-performance inverted perovskite solar cells, *Adv. Mater.* 35 (2023) 2212258.
- [106] Z. Zhang, R. Zhu, Y. Tang, Z. Su, S. Hu, X. Zhang, J. Zhang, J. Zhao, Y. Xue, X. Gao, G. Li, J. Pascual, A. Abate, M. Li, Anchoring charge selective self-assembled monolayers for tin-lead perovskite solar cells, *Adv. Mater.* (2024) 2312264.
- [107] W. Jiang, M. Liu, Y. Li, F. R. Lin, A. K.-Y. Jen, Rational molecular design of multifunctional self-assembled monolayers for efficient hole selection and buried interface passivation in inverted perovskite solar cells, *Chem. Sci.* 15 (2024) 2778-2785.
- [108] D. Vidyasagar, Y. Yun, J. Yu Cho, H. Lee, K. Won Kim, Y. Tae Kim, S. Woong Yang, J. Jung, W. Chang Choi, S. Kim, R. Kumar Gunasekaran, S. B. Kang, K. Heo, D. H. Kim, J. Heo, S. Lee, Surface-functionalized hole-selective monolayer for high efficiency single-junction wide- bandgap and monolithic tandem perovskite solar cells, *J. Energy Chem.* 88 (2024) 317-326.
- [109] W. Wang, K. Wei, L. Yang, J. Deng, J. Zhang, W. Tang, Dynamic self-assembly of small molecules enables the spontaneous fabrication of hole conductors at perovskite/electrode interfaces for over 22% stable inverted perovskite solar cells, *Mater. Horiz.* 10 (2023) 2609-2617.
- [110] H. Bi, J. Liu, Z. Zhang, L. Wang, G. Kapil, Y. Wei, A. Kumar Baranwal, S. Razey Sahamir, Y. Sanehira, D. Wang, Y. Yang, T. Kitamura, R. Beresneviciute, S. Grigalevicius, Q. Shen, S. Hayase, Ferrocene derivatives for improving the efficiency and stability of ma-free perovskite solar cells from the perspective of inhibiting ion migration and releasing film stress, *Adv. Sci.* 10 (2023) 2304790.
- [111] D.-H. Kim, H.-J. Lee, S.-H. Lee, Y.-J. Kang, S.-N. Kwon, D.-H. Kim, S.-I. Na, Mixed self-assembled hole-transport monolayer enables simultaneous improvement of efficiency and stability of perovskite solar cells, *Solar RRL* 8 (2024) 2400067.
- [112] E. Yalcin, E. Aktas, M. Mendéz, E. Arkan, J. G. Sánchez, E. Martínez-Ferrero, F. Silvestri, E. Barrena, M. Can, S. Demic, E. Palomares, Monodentate versus

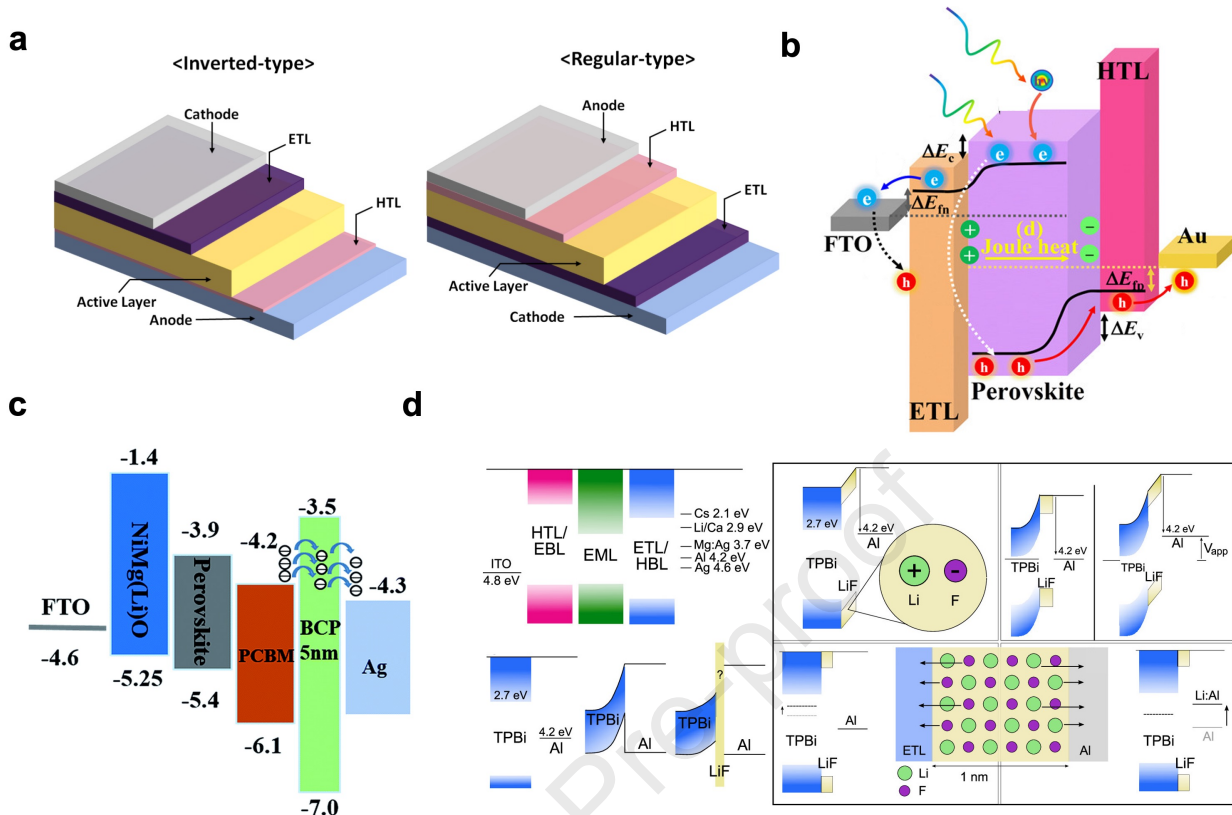
- bidentate anchoring groups in self-assembling molecules (sams) for robust p-i-n perovskite solar cells, *ACS Appl. Mater. Interfaces* 15 (2023) 57153–57164.
- [113] W. Li, M. Cariello, M. Méndez, G. Cooke, E. Palomares, Self-assembled molecules for hole-selective electrodes in highly stable and efficient inverted perovskite solar cells with ultralow energy loss, *ACS Appl. Energ. Mater.* 6 (2023) 1239-1247.
- [114] E. Aktas, R. Pudi, N. Phung, R. Wenisch, L. Gregori, D. Meggiolaro, M. A. Flatken, F. De Angelis, I. Lauermann, A. Abate, E. Palomares, Role of terminal group position in triphenylamine-based self-assembled hole-selective molecules in perovskite solar cells, *ACS Appl. Mater. Interfaces* 14 (2022) 17461–17469.
- [115] C.-Y. Chang, H.-H. Huang, H. Tsai, S.-L. Lin, P.-H. Liu, W. Chen, F.-C. Hsu, W. Nie, Y.-F. Chen, L. Wang, Facile fabrication of self-assembly functionalized polythiophene hole transporting layer for high-performance perovskite solar cells, *Adv. Sci.* 8 (2021) 2002718.
- [116] C.-M. Hung, C.-L. Mai, C.-C. Wu, B.-H. Chen, C.-H. Lu, C.-C. Chu, M.-C. Wang, S.-D. Yang, H.-C. Chen, C.-Y. Yeh, P.-T. Chou, Self-assembled monolayers of bi-functionalized porphyrins: A novel class of hole-layer-coordinating perovskites and indium tin oxide in inverted solar cells, *Angew. Chem. Int. Ed.* 62 (2023) e202309831.
- [117] A. Abid, P. Rajamanickam, E. Wei-Guang Diau, Design of a simple bifunctional system as a self-assembled monolayer (sam) for inverted tin-based perovskite solar cells, *Chem. Eng. J.* 477 (2023) 146755.
- [118] E. Yalcin, M. Can, C. Rodriguez-Seco, E. Aktas, R. Pudi, W. Cambarau, S. Demic, E. Palomares, Semiconductor self-assembled monolayers as selective contacts for efficient pin perovskite solar cells, *Energy Environ. Sci.* 12 (2019) 230-237.
- [119] E. Arkan, E. Yalcin, M. Unal, M. Z. Y. Arkan, M. Can, C. Tozlu, S. Demic, Effect of functional groups of self-assembled monolayer molecules on the performance of inverted perovskite solar cell, *Mater. Chem. Phys.* 254 (2020) 123435.
- [120] E. Arkan, M. Unal, E. Yalcin, M. Z. YigitArkan, S. Yurtdas, M. Can, C. Tozlu, S. Demic, Influence of end groups variation of self assembled monolayers on performance of planar perovskite solar cells by interface regulation, *Mater. Sci. Semicond. Process* 123 (2021) 105514.
- [121] D. A. González, C. E. Puerto Galvis, W. Li, M. Méndez, E. Aktas, E. Martínez-Ferrero, E. Palomares, Influence of the carbazole moiety in self-assembling molecules as selective contacts in perovskite solar cells: interfacial charge transfer kinetics and solar-to-energy efficiency effects, *Nanoscale Adv.* 5 (2023) 6542–6547.
- [122] E. Aktas, J. Jiménez-López, K. Azizi, T. Torres, E. Palomares, Self-assembled zn phthalocyanine as a robust p-type selective contact in perovskite solar cells, *Nanoscale Horiz.* 5 (2020) 1415–1419.
- [123] J. Zhu, Y. Luo, R. He, C. Chen, Y. Wang, J. Luo, Z. Yi, J. Thiesbrummel, C. Wang, F. Lang, H. Lai, Y. Xu, J. Wang, Z. Zhang, W. Liang, G. Cui, S. Ren, X. Hao, H. Huang, Y. Wang, F. Yao, Q. Lin, L. Wu, J. Zhang, M. Stolterfoht, F. Fu, D. Zhao, A donor-acceptor-type hole- selective contact reducing non-radiative recombination losses in both subcells towards efficient all-perovskite tandems, *Nat. Energy* 8 (2023)

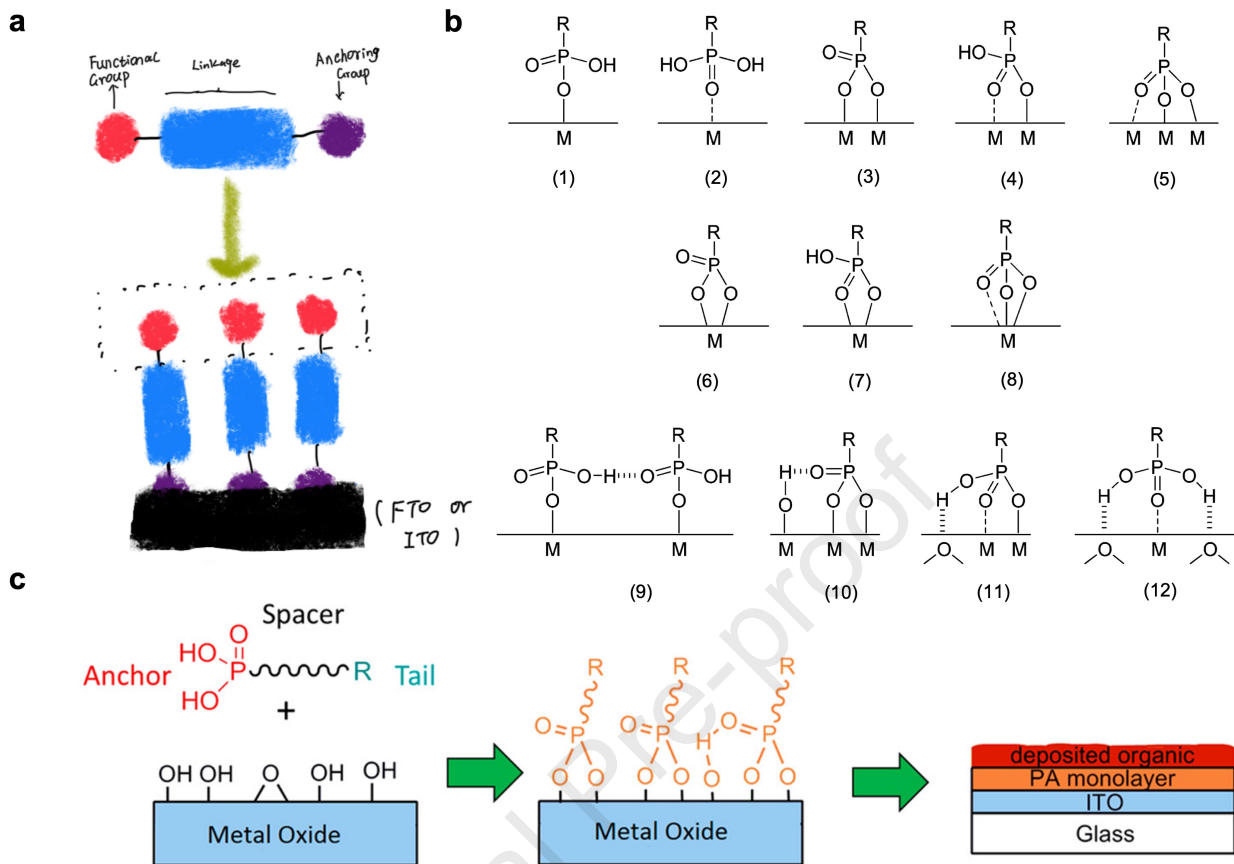
714-724.

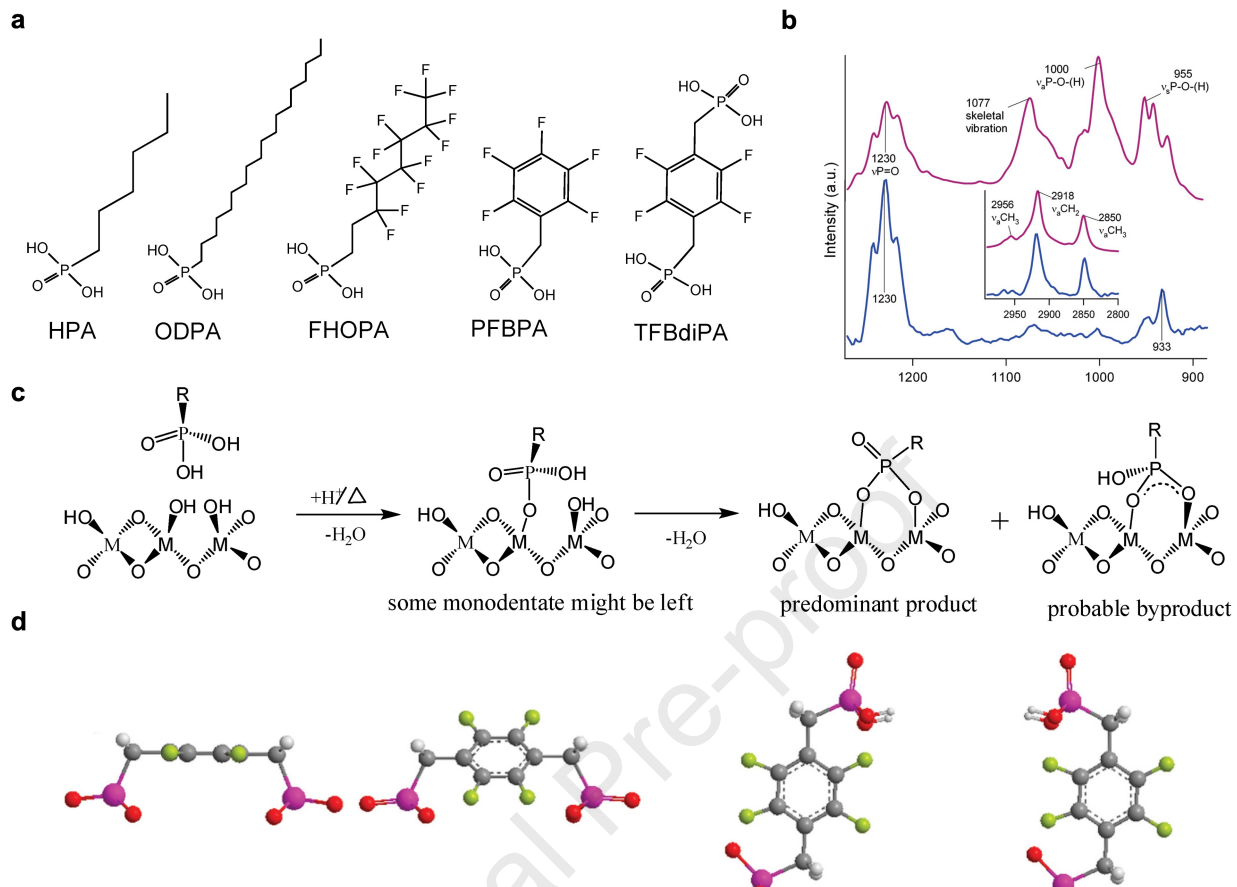
- [124] E. Yalcin, D. A. Kara, C. Karakaya, M. Z. Yigit, A. K. Havare, M. Can, C. Tozlu, S. Demic, M. Kus, A. Aboulouard, Functionalized organic semiconductor molecules to enhance charge carrier injection in the electroluminescent cell, *Opt. Mater.* 69 (2017) 283-290.
- [125] Y. Wang, Q. Liao, J. Chen, W. Huang, X. Zhuang, Y. Tang, B. Li, X. Yao, X. Feng, X. Zhang, M. Su, Z. He, T. J. Marks, A. Facchetti, X. Guo, Teaching an old anchoring group new tricks: Enabling low-cost, eco-friendly hole-transporting materials for efficient and stable perovskite solar cells, *J. Am. Chem. Soc.* 142 (2020) 16632-16643.
- [126] Q. Liao, Y. Wang, Z. Zhang, K. Yang, Y. Shi, K. Feng, B. Li, J. Huang, P. Gao, X. Guo, Self-assembled donor-acceptor hole contacts for inverted perovskite solar cells with an efficiency approaching 22%: the impact of anchoring groups, *J. Energy Chem.* 68 (2022) 87-95.
- [127] Q. Liao, Y. Wang, M. Hao, B. Li, K. Yang, X. Ji, Z. Wang, K. Wang, W. Chi, X. Guo, W. Huang, Green-solvent-processable low-cost fluorinated hole contacts with optimized buried interface for highly efficient perovskite solar cells, *ACS Appl. Mater. Interfaces* 14 (2022) 43547-43557.
- [128] A. V. Kesavan, V. Adiga, G. K. Chandrasekar, K. M. Panidhara, P. C. Ramamurthy, Nanoscale small molecule self-assembled ict for photon harvesting in polymer and perovskite solar cells, *Solar Energy* 240 (2022) 201-210.
- [129] M. Más-Montoya, P. Gómez, D. Curiel, I. da Silva, J. Wang, R. A. J. Janssen, A self-assembled small-molecule-based hole-transporting material for inverted perovskite solar cells, *Eur. J. Org. Chem.* 26 (2020) 10276-10282.
- [130] M. Más-Montoya, P. Gómez, J. Wang, R. A. J. Janssen, D. Curiel, Small molecule dopant-free dual hole transporting material for conventional and inverted perovskite solar cells, *Mater. Chem. Front.* 7 (2023) 4019-4028.
- [131] E. Arkan, M. Z. Yigit Arkan, M. Unal, E. Yalcin, H. Aydin, C. Celebi, M. Can, C. Tozlu, S. Demic, Performance enhancement of inverted perovskite solar cells through interface engineering by TBP based bidentate self-assembled monolayers, *Opt. Mater.* 105 (2020) 109910.
- [132] P. Gómez, J. Wang, M. Más-Montoya, D. Bautista, C. H. L. Weijtens, D. Curiel, R. A. J. Janssen, Pyrene-based small-molecular hole transport layers for efficient and stable narrow-bandgap perovskite solar cells, *Solar RRL* 5 (2021) 2100454.
- [133] Y. Hou, S. Scheiner, X. Tang, N. Gasparini, M. Richter, N. Li, P. Schweizer, S. Chen, H. Chen, C. O. R. Quiroz, X. Du, G. J. Matt, A. Osset, E. Spiecker, R. H. Fink, A. Hirsch, M. Halik, C. J. Brabec, Suppression of hysteresis effects in organohalide perovskite solar cells, *Adv. Mater. Interfaces* 4 (2017) 1700007.
- [134] P. Topolovsek, F. Lamberti, T. Gatti, A. Cito, J. M. Ball, E. Menna, C. Gadermaier, A. Petrozza, Functionalization of transparent conductive oxide electrode for TiO<sub>2</sub>-free perovskite solar cells, *J. Mater. Chem. A* 5 (2017) 11882–11893.
- [135] H. Cheng, Y. Li, M. Zhang, K. Zhao, Z.-S. Wang, Self-assembled ionic liquid for highly efficient electron transport layer-free perovskite solar cells, *ChemSusChem* 13 (2020) 2779-2785.

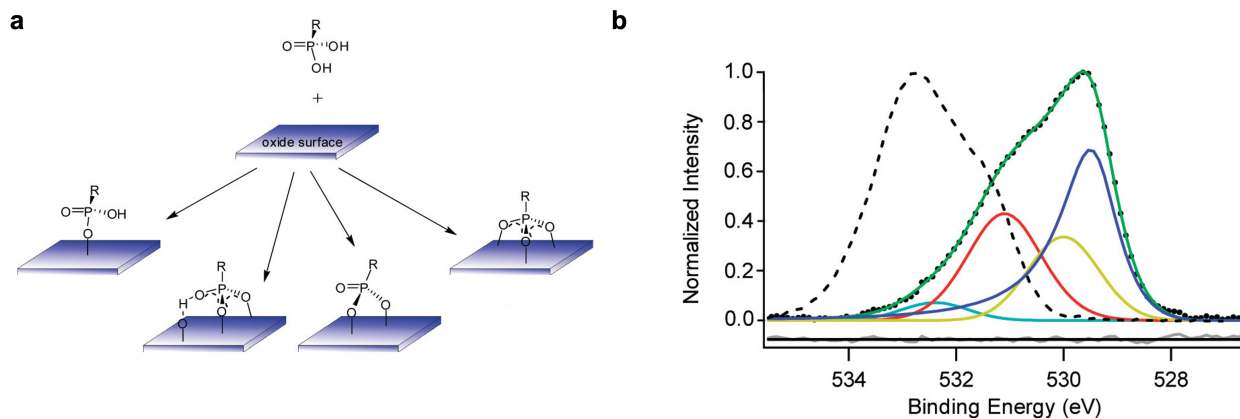
- 
- [136] L. Li, Y. Wu, E. Li, C. Shen, H. Zhang, X. Xu, G. Wu, M. Cai, W.-H. Zhu, Self-assembled phthalimide derivatives as an efficient and low-cost electron extraction layer for n-i-p perovskite solar cells, *Chem. Commun.* 55 (2019) 13239-13242.
- [137] S. O. Fürer, K. J. Rietwyk, F. Pulvirenti, D. P. McMeekin, M. A. Surmiak, S. R. Raga, W. Mao, X. Lin, Y. Hora, J. Wang, Y. Shi, S. Barlow, D. S. Ginger, S. R. Marder, U. Bach, Naphthalene-imide self-assembled monolayers as a surface modification of ito for improved thermal stability of perovskite solar cells, *ACS Appl. Energy Mater.* 6 (2023) 667–677.
- [138] D. AkÄsn Kara, K. Kara, G. Oylumluoglu, M. Z. Yigit, M. Can, J. J. Kim, E. K. Burnett, D. L. Gonzalez Arellano, S. Buyukcelebi, F. Ozel, O. Usluer, A. L. Briseno, M. Kus, Enhanced device efficiency and long-term stability via boronic acid-based self-assembled monolayer modification of indium tin oxide in a planar perovskite solar cell, *ACS Appl. Mater. Interfaces* 10 (2018) 30000-30007.
- [139] C.-Y. Chang, Y.-C. Chang, W.-K. Huang, W.-C. Liao, H. Wang, C. Yeh, B.-C. Tsai, Y.-C. Huang, C.-S. Tsao, Achieving high efficiency and improved stability in large-area ITO-free perovskite solar cells with thiol-functionalized self-assembled monolayers, *J. Mater. Chem. A* 4 (2016) 7903-7913.

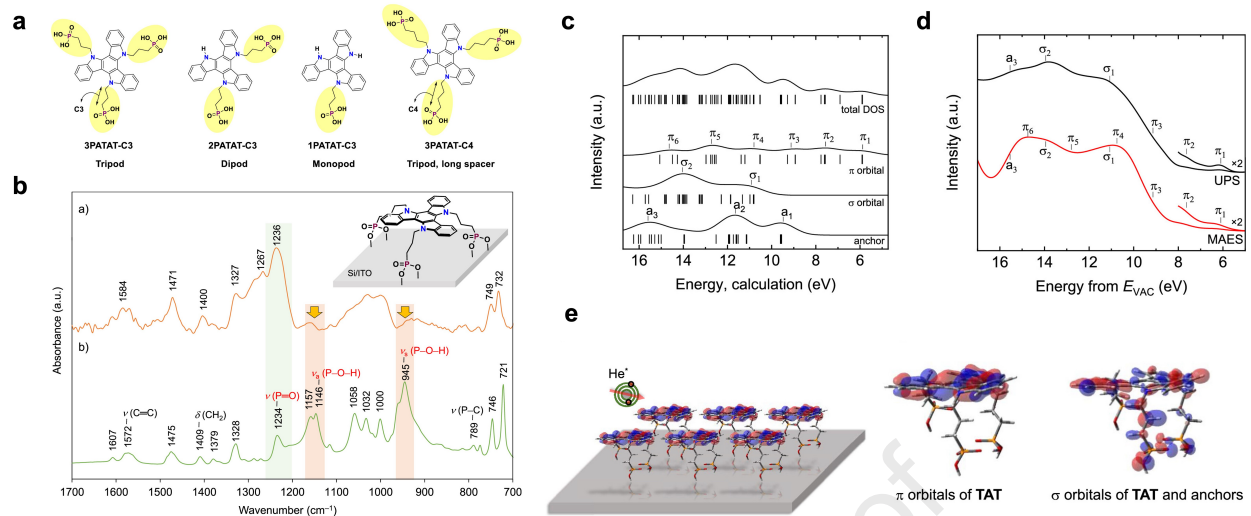


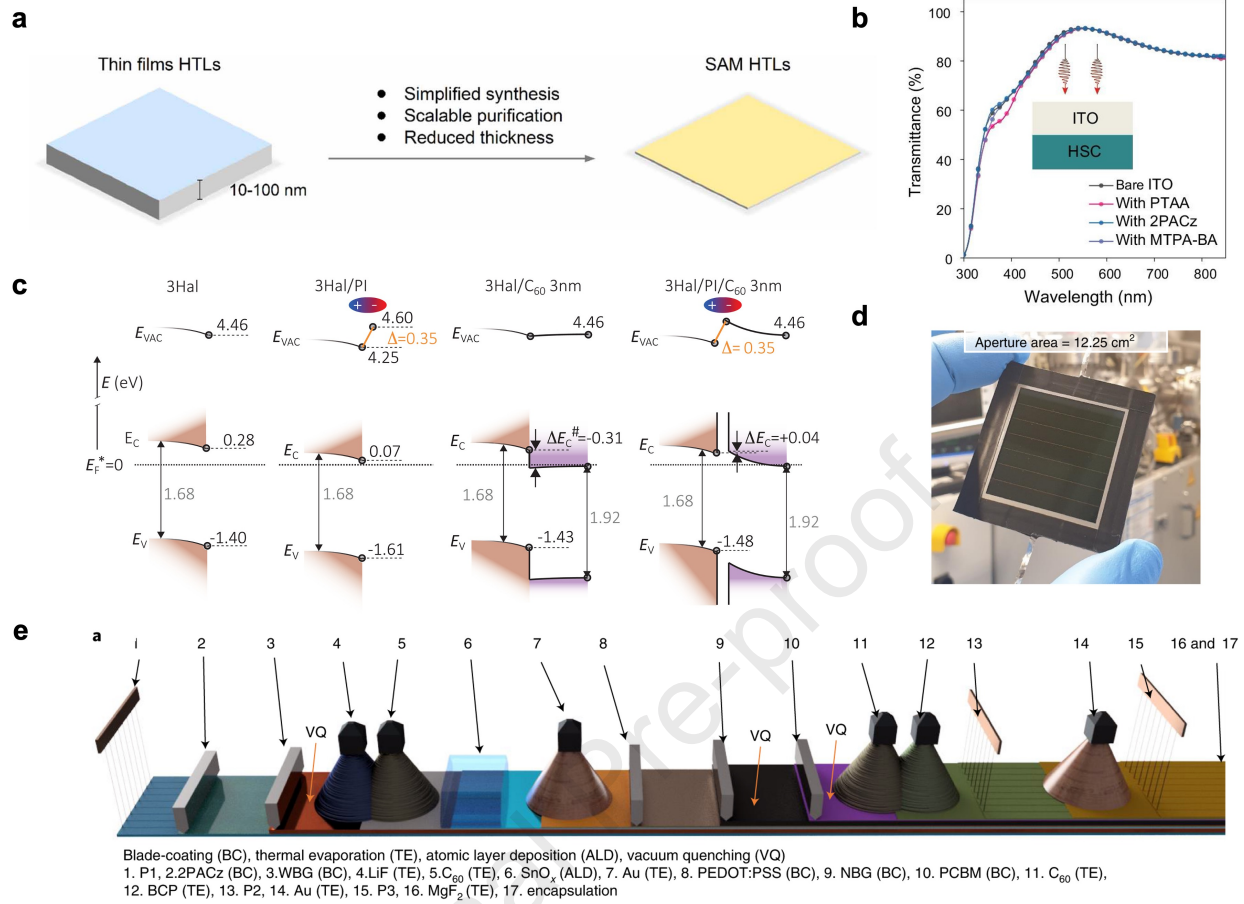


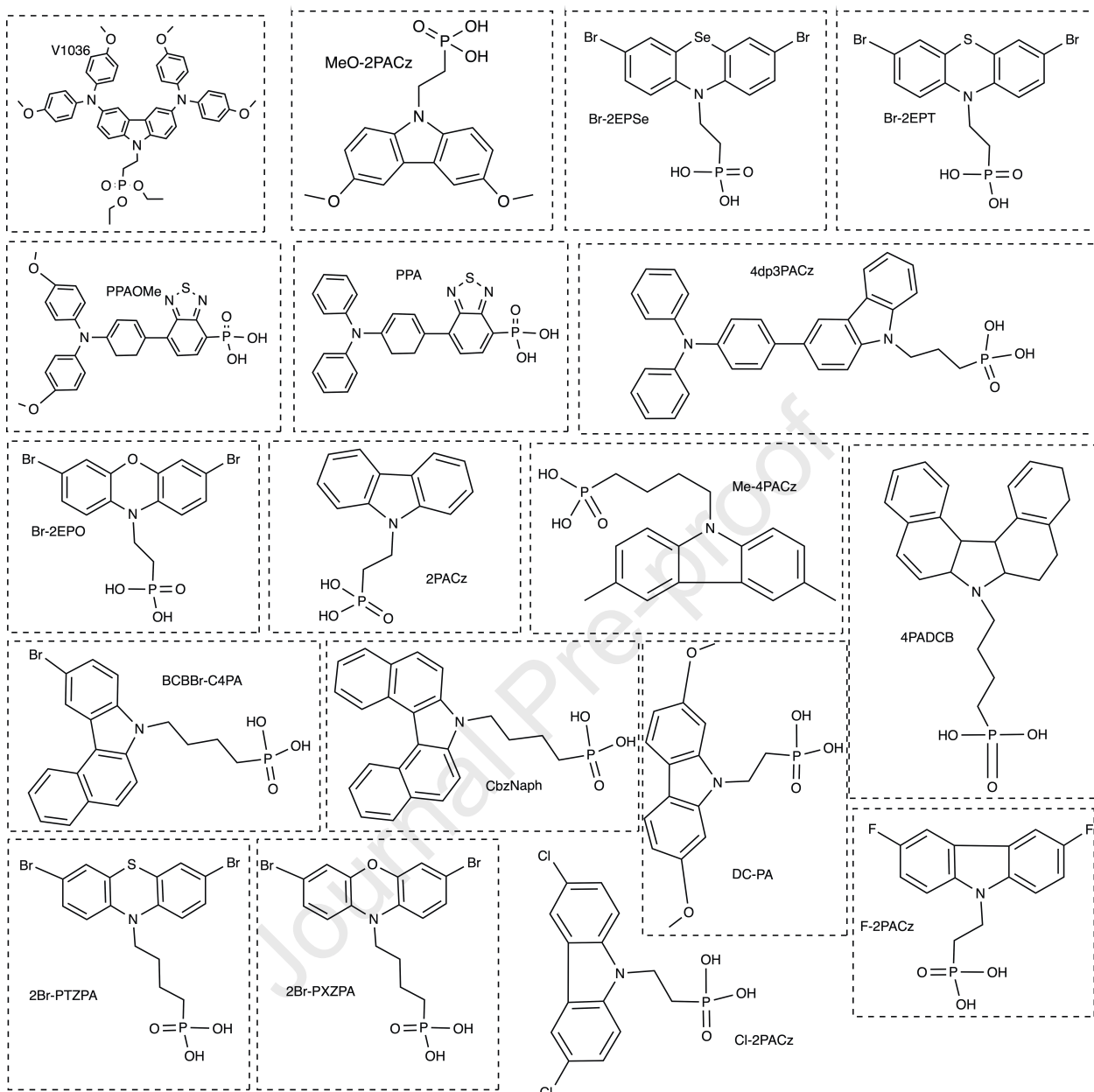


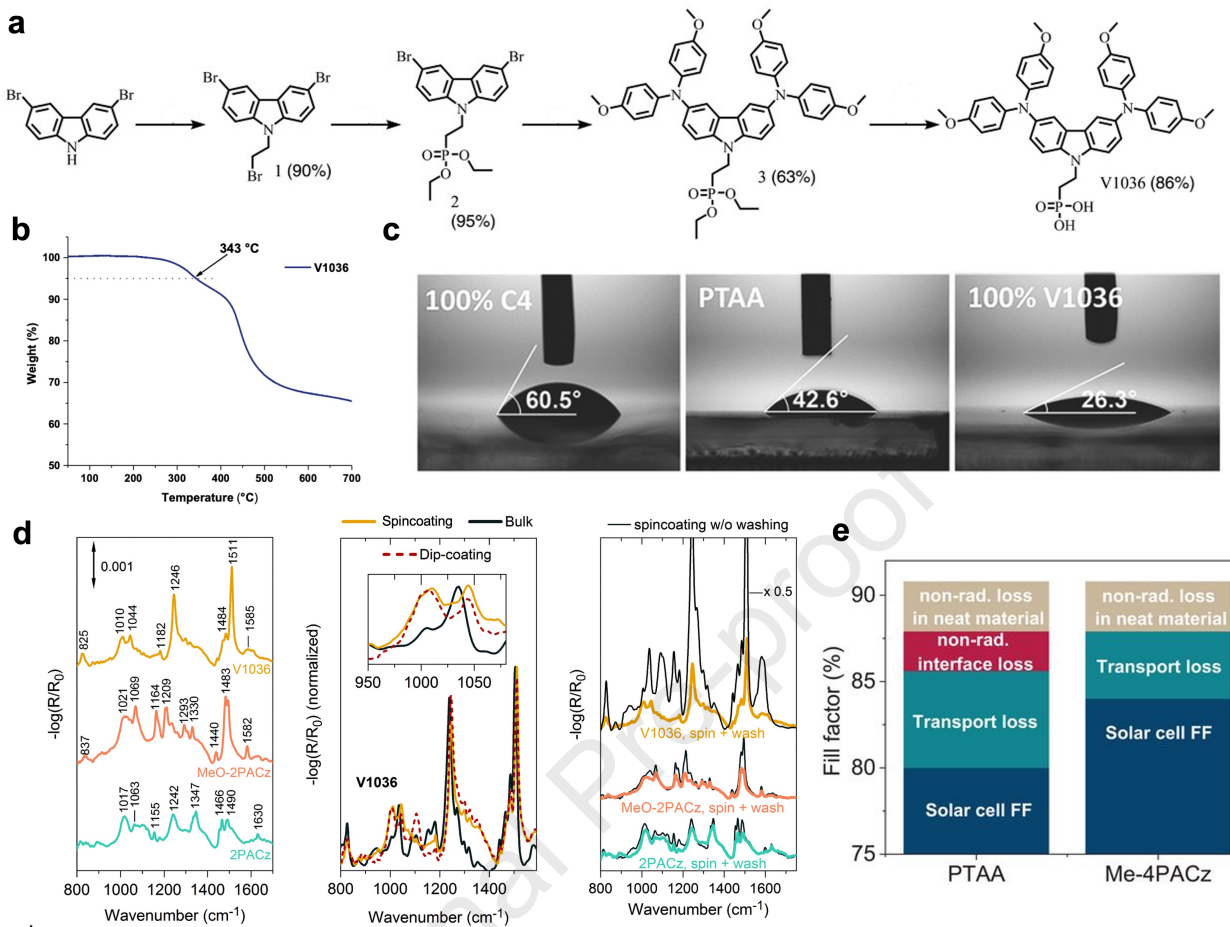


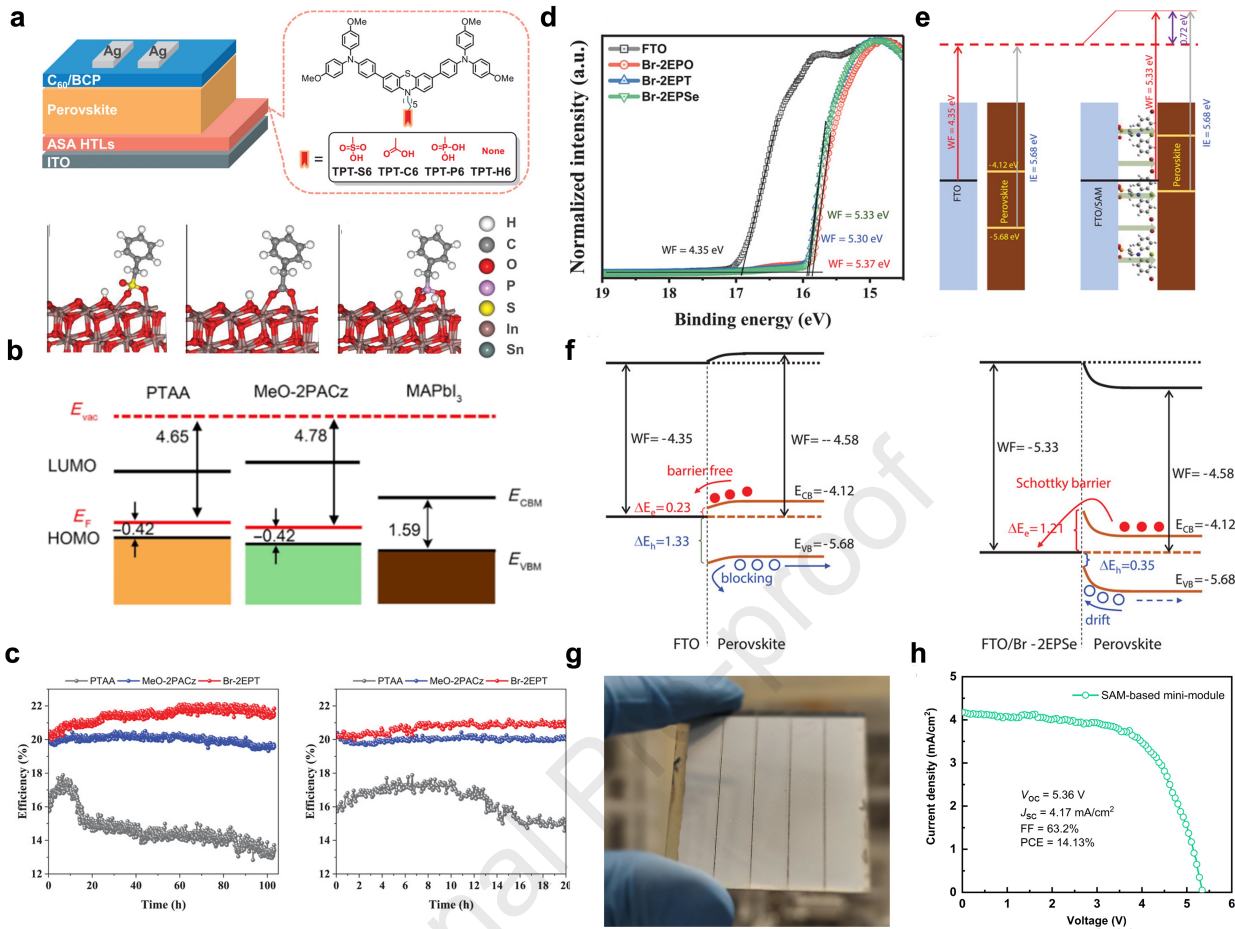


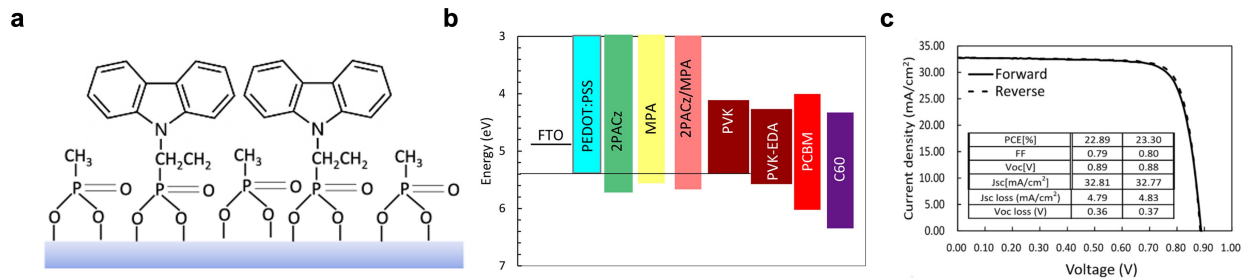


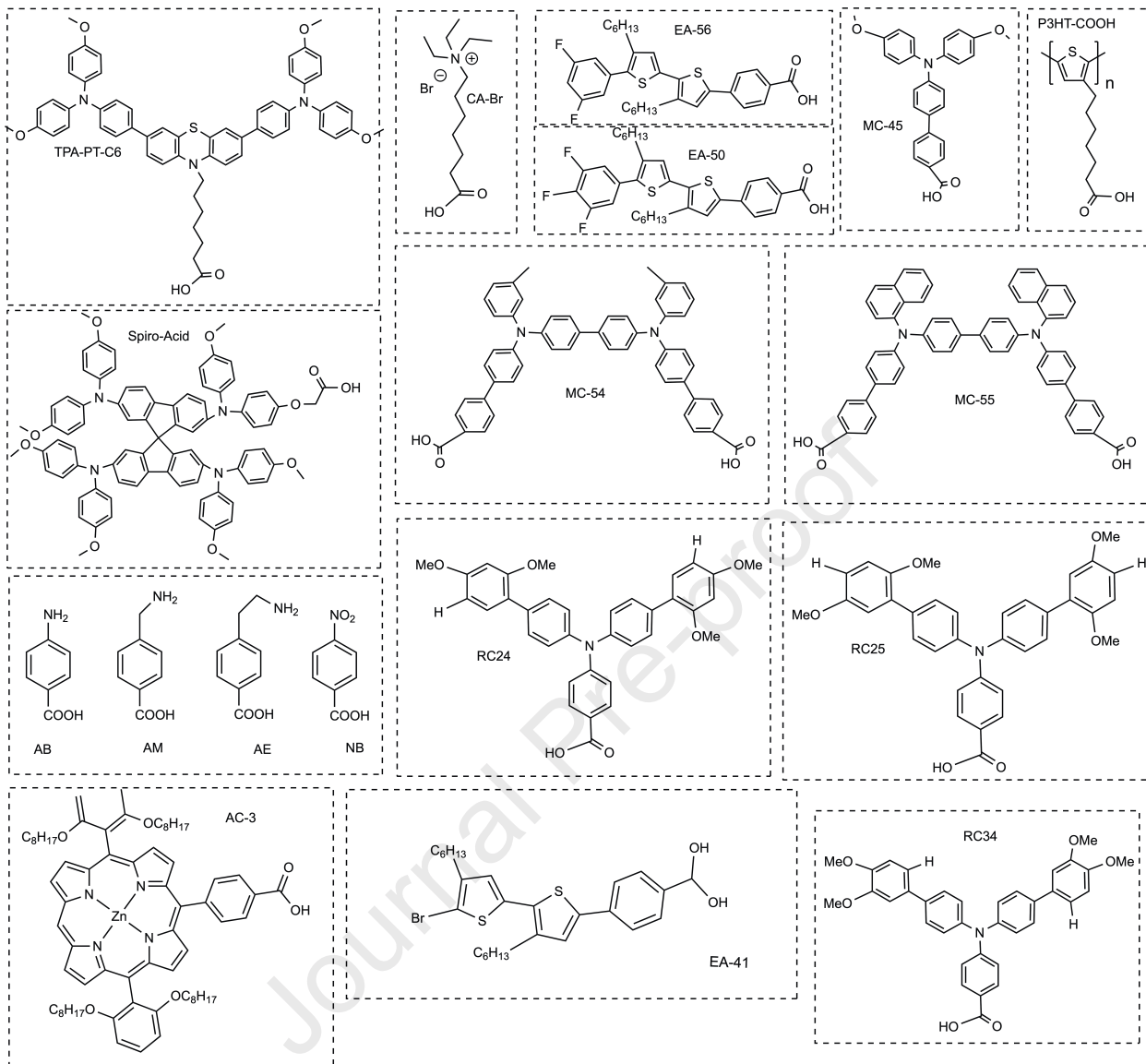


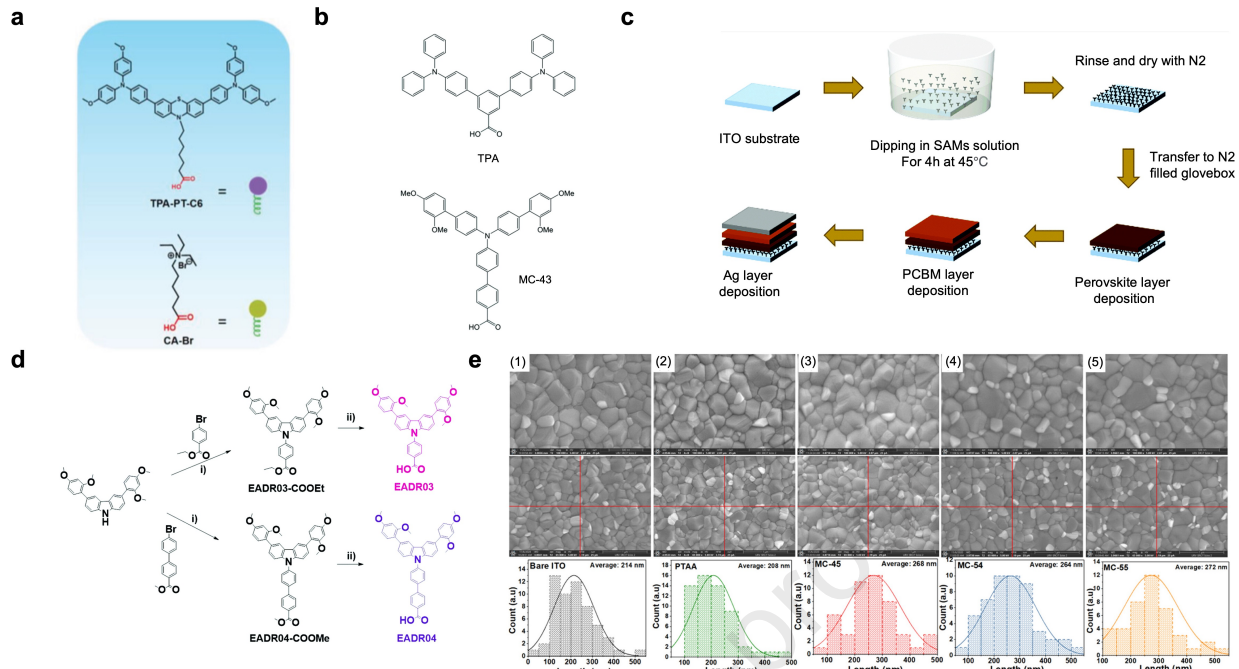


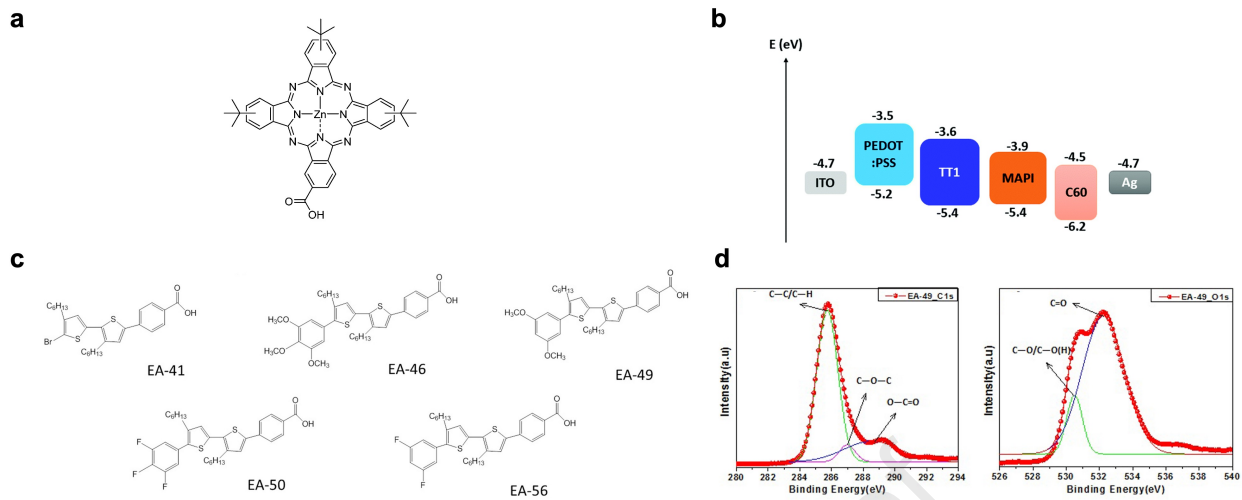


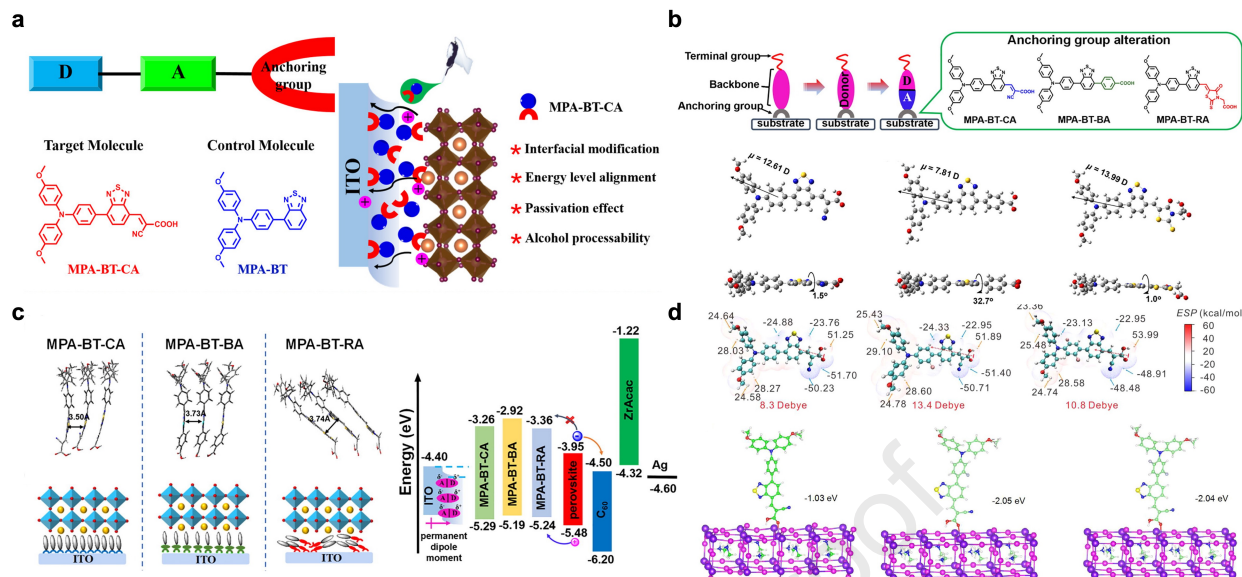


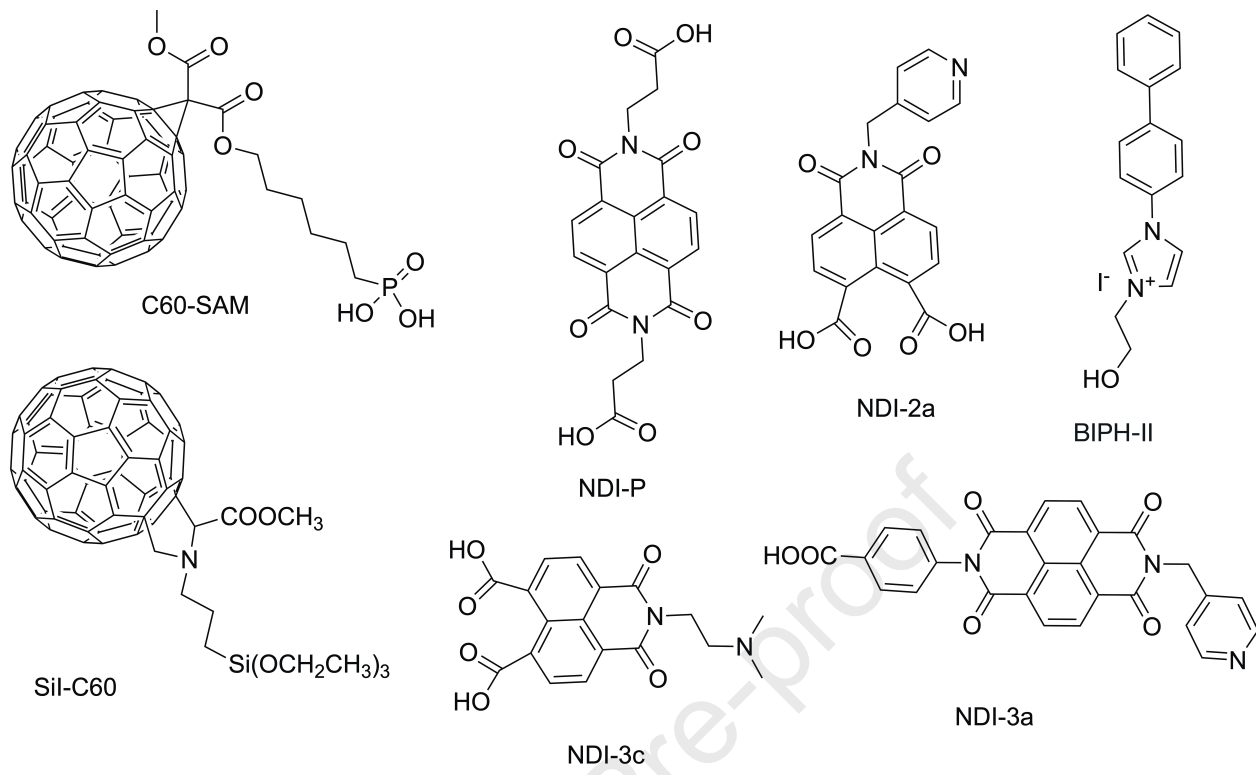












1. The composition, advantages, and potential problems of self-assembled molecules (SAMs) are summarized.
2. The application of SAMs as hole transport layers is reviewed, focusing on common functional groups such as phosphonic acid and carboxylic acid.
3. The application of SAMs as electron transport layers is briefly reviewed.
4. The challenges of using SAMs as a functional layer in perovskite solar cells are laid out, and suggestions are made for the future design and development of SAMs.

**Declaration of interests**

- The authors declare that they have no known competing financial interests or personal relationships that could have appeared to influence the work reported in this paper.
- The author is an Editorial Board Member/Editor-in-Chief/Associate Editor/Guest Editor for *[Journal name]* and was not involved in the editorial review or the decision to publish this article.
- The authors declare the following financial interests/personal relationships which may be considered as potential competing interests:

